ALMA MATER STUDIORUM
UNIVERSITÀ DI BOLOGNA

DEPARTMENT OF INDUSTRIAL ENGINEERING

SECOND CYCLE DEGREE

CARBON EMISSIONS REDUCTION OF ISRU-ENABLED MISSION ARCHITECTURES

DISSERTATION IN SPACE MISSION ARCHITECTURE

Supervisor

Dr. Paolo Tortora

Defended by

Marco Fiorito

Graduation Session December 2025

Academic Year 2025/2026

Acknowledgements

The completion of this thesis would not have been possible without the expertise and guidance of the Space Resources Team at the European Space Research and Technology Centre of the European Space Agency. I wish to convey my deepest gratitude to my internship supervisor, Dr. Melchiorre Conti, my office mate, Ms. Victoria Schein, and Mr. Ryan Jacmohone. Thanks to you all, my time at ESA was full of enjoyable moments and learning experiences; this thesis is as much yours as it is mine.

At the University of Bologna, I wish to thank my thesis supervisor Dr. Paolo Tortora, for the faith placed in me to complete this work, and for his greatly appreciated feedback. To my friends, Rosario and Lorenzo, to whom for their continued support and willingness to help me enter the world of engineering, I owe an unrepayable debt, please accept the food and wine we will share after this thesis has been defended as an initial down payment.

At TU Delft, where I had the pleasure of completing my exchange, I wish to thank Lorenzo, Josh, and Mateo, who suddenly found themselves with a fourth room-mate and 25% less beer. I am pleased to say the friendships are on par with the quality of education.

In Brussels, where this thesis took a year-long break whilst I started working, I wish to thank my colleagues at the European Defence Agency, who provided me with the support to finalise my degree whilst giving me an environment in which to apply my studies, and my girlfriend Rosy, whose constant encouragement enabled me to accomplish more than I could have alone.

Finally, to my parents Alessandro and Daniela, who, for the last 25 years, have passed their extensive life and technical knowledge on to me, and to my sister Alice, who has chosen the somewhat sadistic life of a PhD student: the importance of your continued support in completing this degree can not be overstated, and I will forever be grateful to you all.

Abstract

This thesis explores the critical role of In-Situ Resource Utilisation (ISRU) in space exploration, particularly its impact on mission architecture and carbon emissions. The research provides an extensive analysis of space resources, propulsion technologies, ISRU methodologies, and their integration into future mission designs. By examining the challenges posed by overcoming gravity wells, the study highlights how ISRU can significantly reduce launch mass, costs, and emissions by decreasing dependence on Earth-based supply chains. The strategic importance of ISRU becomes apparent in the context of long-term human presence on the Moon and Mars, where it enables the production of oxygen, water, and fuel directly on celestial bodies.

A key focus of the study is the energy-intensive nature of space travel due to Earth's gravitational pull, which requires a velocity change of approximately 9.8 km/s to reach Low Earth Orbit. Any material sourced from outside Earth's gravity well reduces launch mass and overall mission cost. This consideration makes ISRU a potential game-changer by providing essential resources such as oxygen and fuel through processes like molten salt electrolysis of lunar regolith and the conversion of Martian atmospheric CO2 into breathable oxygen, as demonstrated by NASA's MOXIE experiment. The research also explores asteroid mining as a means of extracting water and metals for in-space manufacturing, further enhancing ISRU's relevance.

The study examines various space propulsion methods, including chemical, electric, nuclear, and solar sail technologies, and evaluates how ISRU can enhance mission efficiency. The potential of electric propulsion combined with ISRU-derived fuels presents a promising avenue for sustained deep-space transport. Additionally, the research quantifies CO2 emissions from different space missions, comparing traditional architectures with ISRU-enabled alternatives. By developing a Δv roadmap, the study systematically analyses emissions at different mission stages and considers how ISRU could mitigate these environmental impacts.

A significant portion of the thesis is dedicated to assessing the ISRU implications for mission models adopted by SpaceX and Blue Origin. The SpaceX model evaluates Starship's fuel requirements and investigates the feasibility of refuelling with ISRU-derived liquid oxygen in Low Lunar Orbit, reducing dependency on Earth-supplied fuel. The Blue Origin model considers the role of New Glenn and BE-7 engines in a broader cislunar transport system. Both models demonstrate that integrating ISRU into mission architecture could substantially decrease carbon emissions by reducing the need for Earth-based fuel production.

The study also explores mission architecture and logistics, particularly the influence of ISRU on the design, mass, and refuelling cycles of lunar surface shuttles and Mars-bound missions. Various plant sizing calculations are conducted to estimate ISRU efficiency and determine feasibility for surface operations on the Moon and Mars. The findings suggest that ISRU is a crucial enabler for sustainable space exploration, allowing for greater mission flexibility and long-term resource independence. However, technology gaps remain in areas such as automation, power generation, and resource characterization, which must be addressed before ISRU can be fully integrated into space missions.

Contents

Acronym List

Acronym	Definition
BLT	Ballistic Lunar Transfer
BMLL	Blue Moon Lunar Lander
BO	Blue Origin
CH4	Methane
CO2	Carbon Dioxide
ConOps	Concept of Operations
CT	Cislunar Transporter (specifically that of Blue Origin's ConOps)
DARPA	Defense Advanced Research Projects Agency
ESA	European Space Agency
ESM	European Service Module
ESTEC	European Space Research and Technology Centre
FFC	Fray Farthing Chen
GTO	Geosynchronous Transfer Orbit
H2	Hydrogen
HLS	Human Landing System (specifically that of the Artemis programme)
HRE-XI	ESA Directorate of Human and Robotic Exploration, Space Resources Team
ISRO	Indian Space Research Organisation
ISRU	In-Situ Resource Utilisation
JAXA	Japan Aerospace Exploration Agency
LLO	Low Lunar Orbit
LMO	Low Mars Orbit
LOX	Liquid Oxygen
LRO	Lunar Reconnaissance Orbiter
LUNA	Soviet robotic space missions programme
MECO	Main Engine Cut Off
MoC	Material of Construction
MOXIE	Mars Oxygen In-Situ Resource Utilisation Experiment
NASA	National Aeronautics and Space Administration
NEO	Near Earth Objects
NGS1	New Glenn Stage 1
NGS2	New Glenn Stage 2
NRHO	Near Rectilinear Halo Orbit
O2	Oxygen
PBAN	Polybutadiene acrylonitrile (Solid rocket propellant)
PEL	Peaks of Eternal Light
PSR	Permanently Shadowed Regions
RTG	Radioisotope thermoelectric generator
SLS	Space Launch System (specifically that developed by NASA for Artemis)
SR	Space Resources
TES	Thermal Energy Storage
TRL	Technology Readiness Level
VHESC	Very High Efficiency Solar Cell
WSB	Weak Stability Boundary

1 Introduction

Space travel is famously difficult; between the hostile environmental conditions, the technological complexity of launch vehicles, and Earth's unwavering desire to keep everything from leaving its surface, there is no scarcity of situations in which a mission can be brought to an end. One of the most problematic challenges to overcome is the large gravitational pull of the Earth, which results in a large addition of energy needed to reach the velocity required for a stable orbit. Depending on the altitude of the desired orbit and the ascent profile used by the launch vehicle, this acceleration (Δv) is around 8 km.s^{-1} plus 1.5 - 1.8 km.s^{-1} to account for atmospheric and gravity drag on the vehicle, giving a total Δv to low earth orbit (LEO) of around 9.8 km.s^{-1}.

1.1 The Rocket Equation

Consider the Tsiolkovsky rocket equation (Equation 1), where m_w indicates the vehicle wet mass - as it is prior to a manoeuvre with both its dry mass and any propellant that will subsequently be burnt - and where m_d indicates the vehicle dry mass - composed of everything except the fuel about to be burnt. Additionally, Isp is the specific impulse of the propulsion system being used, and g_0 is the gravitational constant.

$$m_w = m_d \cdot e^{\frac{\Delta v}{Isp \cdot g_0}} \tag{1}$$

The derivation of this equation, although not trivial, is a simple exercise in calculus built on the principle of momentum exchange, and will not be covered here. The key takeaway is that any particular combination of propulsion system and desired Δv results in a certain scale factor > 1, which represents the ratio of the starting mass to final mass of the vehicle. From here, we can also explicitly express the propellant mass required as

$$m_{prop} = m_d \cdot \left(e^{\frac{\Delta v}{Isp \cdot g_0}} - 1\right) \tag{2}$$

It should be clear here that any increase in Δv results in an exponential increase of the required propellant mass. As an indicative example consider a destination in low Earth orbit (LEO). From the Earth's surface a fully loaded SpaceX Starship (100 tonnes dry mass + 250 tonnes payload in its expendable configuration) requires more than 5.2 million kg of propellant to reach its destination. However, from the Lunar surface, where only 5.9 km.s^{-1} of Δv is neccesary to reach LEO, only 1.4 million kg of propellant is required. This difference highlights the energy cost of launching from Earth compared to difference celestial bodies, and it becomes apparent that anything we can source from outside Earth's gravity well (and thus does not need to overcome the 9.8 km.s^{-1} of Δv) represents a significant propellant saving. In turn this results in cheaper, smaller rockets that produce less emissions.

1.2 In-Situ Resource Utilisation (ISRU)

In-situ resource utilisation (ISRU) is the practice of sourcing and converting local extraterrestrial materials into the consumables and commodities that a mission would otherwise have to launch from Earth. The rationale is simple but far-reaching: every kilogram of oxygen, water, propellant, or structural material produced off-world avoids the exponential launch-mass penalty described in subsection 1.1, unlocking leaner architectures and, ultimately, longer and more ambitious human stays beyond LEO.

For near-term Lunar and Martian scenarios the most valuable indigenous resources are oxidised minerals that can be electrolysed to release oxygen, water ice or hydrated regolith that can be cracked into life-support water and hydrogen/oxygen propellants, and silicate- and metal-bearing soils that can be

refined into construction feedstocks. By turning these in situ reservoirs into breathable air, fuel, and building materials, ISRU promises to shorten Earth-bound supply chains, curb mission-stage CO_2 emissions, and enable surface infrastructures that would be impractical to deliver via launch vehicles.

The concept, first proposed in Apollo-era studies, is now moving from laboratory proof of principle to prototype hardware. Section 4 surveys the present state of the art from molten-salt electrolysis of lunar regolith and Mars-atmosphere oxygen generation to water-ice mining techniques, while Part II quantifies how these technologies reshape mission mass flows and carbon footprints. Throughout the thesis we return to ISRU as both a technological driver and a design variable; here, it suffices to recognise it as the cornerstone on which sustainable human activity in cislunar space and beyond will be built.

As an indicative example to set the stage for the deeper analysis to come, consider an ascent from the lunar surface to low lunar orbit (LLO)[1]. This requires approximately 1.8 $km.s^{-1}$ of ΔV, meaning that each kilo lifted to orbit requires half a kilo of propellant. The real penalty here is not the half kilo on ascent, but in the logistics chain required to bring that half kilo to the lunar surface to begin with. If supplied from Earth, the approximately 16 $km.s^{-1}$ of ΔV means that around 18 kilos of propellant are required to deliver that same half kilo to where it is needed - the gear ratio is approximately 1:36, even before we account for safety margins or additional structural mass neccesary to facilitate such a delivery. It is easy to see how it quickly becomes favourable to have an in-situ production capability when sustained extraterrestrial operations are desired. The cost break-even may come later, especially considering the required research and technology readiness level (TRL) raising efforts, but from a mass balance perspective, break-even can easily be reached within a single mission cycle.

[1] Ranging from approximately 100 to 200 km orbital altitude.

Part I
Space

2 Space Exploration Technologies

Space exploration is a melting pot of technological disciplines, five of which can be augmented by space resources, and thus merit a discussion in the context of this work. These five - propulsion, life support, power generation and storage, construction, and robotics - are discussed below. Others not covered, but undoubtedly crucial to space exploration, include communication systems and navigation and control systems.

2.1 Propulsion

The field of propulsion in space is vast, with the most common being chemical and electric propulsion. New technologies include solar sails, nuclear thermal rockets, and nuclear electric propulsion, and although promising, lack flight-readiness. Within the context of this work, we focus first on the legacy technologies within the context of carbon emissions and mission design for ISRU, and then consider near-future technologies within the context of an ISRU system sizing. Here we provide a brief overview of each technology, including how it works, its advantages/disadvantages, and its maturity in the context of space exploration. At the most general level, all propulsion systems work on the exchange of momentum between the vehicle and a propellant[2]. For this to occur, systems require both the propellant itself, and an energetic source to produce the momentum that is then exchanged.

2.1.1 Chemical Propulsion

Chemical propulsion is the oldest of the four main propulsion categories, with solid propellant rockets dating back to ancient Chinese gunpowder rockets in the 13^{th} century. All forms of chemical propulsion operate with some form of fuel and oxidiser, although the form factor and combinations greatly differ from one type to another. For example, solid rocket propellant is often a homogenised mixture of both in a pre-determined ratio, whereas liquid rockets store both in separate tanks and only combine them at the moment of combustion[3]. Before proceeding, it is important to clarify that propellant is the combination of both fuel and oxidiser neccesary to produce thrust.

Solid propellant is significantly easier to integrate into a rocket when compared to liquid chemical propulsion. It requires no pumps, tanks, or valves, and once ignited, the rocket burns until the fuel is exhausted. The lack of moving parts, and relative stability of the propellant mean solid rockets are cheaper, easier to manufacture, and generally more reliable than their liquid counterparts. However, the very things that led to its early adoption can be limitations when the application becomes more technical. The simplicity of solid rockets means they cannot be throttled, shut down, or restarted once ignited[4]. In many use cases this in not necessarily a problem, especially when you have something like a sounding rocket, who's goal is just to get to space for a short period of time. However, when the goal becomes more technical, such at entering orbit, a greater level of thrust control is required.

[2]Solar sails too, although the "propellant" in this case exchanging momentum with the vehicle is numerous photons.

[3]There are also forms of liquid propulsion with homogenised propellant mixtures, such as mono-propellant rockets that generate thrust by decomposing a single chemical propellant, releasing energy without the need for a separate oxidiser or additional fuel.

[4]Advanced solid rocket designs may actually be throttled through the use of jet deflection vanes and extinguished through the use of vent ports, but this added complexity is rarely justified in the use-case.

The first liquid chemical rocket was launched by Goddard in 1926, using a combination of LOX and gasoline. Not only are the oxidiser and the fuel used in this propellant configuration more energetically dense, but their liquid form factor allows the throttle to be controlled via the flow rate, and also allows for the engine to be shut off and restarted as required. Furthermore, combinations of fuel and oxidiser that spontaneously combust when combined (hypergolic propellants) allow for a theoretically unlimited number of restarts without significantly increasing engine complexity. This increased control on combustion conditions also allows for a more optimised engine design that would not be possible with solid propellant. Combined with the generally higher specific energy of liquid propellants, liquid rocket propulsion is a more efficient and controllable alternative to solid propulsion, albeit at a higher complexity and cost.

With both solid and liquid chemical propulsion, both the reactive energy and the reactive mass required to produce thrust come from the propellant itself. Whilst useful, we will see that other forms of propulsion do not necessarily rely on the propellant itself for both the energetic and massive requirements of a propulsion systems.

2.1.2 Electric Propulsion

Above all else, the key difference between electric and chemical propulsion is that the onboard propellant only represents the mass requirements of the propulsion system, with the required energy for producing thrust coming from an external source. In the majority of cases this is either a set of solar arrays, or an onboard radioisotope thermoelectric generator (RTG). Using this electrical energy to accelerate propellant to very high speeds, thrust is generated more efficiently than traditional chemical rockets. Common types of electric propulsion, like ion thrusters and Hall-effect thrusters, expel ions or plasma to produce continuous, low-thrust acceleration, ideal for long-duration missions and deep-space exploration. Historically, propellants have been limited to noble gases such as krypton and xenon, due to their relatively low ionisation energy and relatively high atomic mass, combined with their non-reactive nature that helps prolong the service life of the electric engine.

By using an external source of energy to accelerate the propellant, vehicles using electric propulsion can be made lighter and can use their onboard propellant more efficiently, enabling longer duration space missions. This efficiency, which is general an order of magnitude higher than chemical rockets, comes at the cost of a much lower thrust. Consequently, electric propulsion is unsuitable for applications requiring high instantaneous thrust or rapid acceleration, such as at launch. However, electric propulsion, combined with effective mission and manoeuvre planning remains an effective choice for long-duration missions or non time-critical operations. It also remains a very suitable choice for continuous low-thrust applications such as station-keeping at Lagrange points[5].

2.1.3 Nuclear Propulsion

Nuclear thermal propulsion is a form of chemical propulsion, where a nuclear reactor produces the heat neccesary to expand, and thus accelerate, the propellant through a rocket nozzle and produce thrust. Like electric propulsion, in this configuration the energetic requirement of the propulsion system does not come from the propellant itself, but from an external, non-consumable source[6]. This allows nuclear thermal propulsion to have a higher efficiency than traditional bi-propellant liquid propulsion, whilst not suffering from the low-thrust of electric propulsion systems.

[5] Foreshadowing the logistics of in-space propellant depots.

[6] Also technically a consumable, but for practical purposes is not depleted during the vehicle's operational lifespan.

Nuclear electric propulsion uses a nuclear reactor to produce the neccesary electrical power for an electric propulsion system. Not only does this allow for greater electrical power, but also removes the dependency on solar radiation, and thus deals with the problem of reduced power generation of solar arrays on deep space missions. This form of electric propulsion is therefore a suitable option for near-future electric propulsion systems, and also allow for the implementation of electric propulsion systems on heavier transport vehicles that require more significant levels of thrust.

2.1.4 Propulsion via radiative pressure

Radiative pressure propulsion systems, namely solar sails or light sails, take advantage of the pressure exerted by photons on the body of a vehicle. In most cases this force is negligible compared to the thrust of the propulsion system, however when the exposed area is greatly increased, the force produced may be significant. In the case of solar sails, the solar radiative pressure is exploited through the use of large sails on the vehicle in order to produce a small, but constant and non-negligible thrust. Similarly, light sails use the same principle but instead of solar pressure, use a ground-based high-powered laser as the source of photons.

The lack of onboard propellant mass, and the continuous thrust, mean that this propulsion system is a suitable choice for long-duration non time-sensitive missions. Furthermore, controlling and navigating with sails can be complex due to their reliance on external light sources, and solar sails become less effective as they move farther from the Sun where photon pressure diminishes. For light sails dependent on ground-based lasers, the need for powerful, accurate laser infrastructure adds significant complexity and expense.

2.2 Life Support

Life-support, also called Environmental Control and Life-Support Systems (ECLSS), is the collection of hardware that provides crews with breathable oxygen, potable water, pressure, thermal regulation, and waste management. Without it, astronauts would survive only minutes once separated from Earth's biosphere. ISRU can transform this indispensable and logistically heavy subsystem into a largely self-sustaining one. On the Moon, molten-regolith and molten-salt electrolysis routes demonstrated in subsubsection 4.1.1 can liberate oxygen from common silicates, turning the very soil into an on-demand air source and eliminating many tonnes of Earth-launched oxygen per mission [1]. Where polar ice or hydrated soils are present, excavation followed by thermal extraction and water electrolysis closes both the water and oxygen loops (described in more detail in subsubsection 4.1.2 and 4.2.2) [2]. Mars has already field-tested an atmospheric pathway: the MOXIE (refer to subsubsection 3.4.3) stack splits carbon dioxide into oxygen, proving that future habitats can refill tanks and EVA suits directly from the ambient air, which coupled with the capture of buffer gases such as nitrogen and argon from the same atmosphere, could relieve the supply chain, extend mission duration, and lay the technological foundation for closed-loop life-support ecosystems on other worlds.

2.3 Power Generation and Storage

Power generation, like propulsion, can be split into a clearly defined set of legacy technologies and near-future technologies. Legacy tech includes solar arrays, batteries, and RTG's; the methods that have been used since the start of the space age to reliably provide electrical power to spacecraft. They are often on the cutting edge of their respective technological fields, with the developments and advances eventually being applied to terrestrial versions of the same tech. Two key examples of this occurring within the field of solar cells are the the activities of Spectrolab and DARPA.

Spectrolab, a Boeing subsidiary, began developing high-efficiency solar cells in the 1950's, and since then has supplied the cells for a multitude of satellites, including the ISS's roll-out solar arrays. [3]. Their development of multi-junction solar cells, capable of exceeding 40% efficiency, has been a game-changer, with these high-efficiency cells providing more power from smaller, lighter panels [4]. Likewise, the Very High Efficiency Solar Cell (VHESC) initiative funded by DARPA to develop ultra-high-efficiency, lightweight solar cells for military and space applications resulted in technological advancements such as new materials and cell designs, which transitioned into civilian markets, enhancing the efficiency and reducing the cost of terrestrial solar panels [5, 6, 7].

Within the context of ISRU on the lunar surface and ISRU in service of lunar resource extraction, technologies such as concentrated solar power and thermal energy storage (TES) are particularly promising as any lunar-based ISRU system (except those in peaks of eternal light (PEL's)) will be required to survive the night. Already a mature technology in terrestrial applications, both concentrated thermal power and thermal energy storage could be adapted relatively easily for use on the lunar surface. In combination with the lunar resources available, these technologies could provide a means to continue ISRU operations throughout the 14-day lunar night, and avoid the plant downtime that would otherwise occur. Not only is regolith abundant on the lunar surface, but its melting point ranging from 1373 K to 1653 K makes it suitable for efficiently storing high-temperature thermal energy [8, 9]. The ability of a TES system to provide continuous power throughout the night is key in allowing the continued and sustained operation of a lunar base without the reliance on a periodic supply such as solar, or a potentially dangerous source such as nuclear [10, 11]. Lunar regolith does, however, present a key problem on account of its highly abrasive nature. The need for robust high-temperature containment systems as part of a lunar regolith TES system necessitates the development of new materials capable of enduring abrasion, thermal cycling, and corrosion [12].

2.4 Construction

Human-rated habitats, landing pads, and radiation shielding weigh far more than any rocket can practically haul from Earth, so long-duration exploration will only scale once construction materials are manufactured on-site [13, 14]. ISRU closes that gap by turning local resources (regolith and atmosphere) into bricks, binders, metals, and composites, which moves structural mass from Earth to the planetary surface itself. The simplest pathway is to dig, heat, and fuse. Lunar and Martian simulants have been microwaved to 1100 Celsius in minutes, sintering them into ceramic tiles with compressive strengths of 50–120 MPa [15]. This is adequate for landing-pad pavers and radiation berms. Laser or electron beam powder-bed fusion pushes that concept toward full additive manufacturing of vaults and arches.

Parallel work on extrusion-based regolith concrete demonstrates segments printed in vacuum chambers, validating autonomous layer deposition and shrinkage control under lunar thermal cycling. Binder-based routes offer lower processing temperatures: sulfur, for example, exists in both lunar pyroclastic deposits and Martian regolith, can melt at 115 Celsius, and reacts with dust to form a dense, recyclable sulfur concrete whose strength rivals that of terrestrial Portland cement [16]. Alternatively, alkaline activation of aluminosilicate fines yields geopolymer mortars. A 2025 study printed zig-zag geopolymers from lunar simulant, achieving 35 MPa strengths while embedding voids that double as thermal-insulation layers [17]. Both approaches minimise energy demand, making them attractive for early surface infrastructure that must bootstrap itself from kilowatt-class power plants.

For lighter, radiation-damping shells, basalt fibres drawn from regolith glass can reinforce sulfur or geopolymer matrices. Mechanical testing of such fibre composites reports 2-3x gains in flexural

strength over plain regolith concrete, enabling thinner shells and lower excavation volumes [18]. In aggregate these techniques, sintering, binder concretes, and electro-metallurgy form a tiered construction toolkit that scales with available power and mission duration, delivering everything from emergency berms to pressurised habitats, all whilst feeding excess oxygen and metals into the wider ISRU economy.

3 Space Resources

3.1 Implications

The presence, and perhaps more importantly the availability, of resources in locations of interest has several important implications in mission design, cost, and sustainability.

3.1.1 Water

Water in any form on an extra terrestrial body has far-reaching implication, including but not limited to those regarding propellant production and life support augmentation.

The progression of our understanding where and how water is located on the moon is better described in subsection 3.3, but the general trend is that whilst originally assumed to be anhydrous, new remote sensing results indicate that most of the lunar surface is in fact hydrated, with the majority of water being contained either in structurally-bound OH^- or in H2O absorbed onto the lunar soil grains [19]. Although we now know with a high degree of certainty that there is water on the moon, the uncertainty regarding its abundance, distribution, and form mean that designing a mission around water as a key lunar resource is still not viable.

From a pure mass perspective, the presence of water most significantly impacts the role that propellant mass plays in current space missions. Even with a substantial number of astronauts on board, the fraction of water resources dedicated to propellant is at least an order of magnitude larger than that given towards life support [20]. To reiterate, oxidiser constitutes approximately six sevenths of the propellant mass for hydrolox propulsion systems and approximately seven ninths of the propellant mass for methalox propulsion systems. For a fully loaded lunar-launched Starship destined for LLO, this represents an oxidiser mass of 498 tonnes (refer to Figure 8). In comparison, an astronaut performing a standard mission including exercise uses approximately 0.8 kg of O2 per day [21].

Although a small output in comparison to propellant, the ability to produce, in-situ, this one kilo per astronaut per day cannot be overstated. It removes reliance on Earth delivery for one of, if not the, most critical consumable required for humans to survive in space. The presence of water in space allows for the immediate and scalable production of life-support O2 through proven and reliable electrolysis [22, 23].

3.1.2 Metals

Metals, including iron, silicon, aluminium, and titanium, are abundant on the lunar surface, asteroids, and other bodies. The composition of lunar regolith includes significant amounts of silicon dioxide (SiO2) at an average weight percentage of 44%, alongside elemental silicon (21%), aluminium oxide (Al2O3) at 19%, and iron oxide (FeO) at 11%. These elements can be harnessed to support the construction of habitats, spacecraft, and essential infrastructure directly on the Moon or Mars. In the absence of these local metal resources, such materials would need to be transported from Earth, imposing significant financial and logistical burdens (refer to Appendix A, Table 28).

The ability to mine and process these metals directly in space can drastically reduce this dependency, enabling on-site manufacturing of essential structures and tools. This in-situ extraction and utilization of metals would support the creation of larger and more complex installations, such as lunar bases or Martian habitats, which would otherwise be limited by the constraints of Earth-based launches.

For instance, the presence of aluminium provides a potential resource for producing structural components for habitats and spacecraft. Similarly, iron and titanium could be used to build tools and reinforce structures, thus supporting long-term sustainability for human missions. The presence of metallic resources supports the broader vision of establishing a self-sufficient space economy, where the infrastructure needed for further exploration can be built using locally available resources [24, 25].

Calcium, an alkaline earth metal, has a key implication when considered in the context of propellant for near-future electric propulsion systems. Primarily found in the form of plagioclase minerals like anorthite, if extracted and purified it can be used as a propellant and reduce dependency on earth-based resupplies. There are, however, some limitations to its integration. Firstly, given its role as a propellant for electric propulsion systems, it must be delivered to an orbital depot before being used, which requires use of chemical propellant. Secondly, the extraction and purification of calcium metal is energy-intensive, and would likely require specialised infrastructure, the cost of which may negate the benefits.

3.1.3 Volatiles

Volatiles such as carbon dioxide (CO2), methane, and ammonia play a crucial role in sustaining human activities and supporting various chemical processes in space. CO2, for example, can be processed to generate breathable oxygen, while methane holds potential as a fuel source. The availability of volatiles on planetary bodies like the Moon, Mars, and certain asteroids offers significant opportunities for the establishment of in-situ life support systems and fuel production capabilities. Unlike Earth-based supply logistics, relying on volatiles extracted in space can greatly simplify mission requirements, reduce costs, and enhance the sustainability of space operations. Telescopic spectroscopy and exploratory missions have shown that volatiles are distributed across different regions of these celestial bodies, providing valuable information for mission planners. By utilising these in-situ resources, long-duration missions can become more feasible, and the foundation for permanent human settlements on other planets can be established. This in turn forms an essential step toward building a sustained human presence beyond Earth, supported by efficient, closed-loop life support systems and in-situ energy production [26, 27, 28].

The implications of volatiles for mission design are significant when comparing missions that can and cannot utilise these resources. Missions that are able to make use of local volatiles benefit from greater flexibility and reduced dependency on Earth-based resupply, which allows for more ambitious mission profiles and extended durations. For instance, the ability to generate fuel from Martian atmospheric carbon dioxide means that return missions from Mars can be more economical, as they do not need to carry all the necessary propellant from Earth. On the other hand, missions that cannot rely on local volatile resources face greater logistical challenges, as they must carry all necessary life support and propulsion materials with them, leading to increased launch mass and costs. This limitation can restrict the scope of exploration activities and make long-term human presence in space much more challenging. The ability to harness in-situ volatiles, therefore, represents a key enabler for sustainable and scalable human exploration of the solar system.

3.2 Pre-1969 Methodology

Prior to the 1969 Apollo 11 sample return missions, our understanding of lunar resources, and their mineral composition, was largely based on a combination of three things; the Earth-Moon similarity hypothesis, the study of meteorites, and telescopic spectroscopy.

The Earth-Moon similarity hypothesis is the oldest of the three, and was(is) based on the theory that both share similar origins, and such they are also composed of primarily the same minerals. The earliest known instance of this theory is by Darwin[7] (1879) who proposed that the Moon was formed as a result of rapidly spinning Earth, whose outer equatorial mass scummed to centrifugal force and detached to become a separate orbiting body [29]. Darwin's theory was challenged in 1964 by Daly, who agreed with the common origin of the two bodies, but instead proposed an impact as the cause as opposed to centrifugal forces [30]. Following the Apollo lunar sample returns and the subsequent mineral composition analysis, these common-origin theories became the the Giant Impact Theory, that proposes the Moon was formed after a large body, known as Theia, collided with a primordial Earth, ejecting debris that eventually consolidated and joined to form the Moon.

For a community that lacked the technological capability to collect and return samples from space, the analysis of meteorites was an essential tool for understanding the mineral composition of space resources. Multiple publications prior to 1969 explored the chemical compositions of meteorites to understand their formation and potential as analogues for planetary materials, and confirmed the presence of metallic and silicate minerals that would go on to inform future discussions on ISRU [31, 32]. In particular, the work done in this period by J.R. Arnold and his colleagues provided key insights into the specific composition and distributions of these metallic and silicates, and helped create a knowledge base on which ISRU could grow [33, 34, 35].

The final of the three, telescopic spectroscopy, was another crucial technology that helped build the knowledge base of extra-terrestrial resources and their mineral composition. Unlike meteorite analysis, telescopic spectroscopy allowed the community to perform targeted studies of a known region (i.e. lunar mare or highlands) instead of being constrained to samples of unknown origin. The ability to directly analyse specific areas, and compare their mineralogical composition (as was done in the case of suggested Apollo landing sites [36]), proved more accurate and provided a direct understanding of the Moon's composition without the need for physical samples - a method whose accuracy has been validated post-factum with comparison to Apollo samples [37]. Moreover, telescopic spectroscopy could cover large portions of the lunar surface, offering a regional perspective on resource distribution, whereas meteorite samples only provided insights into localised samples (if they even were of lunar origin) [38].

3.3 Past SR-related Missions

There is, in the true sense of ISRU, only one historical example of this technology being used in the context of a space mission - MOXIE. We describe and discuss this mission shortly, but first let us cover the role that space resources have played in ISRU-precursor missions. Figure 1 shows a timeline of MOXIE-precursor missions that helped lay the groundwork for the first true ISRU technology demonstrator.

3.3.1 Luna Program (1959-1976)

The Soviet LUNA programme conducted three successful sample return missions (Luna 16 in 1970, Luna 20 in 1972, and Luna 24 in 1976), and demonstrated the technical viability of automated sample return missions [39, 40]. In the years following, these samples were studied by Soviet and non-soviet teams alike, and the samples were found to contain a variety of minerals including silicates such as pyroxenes[8] and plagioclase[9], which provided early indications that use-cases of lunar materials could

[7] Sir George Howard Darwin; second son of the perhaps more well-known naturalist and biologist Charles Darwin.
[8] Often contain iron and magnesium.
[9] Contains aluminium.

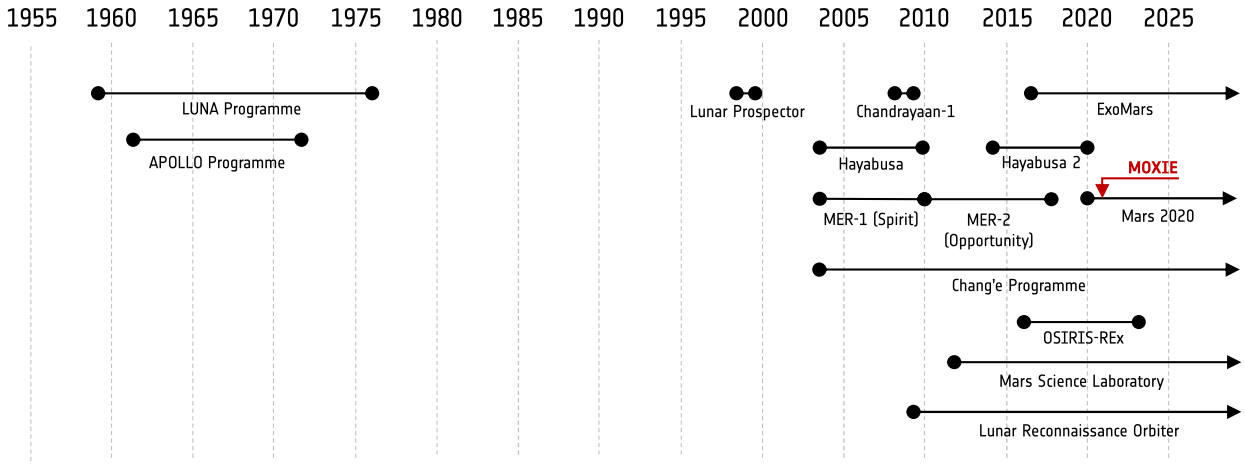

Figure 1: Timeline of missions related to space resources

extend to construction and manufacturing [41, 42, 43].

3.3.2 Apollo Missions (1969-1972)

The return of 58 samples totalling 21.5 kg during the 1969 Apollo 11 mission represented the first time in human history that extra-terrestrial materials were brought back to Earth[10] for detailed analysis [44]. The return of these samples was, in and of itself, one of the greatest scientific achievements of the 20th century, and in the context of ISRU represented the first tangible samples with which to determine the mineral composition of a key space resource.

The quantity of returned lunar samples increased each Apollo mission, reaching a high of 741 samples totalling 110.5 kg in the final Apollo 17 mission. Over the course of the programme, the six missions collected 2196 samples totalling 382 kg. These samples laid the groundwork for understanding lunar regolith composition and potential resources, particularly the oxygen bound in lunar minerals like ilmenite, and are still used to this day for studies on ISRU technologies [45].

3.3.3 Lunar Prospector (1998-1999)

As a mission designed to map the Moon's surface composition and magnetic/gravity fields, with a specific focus on identifying resources such as water ice and hydrogen, Lunar prospector was destined from the get-go to play a crucial role in shaping our understanding of space resources. The discovery of higher-than-expected concentrations of hydrogen at the poles, particularly in permanently shadowed regions (PSR), suggested the presence of water-ice [46]. As discussed in subsubsection 3.1.1, water-ice on the Moon has several important implications regarding mission design and ISRU technologies. In addition to this key discovery, Lunar Prospector's gamma-ray spectrometer and a neutron spectrometer were used to map the distribution of key elements including iron, titanium, thorium, and potassium across the surface [47, 48, 49].

3.3.4 SMART-1 (2003-2006)

SMART-1 was Europe's first mission to the Moon, and had a significant impact on the study of lunar resources, building on the discoveries of Lunar Prospector in several key areas. The higher resolution

[10]Extra-terrestrial material has, of course, always made its way to the Earth's surface in the form of meteorites.

imaging cameras onboard allowed detailed mapping of the lunar poles, especially the permanently shadowed regions where water ice might exist [50, 51, 52]. This detailed mapping was augmented by the mission's focus on the polar region, allowing it to spend more time analysing areas of key importance for future ISRU implementation - namely PSR's and PEL's [53, 54]. SMART-1's X-Ray and Infrared spectrometers also providing a more comprehensive understanding of the Moon's mineralogy than Lunar Prospector.

3.3.5 Chandrayaan-1 (2008-2009)

Chandrayaan-1, ISRO's first lunar mission, made significant contributions to the understanding of lunar resources. The mission's Moon Impact Probe detected water molecules on the Moon's surface, which was a groundbreaking discovery that transformed how scientists viewed lunar volatiles. The onboard Moon Mineralogy Mapper (M^3) provided spectral data of the lunar surface, and identified hydroxyl and water signatures near the poles [55, 56].

3.3.6 Hayabusa and Hayabusa 2 (2003-2010, 2014-2020)

JAXA's Hayabusa mission was the first successful attempt to return samples from an asteroid to Earth. The mission targeted a sub-kilometre asteroid named Itokawa, and provided invaluable insights into asteroid composition [57]. The samples returned by Hayabusa revealed a mixture of silicate minerals, iron, and trace metals; all potential sources of raw materials that could be utilised for construction, fuel, and life support in space [58]. Its successor, Hayabusa 2 targeted the carbonaceous asteroid Ryugu, and collected subsurface samples, returning them to Earth in 2020. The analysis of these samples revealed organic and hydrated compounds, indicating the presence of water bound to the minerals [59].

Aside from the substantial technological accomplishment of both Hayabusa missions, they demonstrated how small bodies in the solar system can serve as resource-rich targets, and their potential for supporting long-term missions beyond Earth.

3.3.7 Mars Exploration Rovers (Spirit and Opportunity, 2004-2018)

NASA's twin Mars Exploration Rovers (MER) were delivered to Gusev Crater (Spirit) and Meridiani Planum (Opportunity) in January 2004 to follow the water and reconstruct early Martian environmental conditions. Spirit encountered basaltic plains overprinted by silica-rich opaline deposits , which were interpreted as hydrothermal precipitates. This is direct evidence that hot water once interacted with the crust and could have concentrated economically interesting phases such as silica and sulfates. Opportunity spent more than 14 years traversing an ancient hematite-bearing terrain, and it documented jarosite-rich sulfate sandstones, Fe-Mn nodules and fracture-filling gypsum veins that unambiguously record groundwater circulation. These minerals constrain Mars' aqueous history and provide ground-truth for future ISRU feedstocks (Fe-oxides, sulfates, silica) [60].

By the time dust finally silenced Opportunity in June 2018 the rovers had driven more than 54 km and returned more than 400 000 images plus in situ Mössbauer, APXS and miniTES measurements that remain the baseline mineralogical map for Mars surface-resource assessments [61].

3.3.8 OSIRIS-REx (2016-2023)

OSIRIS-REx is NASA's first asteroid-sample-return mission dedicated to primitive, volatile-rich near-Earth objects [62]. Launched in September 2016, the spacecraft used an Earth-gravity assist in

September 2017 to set up its Bennu rendezvous in December 2018, then executed a year-long global-reconnaissance campaign (PolyCam imaging, OLA/LIDAR and radio science) that produced a 5 cm-resolution shape model and revealed Bennu's unexpectedly boulder-rich, high-porosity "rubble-pile" surface [63, 64, 65]. Those surveys (2018–2019) also mapped ubiquitous hydrated phyllosilicates with embedded water and constrained bulk porosity to 40 wt %, strengthening the case that C-type NEOs carry easily liberated hydrogen and carbon-bearing materials valuable for in-space propellant production. A formal landing-site down-select in December 2019 led to rehearsal descents in April 2020 (Checkpoint) and August 2020 (Matchpoint) and, on 20 Oct 2020, a 6-second TAGSAM touch-and-go that collected 250 g of regolith [66]. The return cruise culminated with the sample return capsule landing in Utah on 24 Sep 2023. Early laboratory analyses of the returned material are already detecting soluble organic species and carbonates that inform early-solar-system volatile budgets and the feedstock quality for asteroid mining [67].

3.4 Current SR-Related Missions

The present decade marks the transition from reconnaissance to practice, as multiple flight programmes now probe, extract, and even prototype the use of local resources in real time.This section reviews five current missions whose instruments and technology demonstrators span cislunar, Martian, and small-body environments, and are laying the operational groundwork for a fully integrated ISRU economy.

3.4.1 Chang'e Programme (2004-present)

China's Chang'e architecture has progressed from global-mapping orbiters (Chang'e-1/2) to precision landers and rovers (Chang'e-3/4) and, most recently, robotic sample return (Chang'e-5 in 2020 and Chang'e-6 in 2024) [68, 69]. These missions have delivered high-resolution spectral, radar, and in-situ data for every major lunar province and returned nearly 2 kilos of pristine regolith to terrestrial laboratories.

The programme's scientific focus is unambiguously resource-oriented; orbital gamma ray spectrometers mapped iron, titanium and potassium bearing basalts; Yutu and Yutu-2 ground penetrating radar sounded regolith to depths of 100 metres, revealing ice-free basalt flows, buried palaeoregoliths[11] and megaregolith[12] structure that control thermal mining economics[13] [70, 71]. Chang'e-5 basalts proved unexpectedly young and volatile-poor, whereas the area mapped by Yutu-2 on the farside contain enhanced iron oxide and crystalline plagioclase, both key feedstocks for molten-salt electrolysis oxygen plants. The upcoming Chang'e-7/8 landers add a multi-spectral drilling station, a water-molecule analyser and an ISRU test bench aimed at sintering bricks from regolith and extracting volatiles at the lunar south pole.

Technologically, Chang'e has demonstrated autonomous ascent, orbital rendezvous, and cislunar sample-return logistics, providing a reusable pathway for bulk cargo from the lunar surface. Together with mantle-derived farside samples, polar volatile prospecting, and on-board ISRU payloads, the programme is laying both the geological knowledge and the flight heritage required for a permanent, resource-powered research station envisioned in the Chinese-led International Lunar Research Base.

[11] Palaeoregoliths are ancient regolith layers that were exposed at the lunar surface long enough to accumulate solar-wind–implanted volatiles and micrometeorite glass, then became entombed beneath later lava flows or ejecta blankets.

[12] The megaregolith is much thicker than Palaeoregoliths, and is a highly fractured crustal layer created by billions of years of large impacts; its blocky, void-rich fabric governs how heat propagates through the subsurface.

[13] The depth, porosity, and thermal conductivity of these buried regolith units determine how efficiently artificial heat can be delivered to release trapped water or other volatiles, and how much energy is lost to the surrounding rock.

3.4.2 Mars Science Laboratory (Curiosity, 2011-present)

NASA's Curiosity rover landed in Gale crater in August 2012 to assess past habitability and to survey materials that could matter for ISRU. In its first Martian year, Curiosity found clear signs that Gale once hosted long-lived standing water, specifically a lake system with water that wasn't strongly acidic or alkaline. The rocks record fine muds that formed in that water and layered soils showing chemical energy gradients that life could have used in the past.

For ISRU-relevant sensing, Curiosity's Dynamic Albedo of Neutrons[14] (DAN) instrument counts neutrons to map near-surface hydrogen, revealing metre-scale patches with up to 6 wt% water-equivalent content in both mudstones and sands—i.e., materials that either hold water in their structure or are mixed with hydrated salts. CheMin, a mini X-ray lab on the rover, identifies mineral types and their abundance, flagging those that lock in water or oxygen-bearing compounds and could be processed to release oxygen or support metal production. The SAM ovens and mass spectrometers have heated samples and detected simple organic molecules and sulphur-bearing gases, indicating accessible carbon and sulphur that could feed future bioregenerative life-support loops.

For ISRU mission planners the take-away is two-fold. First, Gale's mineral-fertile sediments demonstrate that mid-latitude basins harbour both structural water and redox-active phases suitable for oxygen extraction and metal production. Second, DAN's centimetre-deep hydrogen maps provide the first calibration set for orbital neutron detectors, improving resource prediction at scales relevant to landing-site certification and propellant-plant siting .

3.4.3 Mars 2020 (Perseverance) & MOXIE

Landing in Jezero crater on 18 February 2021, Perseverance carries a payload expressly geared toward resource prospection. The onbobard instruments are PIXL micro-XRF for trace metals, SHERLOC deep-UV Raman for organics, RIMFAX ground-penetrating radar for ice lenses, and the first flight ISRU experiment MOXIE. Orbital and rover observations show the crater floor is an olivine-cumulate intruded by aqueously altered igneous rocks; an inventory of carbon, hydrogen and oxygen bearing minerals all highly attractive for propellant and construction feedstocks [72, 73, 74, 75, 76].

MOXIE is a 15 kilo, toaster-sized experiment inside the Perseverance rover that turns the Martian atmosphere into oxygen. It draws ambient carbon dioxide through a HEPA filter and scroll compressor, pressurises it to around 1 bar, and then heats the gas to around 800 Celsius before feeding it into a solid-oxide electrolysis (SOXE) stack made of yttria-stabilised-zirconia. Under an applied voltage, the ceramic conducts O^{2-} ions from the cathode (where carbon dioxide is split) to the anode, where pairs of ions recombine to form oxygen gas and the by-product carbon monoxide is exhausted back to the atmosphere. MOXIE's channels, heaters, and sensors are all governed by a feedback controller designed to hold the temperature and current density within a narrow limit while keeping power below its 300 watt allocation, demonstrating that compact and regenerable electrolysis can survive the Martian diurnal cycle [77, 78, 79].

Since landing, MOXIE has been activated 16 times, covering day and night time operations, four Martian seasons, and a range of atmospheric pressures. During those runs it produced a cumulative 122 grams of more than 98% pure oxygen, peaking at 12 grams per hour (double its design requirement) with stable voltage and minimal cell degradation. An 18 month performance review reports

[14] This spectroscope works by firing neutrons into the ground and measuring the returning *albedo* neutrons to map near-surface hydrogen that represents water-equivalent content in roughly the top 50–60 cm of Martian soil.

that thermal transients shortened start-up times from 120 min to 60 min by the end of the campaign, while purity, flow, and energy efficiency all met or exceeded the thresholds identified for a full-scale propellant plant [80]. Importantly, MOXIE operated successfully during the planet-wide dust storm of Martian Year 36, validating its filter and thermal-management design under worst-case conditions.

These results close a critical technology gap; modelling studies show that a 2 tonne MOXIE-derived plant run for 14 months before crew arrival could deliver the 30 tonnes of liquid oxygen needed for a six-person Mars Ascent Vehicle, reducing Earth-launch mass by approximately 80% compared with pre-supplied oxidiser [81]. The experiment also provides a calibration data set for atmospheric resource forecasting models that couple dust loading, diurnal pressure swings, and compressor work requirements to guide power-system sizing for future missions.

These demonstrations advance Mars ISRU from laboratory to TRL-7; MOXIE proves solid-oxide electrolysis survivability in the diurnal pressure cycle, PIXL and RIMFAX supply feedstock grade control, and the sample caching campaign starts a mineralogical database essential for scaling propellant plants, habitat shielding, and additive-manufacturing feeds.

3.4.4 ExoMars (2022)

ExoMars is an active two-part programme in which the Trace Gas Orbiter (TGO) continues global reconnaissance while the Rosalind Franklin rover mission has been re-phased under a new European landing system. TGO's NOMAD and FREND suites are still delivering the highest-resolution hydrogen maps to date—pinpointing metre-scale ice/hydrate reservoirs and refining present-day water budgets via detections such as HCl and D/H profiles—data that directly feed SR/ISRU site selection and volatile-harvesting models[82, 83].
On the surface segment, the Rosalind Franklin rover and associated flight hardware remain preserved after the 2022 ESA–Roscosmos suspension; the mission retains its 2-m drill, WISDOM ground-penetrating radar, and the nine-instrument Pasteur payload aimed at accessing and characterising subsurface volatiles and organics at Oxia Planum—capabilities that are central to validating extraction scenarios for propellant-grade water and in-situ oxidiser production. A European landing system is in development to deliver this payload, and the overall ExoMars architecture (orbital mapping plus deep drilling) continues to provide operationally relevant inputs for planning near-term resource utilisation campaigns[84, 85, 86].

3.4.5 CLPS (Commercial Lunar Payload Services)

The Commercial lunar payload services is not actually a single mission or programme, but NASA's rapid-acquisition framework that purchases end-to-end delivery to selected lunar locations from U.S. vendors such as Astrobotic, Intuitive Machines, and Firefly. The fixed-price contracts offload lander development while NASA focuses on science and ISRU payloads, enabling more than 2 missions per year at a fraction of traditional costs [87, 88, 89].

The service mission manifest is heavily resource-centred; PRIME-1 (2025) will emplace the TRIDENT one-metre auger and the MSolo mass spectrometer at 80 degrees south latitude to drill, heat, and sniff polar regolith for water vapour, providing the first ground truth on ice concentration versus depth [90]. The follow-on VIPER rover (Griffin lander) will traverse up to 20 km, map hydrogen with a neutron spectrometer, and excavate 1 metre cores at five sites to quantify ice grain size, salt content, and microwave extractability [91, 92]. Additional flights will test regolith-sintering tiles, autonomous prospecting algorithms, and cryogenic propellant tanks.

By commercialising transport, CLPS lowers cadence risk and accelerates technology iteration, with each landing incrementing polar volatiles statistics, maturing drill/heater designs, and rehearsing logistics for Artemis surface systems [93, 94]. In effect, CLPS is building the pre-ISRU supply chain with the validated resource maps and industrial partners needed before megawatt-class oxygen plants can be deployed.

3.4.6 Lunar Reconnaissance Orbiter (LRO, 2009-present)

The Lunar reconnaissance orbiter (LRO) has circled the Moon for over 15 years, providing the baseline geodetic and resource data set that underpins every modern lunar polar prospecting mission. Its LEND instrument produced the first metre-scale hydrogen maps, identifying cold spots with up to 4 wt% water-equivalent hydrogen in permanently shadowed regions (PSR)[95], and complementary Mini-RF S-band radar mosaics revealed decametre-scale dielectric anomalies consistent with buried ice lenses, which demonstrated that not all hydrogen resides in optical PSRs [96].

Lunar Orbiter Laser Altimeter (LOLA) topography, Diviner thermometry, and LAMP far-UV spectroscopy combine to delineate surface temperatures, regolith roughness, and night-side frost signatures, refining models of volatile stability and harvestability [97, 98]. Continuous epithermal neutron monitoring further tracks regolith hydration loss after micrometeoroid impacts, informing volatile retention timescales important to mining economics.

For ISRU strategists LRO remains indispensable, as its decade-long climatology constrains thermal cycling loads on cryogenic storage, its hydrogen maps define high-value mining concessions, and its topography underpins power-beaming and communications line-of-sight analyses. No lunar propellant or construction scenario closes without LRO's geospatial foundation [99].

3.5 Future Role

Looking beyond the present flight campaigns, space resources are set to evolve from optional demonstrators into primary design drivers that dictate how and where humans extend their reach beyond LEO. This section explores this architectural pivot, focusing on the Lunar Gateway and Artemis surface systems to show how ISRU-enabled logistics could reshape power, mass, and risk trades across the entire cis-lunar stack.

3.5.1 Lunar Gateway

The Lunar Gateway is a small, crew-tended station that will follow a 7-day Near-Rectilinear Halo Orbit (NRHO) around the Moon, providing a staging node between cis-lunar space and every point on the lunar surface [100].

From the outset, Gateway is being engineered as a logistics multiplier for ISRU. The 60 kW-class power and propulsion element solar-electric thrusters furnish the ΔV margin to shift the station's argument of perigee, allowing its docking ports to remain in sun-synchronous attitude for kilowatt-level power export and uninterrupted optical comms relays down to polar mining sites [101]. Internal avionics, life-support interfaces, and high-rate Ka-band links have been sized to handle multi-tonne cargo tugs that would ferry oxygen, metal feedstock, or water produced on the surface to orbit for long-term storage or onward transit. Under NASA's logistics-to-propellant analyses, such a depot cuts the total launch mass of an Artemis-class lander campaign by more than 30% because of the reduced ΔV requirements from Earth.

Recent architecture studies extend the concept, with Gateway's exterior pallets capable of hosting ISRU experiments in similar condition to the Lunar surface. Once operational, Gateway will not only serve as a lunar supply depot, but also as a critical infrastructure node in facilitating and ISRU economy [102, 103].

3.5.2 Artemis Program

The Artemis campaign is conceived in escalating blocks. The first is foundational exploration (Artemis I–III) to validate the Orion and SLS transportation stack, and land the first south-polar crews. The second is sustained lunar exploration (Artemis IV–VI) to establish a semi-permanent Base Camp supplied through Gateway, and the third is a transition to Mars in the early-2030s that leverages that cis-lunar supply chain to stage crewed Mars vehicles [104, 103].

From its first trade studies, Artemis has treated ISRU as a core sub-architecture. NASA's ISRU plan sets two guiding rules; to start with the easiest resources to mine and focus early efforts on the south-polar volatiles that most reduce launch mass [105]. The result is the two-site concept in which excavators harvest ice inside a permanently shadowed crater and haul water a few kilometres to a sun-lit propellant production plant that electrolyses, liquefies, and stores hydrolox for landers and life-support systems [106]. Site-selection studies show several Shackleton-rim and Nobile-basin scenarios already meet the 5 km distance and less than 20 degree slope rules needed for early operations, with a 1 km ice patch able to sustain hundreds of ten-tonne oxygen production cycles [107]. Embedding that ISRU chain into the campaign architecture promises a step-change in logistics: polar propellant can cut the Earth-launch mass of a surface sortie by roughly one-third and positions Gateway to evolve into an orbital depot during the foundational exploration segment [108]. As production scales toward hundreds of tonnes per year, ISRU also supplies construction feedstocks and radiation shielding for the Base Camp, seeding the commercial markets that Artemis is counting on to make a permanent human lunar presence affordable and resilient.

4 ISRU State of the Art

ISRU technologies were once considered speculative, but have now progressed to the point where they define not only what is possible in planetary exploration, but also what is economically and environmentally viable. This section provides an overview of the current state of ISRU research and its implementation, focusing on the techniques, proven performance, and challenges associated with extracting resources from the Lunar and Martian environments [109].

4.1 Lunar ISRU Techniques

The Moon differs significantly from either Earth or Mars, for all practical purposes it has no atmosphere, its surface gravity is approximately one sixth Earth's, and its surface undergoes extreme diurnal temperature fluctuations. The techniques required to survive and thrive on its surface are considerably different to those currently used in space exploration. For starters, the absence of an atmosphere means lunar equipment must shed heat by radiation alone, and that thermal gradients of more than 300 kelvin exists between sun-lit and shadowed regions. The same vacuum permits clean high-temperature processing without oxidation, a major advantage for pyrometallurgical ISRU systems. Lunar gravity lowers bearing loads but calls for augers and bucket wheels that can bite into loosely consolidated regolith without relying on weight.

4.1.1 Oxygen Extraction

The value of oxygen extracted from lunar resources is immediately apparent. Not only is is a neccesary consumable for human life support, but its role as a majority component in hydrolox means it is indispensable as a facilitator of sustainable access to the lunar surface from cislunar space.

Electrolytic reduction works by separating the oxygen bound to metal elements in lunar regolith, freeing elemental oxygen and allowing us to obtain metals as a byproduct. As a process, the electrodeoxidation of metals and metal oxides using the Fray Farthing Chen[15] (FFC) method is already at TRL9, and used commercially by Metalysis to produce metals at a range of grades. The applicability of molten salt electrolysis on lunar regolith as a means of oxygen extraction has already been demonstrated, with Lomax et. al. successfully producing oxygen from Apollo samples. Ongoing optimisation at ESTEC targets continuous anode architectures and gas-tight cell designs aimed at raising the lunar-specific TRL from 4-5 to an operational prototype.

Vacuum thermal decomposition, also termed vacuum pyrolysis, uses direct heating of raw regolith under the ambient lunar vacuum to dissociate oxides into oxygen and sub-oxides. Because only thermal energy is required, the method couples naturally to concentrated solar furnaces or resistive heaters. Thermodynamic modelling shows that peak oxygen release occurs between 2000–2500 Celsius, with theoretical recoveries of 15–20 wt % from typical highland regolith [110, 111]. However, there are still significant challenges to reach TRL 9, particularly maintaining the high-temperature vacuum seal and continuously removing both oxygen gas and metallic vapours to avoid re-oxidation.

Hydrogen reduciton of ilmenite ($FeTiO_3$) enriched in the lunar maria offers the highest oxygen yield per unit mass of any single mineral (approximately 30 wt %). In hydrogen reduction, regolith is heated to 900–1050 Celsius in a flow of hydrogen and liberated water vapour is then electrolysed,

[15]The FFC process is a molten-salt electrodeoxygenation in which a solid metal-oxide cathode is immersed in $CaCl_2$ at $\sim 900\,^{\circ}C$ and, under an applied potential, its O^{2-} ions migrate into the electrolyte and are discharged at a carbon anode as CO/CO_2, leaving metallic powder or a consolidated part. This provides a direct, energy-efficient conversion of oxides to metal.

recycling the hydrogen and delivering pure oxygen. Laboratory and analogue tests have demonstrated conversions of 5–10% per pass, and ESA's PROSPECT/ProSPA package will flight-test the reaction on the south-pole lander [112, 113]. The process benefits from moderate temperatures but requires imported H_2 or an upstream lunar source and pre-beneficiation to raise ilmenite concentration.

Carbothermal reduction treats bulk regolith with carbon monoxide or methane at 1600–1800 Celsius, forming CO_2 (or $CO/H_2/H_2O$ mixtures) that are subsequently electrolysed [114]. Recent numerical and bench-scale work confirms oxygen recoveries above 50% with methane recycling and shows compatibility with vacuum furnaces and rotary kilns [115]. Although energetically intensive, the technique co-produces silicon-rich metal alloy feedstock useful for in-situ construction and electronics [116].

4.1.2 Water Replenishment

Like elemental oxygen, the benefits of being able to produce water in-situ are clear. Given a sufficiently large and sustainable water source, oxygen extraction from regolith becomes moot. However, the presence of water, its accessibility, and its volume all remain unclear.

For regions where volatiles occur as macroscopic ice grains mixed with regolith (most likely at high-latitude PSRs where ice concentrations may reach 10–30 wt%) simple heating is the simplest option. Temperatures just above 0 Celsius suffice for loose icy soil, whereas hydration locked inside mineral lattices can require more than 150 Celsius. Engineering concepts range from static hot-box kilns to mobile heaters and large heliostats or Fresnel mirrors that beam concentrated sunlight onto PSR floors [117]. Recent modelling shows that a 5 metre diameter mirror operated at Shackleton crater could sublime around 40 kilos per hour of water vapour from a 15 wt% ice deposit, which is then captured on cold traps cooled by the ambient environment [1]. The approach avoids imported reactants but must contend with deep-crater logistics, cryogenic dust, and the need for continuous vapour capture to prevent re-condensation.

Microwave or radio-frequency heating volumetrically couples energy into icy regolith which allows sub-surface desorption without large area excavations. Lab work with LHS-1 and icy simulants has demonstrated more than 80 % water release at less than 300 watt per kilo specific power, with condensate collected on chilled fingers [118, 119]. Integrated drill-and-microwave heads are scheduled to fly on PRIME-1/TRIDENT under NASA's CLPS programme in 2025, providing the first in situ validation of the technique at depths down to 1 metre under the surface [120]. However, there are key uncertainties are power scalability under PSR illumination constraints and the electromagnetic behaviour of regolith and ice mixtures.

Outside the polar cold-traps, bulk water ice is scarce. However, the titanium rich mare basalts contain ilmenite that reacts with hydrogen gas at 900–1050 Celsius to form metallic iron and water vapour [121]. Because hydrogen can be recycled by electrolysis of the produced water, only makeup H_2 (or methane/CO) is required. Experimental yields correspond to about 9 tonnes of H_2O per 76 tonnes of processed ilmenite, and recent lab tests report more than 50 kilos of H_2O per tonne of regolith when reaction temperatures exceed 1200 Kelvin [122]. The process shares reactors, heaters and gas-separation hardware with carbothermal oxygen production from subsubsection 4.1.1, but its economics depend on hydrogen logistics, namely imported cryogenic H_2 and electrolysed polar water or solar-wind hydrogen harvested from regolith fines.

4.1.3 Silicon and Metal refining

Early NASA studies proposed heating regolith in the presence of fluorine salts so that fluorine displaces oxygen in the silicates and volatilises silicon as silicon tetrafluoride (SiF_4) gas, and the metal fluorides remain in the residue. SiF_4 can then be condensed and reduced by hydrogen, magnesium or plasma methods to yield high-purity silicon, while fluorine is recycled via electrolysis of the spent salts [123]. Mass balances from that same study indicate that approximately 1 kilo of fluorine could process more than 50 kilos of regolith [124]. The approach operates at relatively low temperatures (750–900 °C) compared to other ISRU processes and cleanly separates silicon from iron-group metals, but it introduces a hazardous halogen loop and demands fluorine-compatible reactors.

Beyond oxygen liberation, the same FFC molten-salt electrolysis process described in subsubsection 4.1.1 can also yield a silicon-rich metal sponge at the cathode. Once the anodic oxygen evolution rate stabilises, continued electrolysis progressively reduces the residual iron, aluminium, and titanium silicates so that elemental silicon, iron, aluminium and titanium precipitate as a porous alloy. Metalysis has already industrialised the process on terrestrial oxides to produce high-purity Ti and Al powders for additive manufacturing [125]. Laboratory campaigns with JSC-1A simulant and Apollo 16 samples have replicated this behaviour in a lunar context, delivering cathode products containing more than 45 wt% silicon while maintaining oxygen release at the anode [126, 127]. ESA's work demonstrated continuous operation of such cells with approximately 30 grams per hour of O_2, confirming that the co-produced alloy can be separated by vacuum distillation and selective leaching without degrading the molten salt electrolyte. The current work at ESTEC views FFC as a dual-output refinery, where oxygen is vented from the anode and silicon and metals are harvested from the cathode.

At higher temperatures (around 1550 to 1700 Celsius) the regolith can be melted directly to form its own conductive oxide bath. Electrolysis then releases oxygen at the anode and precipitates a silicide/metal alloy layer at the cathode. NASA's Molten Regolith Electrolysis test beds have demonstrated oxygen yields of 750 $g.m^{-2}.h^{-1}$ and continuous operation for over 100 hours with no consumable reagents [128]. This technology eliminates molten salt logistics but must the scaling of megawatt-class power supplies.

As with oxygen production in subsubsection 4.1.1, injecting carbon monoxide or methane into molten regolith at 1600 to 1800 Celsius reduces metal oxides to an Fe-Si alloy while generating CO_2 (or CO/H_2) that can be re-electrolysed. Laboratory crucible tests have achieved more than 60% metallisation of silicon within two hours [129].

4.2 Mars ISRU Techniques

The Martian environment provides three principal resource reservoirs: its CO_2-rich atmosphere, extensive shallow ground-ice deposits, and a globally basaltic regolith. ISRU research therefore clusters around atmospheric processing, water acquisition, and regolith conversion, each with a different technical maturity [130, 131].

4.2.1 Atmospheric Processing

Solid-oxide electrolysis has advanced furthest, driven by MOXIE (recall subsubsection 3.4.3) aboard NASA's Perseverance rover. MOXIE draws ambient CO_2, compresses and heats it to approximately 800 Celsius in a yttria-stabilised-zirconia cell where it is split into O_2 and CO. In its first campaign the instrument produced 6 grams per hour of 99.6%-pure oxygen, meeting its design target and validating closed-loop control under fluctuating Martian diurnal pressures[132, 79]. Subsequent runs have

confirmed stable operation over more than 15 thermal cycles, demonstrating TRL 7 for kilo-per-day oxygen generators.

For ascent-vehicle propellant oxygen must be paired with a locally synthesised fuel, with the current reference route being the Sabatier/RWGS sequence [133]. Atmospheric CO_2 is first reacted with imported (or electrolysed) H_2 over Ru-Al_2O_3 catalysts at 350 Celsius to form CH_4 and H_2O. The water is electrolysed, recycling hydrogen, while the methane is liquefied together with the oxygen stock. Laboratory reactors at NASA-SSI and JSC have achieved methane throughputs of 2.5 kilos per hour with 95% carbon utilisation[134, 135], and integrated tests have logged more than 1000 hours without measurable catalyst deactivation[136]. Scaled up studies for the Mars Design Reference Architecture (DRA 5.0) show that a 30 tonne O_2/ 7 tonne methane plant requires approximately 170 kW of electrical power sustained for 480 sol, placing the system at TRL 5 [137].

Alternatives under exploration include CO/O_2 bipropellant production by high-temperature electrolysis (bypassing methane synthesis) and plasma dissociation of CO_2 to CO + O_2 at lower thermal loads; both remain at laboratory TRL 3–4.

4.2.2 Water Acquisition and Processing

Neutron, radar, and thermal-inertia data from Mars Odyssey, SHARAD and MRO suggest that more than 100,000 km^3 of water ice lies within the top five metres at mid-latitudes, with local volumetric fractions exceeding 60% [138, 139]. Engineering concepts for extraction bifurcate into mechanical mining and sub-surface heating.

Radar and neutron spectrometry supported by impact crater observations and thermal emission measurements confirm widespread shallow subsurface ice across Mars' mid latitudes. Ice depths can be as shallow as less than a metre and thicknesses can exceed 100 metres, with volumetric fractions of excess ice significantly above regolith porosity, reaching more than 60% in some locations such as Arcadia Planitia and Milankovič Crater [140, 141]. Engineering approaches to exploit this resource bifurcate into mechanical excavation and thermal in situ mining.

Mechanical extraction draws from polar and permafrost mining analogues. Drilling campaigns such as Icebreaker have achieved 1 metre penetration in an hour with less than 100 Watts of power and less than 100 Newtons weight-on-bit, acquiring frozen samples in approximately 10 centimetre increments without inducing phase changes [141]. Designs based on rotary-percussive or auger mechanisms have demonstrated viability for deployment in Mars analogue environments and Mars simulation chambers [141, 142]. Material conveyance remains a critical link, with cryogenic belts and bucket-chains showing they can keep ice below -40 Celsius during transfer, minimising sublimation and preserving sample integrity [143].

In contrast, in-situ thermal mining avoids excavation by delivering heat directly through conductive rods inserted into the exposed ice. This method sublimates the ice allowing water vapour to be collected via condensation traps or vacuum pumps. Models show that single-rod configurations can sustain sublimation for low-demand operations while high-throughput designs require multi-rod arrays with total power inputs approaching several hundred watts per kilogram of ice released [140]. Sublimation rates depend strongly on rod geometry and the purity of the ice.

Both strategies ultimately aim to feed electrolysis systems for hydrogen and oxygen production. Technologies derived from proton-exchange membrane electrolysers (initially used in life-support systems)

have demonstrated 2 kilo per hour throughput at approximately 3.5 kWh per kilo specific energy input [144]. The combination of subsurface access, thermal control, and regolith-handling reliability forms the primary engineering barrier to scalable Martian water ISRU.

4.3 Technology Gaps

The development of ISRU capabilities for the Moon and Mars has progressed rapidly in recent years, yet significant technology gaps still remain before these methods can be deployed at the scale required to support human missions. In particular, there are key gaps in the fields of oxygen and fuel production, water acquisition, and metal refining, as well as issues regarding the integration of these techniques into autonomous resource processing systems.

4.3.1 High-throughput Oxygen Plants

Laboratory campaigns of molten-salt and molten-regolith electrolysis now release tens of grams of O per hour and have run continuously for up to 100 hours, lifting the generic technology to TRL 4–5. The decisive gap is scaling those bench cells to the multi-kilowatt, multi-month reactors that a surface propellant plant demands. Doing so entails (i) materials handling of abrasive, electrically conductive melts at 1600–1700 Celsius, (ii) thermal management in a vacuum where convective cooling is absent, (iii) mitigation of electrode corrosion over millions of ampere-hours and (iv) fully autonomous control to accommodate duty-cycle interruptions such as the 354-hour lunar night or the seasonal pressure swings on Mars. The first partial closure of this gap came only in 2024, when a NASA and Lunar Resources prototype extracted O_2 from 25 kilos of simulant inside a large vacuum chamber—roughly an order of magnitude up-mass on prior trials and the first test under a mission-like environment [145]. Although heralded as commercial-scale, the run length was still less than 8 h and no study yet couples such reactors to an in-situ power system or to continuous product storage.

The MOXIE experiment (subsubsection 3.4.3) elevated solid-oxide electrolysis to TRL 7, yet its 6–10 gram per hour output would have to rise by two orders of magnitude to prefuel a Mars Ascent Vehicle. Analyses of a full-scale MOXIE indicate electrical loads of approximately 25 kiloWatts and coolant rejection of comparable magnitude for about 500 sols to accumulate 30 tonnes of O_2 [146]. The open engineering items are therefore compressor reliability in dust-laden CO_2, thermo-mechanical cycling of the solid-oxide stacks over diurnal swings, and integration of high-power electronics into a martian thermal-vacuum environment—all over multi-year lifetimes without maintenance.

4.3.2 Methane and Complete Propellant Loops

Sabatier reactors with Ru-Al_2O_3 catalysts have already logged more than 1000 hours in Earth testbeds at conversion efficiencies over 95%, but no system has yet operated on Mars. The gap is thus less in chemistry than in the end-to-end loop: collecting and compressing more than 30 tonnes of CO_2, importing or recycling about 8 tonnes of H_2, electrolysing and liquefying both product streams, and storing cryogens through a martian winter night. Design reference studies suggest approximately 170 kW continuous power for a 30 tonne O_2 / 7 tonne CH_4 plant [147], making power generation, radiator sizing and autonomous fault-management the critical unknowns.

4.3.3 Water Acquisition

Hydrogen reduction of ilmenite, microwave sublimation of polar ice, and regolith auger-sampling each mature to different TRLs under Earth conditions, yet no method has proven it can deliver the hundreds of kilos per day that a fuel-grade electrolyser demands. In particular, resource heterogeneity (lateral

and vertical variations in ice fraction or ilmenite grade) remains poorly mapped below the metre scale and directly affects plant sizing and economics [148]. Demonstrations such as PRIME-1 and VIPER will constrain the variability, but until continuous excavation, transfer, and beneficiation are shown in low gravity (1/6-g for Lunar or 3/8-g for Martian systems), mining remains the dominant risk driver for water-derived propellant architectures.

5 Mission Architectures

What does the choice of mission architecture really buy us in ΔV, cost, and CO_2, and how does ISRU change the answer?

A mission architecture is the ordered set of launches, orbital rendezvous, propellant and consumables transfers, and supporting operations needed to execute a mission. Each architectural choice fixes the sequence of propulsion events, and thus the total ΔV requirements. Through subsection 1.1 and Equation 1 it is evident that an increase in ΔV exponentiates the propellant mass, driving both launch cost and the CO_2 emitted. Here we describe five progressively ISRU-reliant categories of mission architecture, and show how they differ in logistic assumptions, how they govern vehicle sizing, and how they lay the groundwork for subsequent mission-design analyses.

5.1 Single Launch

The single-launch model places every element, from the crew, lander, return stage, and consumables on the same booster. Its pedigree runs from Luna 16 through Apollo 11, whose 2.9×10^6 kg Saturn V delivered the entire trans-Earth stack in one launch. Operational simplicity is offset by demanding performance: closing the ΔV budget in one burn drives the initial mass-to-payload ratio above 23 for lunar sorties, which in turn inflates propellant production energy and CO_2 release [149]. No ISRU is possible, because nothing remains on the surface long enough to harvest local volatiles, and every gram of propellant, life-support consumable, and structure originates in Earth's industrial base. This architecture serves as a high-carbon and high-cost reference point..

5.2 Multiple Launches

Multi-launch concepts break the "all-up" stack into smaller pieces that assemble by docking, either in LEO, at the destination, or as sequential staged flights. NASA's Artemis Phase 1 profile dispatches SLS with Orion while a commercial lander and logistics module depart on separate boosters before rendezvous at Gateway in NRHO [150]. Distributing mass reduces peak booster thrust, but the propellant driving every rendezvous still comes from Earth. ISRU is absent from the baseline design, although the architecture is ISRU-ready, as once surface propellant becomes available, the lander segment alone can be redesigned without altering the LEO assembly chain. Carbon cost scales with the number of launches, but each leg remains energetically identical to single-launch equivalents, so the absolute CO_2 per delivered tonne falls only modestly.

5.3 In-Space Depots

Propellant depots add cryogenic storage nodes, typically LH_2/LOX or CH_4/LOX tanks, at energetically useful way-points such as LEO or in NRHO. A frequently cited design is the "Simple, Robust Cryogenic Propellant Depot" demonstrator, conceived to store Centaur-derived propellant for up to a year and enable modular scaling to Mars-class missions [151, 152]. Depots decouple launches from departure windows and reduce the ΔV carried on any single stage, improving dry:wet ratios. In their pure form the storage nodes are still fed by Earth launches, so ISRU is optional. Nevertheless, standardising fluid-transfer interfaces and boil-off management makes later insertion of lunar-sourced LOX straightforward.

5.4 ISRU-Assisted

Here the mission plan assumes at least one propellant constituent is produced off-world. The MOXIE has already electrolysed Martian CO_2 into 6 $g.h^{-1}$ of O_2, proving the chemistry at planetary scale

subsubsection 3.4.3. Lunar concepts adopt the same principle: land a tanker with only CH_4, extract oxygen from regolith, and back-haul LOX to an orbiting depot, cutting Earth-launch mass by 40 % in some trade studies [153]. Because only part of the propellant stream is indigenous, launch cadence remains non-zero, yet life-cycle CO_2 per delivered tonne falls steeply once the surface plant mass is amortised Part II.

5.5 Full ISRU

A full ISRU architecture treats the destination as a self-supplied industrial estate, with power generation, volatile extraction, and high-temperature metallurgy run side-by-side so that propellant, structural metals, life-support consumables, and eventually export goods are all produced locally. Because outbound vehicles depart with empty tanks and return with marketable cargo, the classic exponential link between ΔV and Earth-launched mass collapses to a far slower, roughly linear growth with surface-plant throughput. A lunar implementation couples two resource streams. At the poles, water-ice mined from permanently shadowed craters is cracked into LH_2/LOX and stored cryogenically; in sunlit highlands the molten-salt electrolysis produces oxygen and metals. Linking these plants to a reusable lunar shuttle cuts the surface-to-NRHO gear-ratio to about 2:1, where two tonnes of propellant are produced for every tonne delivered in orbit.

6 Impacts of Mission Architecture Choices

The impact of which mission architecture is chosen is not limited to the flight vehicle, but cascades through every layer of the programme, from the factory floor to the astronaut's risk envelope and the economics of an emerging cislunar market.

First, architecture fixes the shape of the terrestrial industrial base that must exist before each launch campaign. A single-launch calls for one surge-capacity booster line and a narrowly timed materials flow, whereas a depot or ISRU-centred campaign drives demand for cryogenic-tank fabrication, autonomous transfer valves, surface robotics, and multi-megawatt power plants. A NASA supply-chain study showed that as much as 70–80 % of recurring operations cost are locked in during this early design phase, and that disciplined supply-chain management can cut total life-cycle expenditure by a third; savings that no vehicle-level optimisation can recover later [154]. Furthermore, a 2023 sustainability review came to the same conclusion: risk, cost, and carbon are co-determined by the agility of the upstream supply chain, not by launcher performance alone [155].

Second, the choice of architecture alters the operational logistics on Earth. Multi-launch rendezvous increases launch pad operations, number of propellant-handling events, and range conflicts. On the Shuttle programme every additional hypergolic-servicing task required bespoke safety procedures and elongated the critical path [156]. Orbital depot architectures relocate part of that logistic load to orbit, but substitute long-duration cryogenic storage. Recent analyses list boil-off control and autonomous tank-to-tank transfer as the dominant power draws and mass drivers in the ground segment that builds and checks those systems [157]. Full-ISRU concepts invert the picture again, pushing the heavy industrial plant and its electrical burden onto the lunar surface. NASA's 2022 ISRU roadmap projects commodity flows of hundreds to thousands of tonnes per year each traceable to surface power and mining throughput rather than launch rate [158].

Third, architecture is inseparable from human-rating and safety. Every new interface, from docking port to propellant lines and surface processing adds failure modes that must be closed by redundancy or abort capability under human-rating standards [159, 160]. Historical system safety work on in-space propellant logistics shows that transfer operations in LEO introduce hazards equivalent to a second launch phase, with cryogenic line rupture and residual propellant ignition topping the risk matrix [161]. Interestingly, architectures that shorten crewed mission phases, possibly by sending landers up dry to be fuelled robotically, can reduce exposure time and thus risk even if they add uncrewed flights.

Finally, as we see in Part II, architecture dictates the macroeconomic and environmental footprint. A 2019 collaborative study finds that meeting a near-term demand of 450 tonnes of propellant per year in cis-lunar space favours a commercial ice-mining operation processing 2,450 tonnes of lunar water, with break-even capital in the billion dollar range and a dramatic cut in Earth-launch mass [162]. Yet that benefit materialises only after the surface power plant grows beyond the megawatt scale, reframing carbon accounting from rocket exhaust to lunar energy generation. In single launch or multi launch architectures the dominant emissions source remains terrestrial propellant production, and in depot-based architectures it shifts to boil-off and refrigeration losses. Thus, choosing an architecture is equivalent to choosing where industry, risk, jobs, and emissions will be.

Part II
The Impact of ISRU on our Carbon Footprint

7 Methodology

The following section serves to outline the general methodology employed throughout the study. Methods that are model or vehicle specific are not covered here, but in their respective sections.

7.1 Δv road map

The following road map was built to organise the logistics of transferring from various orbits. All manoeuvres are assumed impulsive, and unless otherwise specified, orbital velocities and Δv's are calculated using Keplerian mechanics. For the transitions between LEO and Weak Stability Boundary (WSB) orbits, and between WSB and Near Rectilinear Halo Orbits (NRHO), Figure 2 uses data from several internal ESA mission analyses and from theoretically-ideal Hohmann transfers to orbit from the lunar surface to LLO [163, 164]. This was done as both WSB and NRHO are non-Keplerian n-body problems. The ability to arrive in NRHO via WSB is included as pathway that requires less ΔV at the expense of taking approximately 30-60 times longer [165]. As such, it is not implemented for any crewed missions, but explored as a supplementary orbit for non-time-critical transitions into cislunar space.

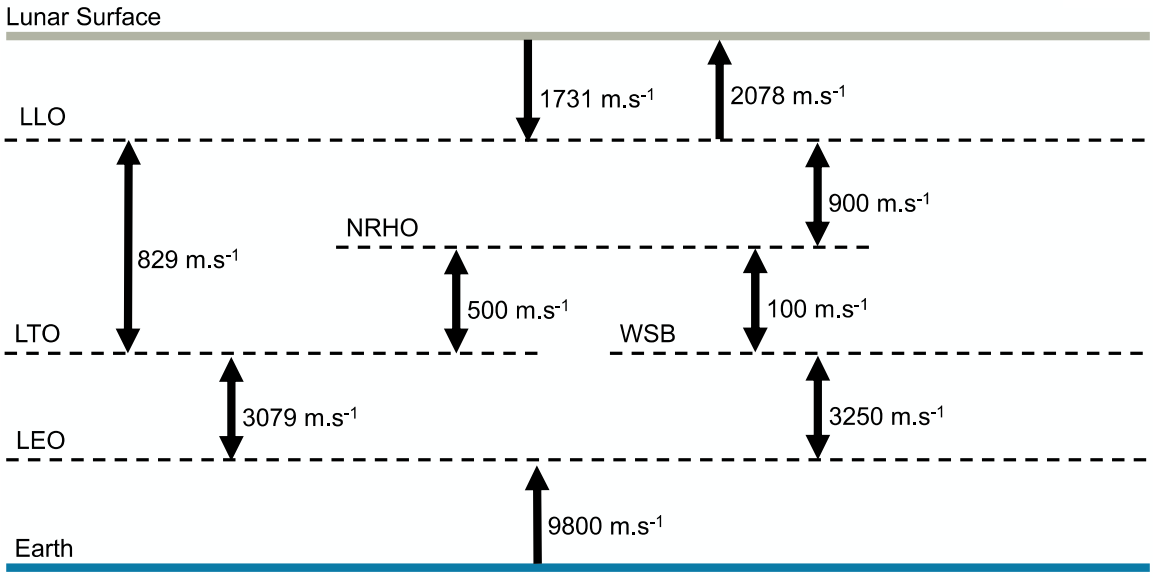

Figure 2: Δv map of cislunar space

For Mars descent using aerodynamic deceleration techniques (for example with a combination of inflatable heat shields, ballutes, drogue chutes, parachutes, etc.), and indicative Δv of 0.5-0.8 km/s^{-1} is used [166]. This value can change depending on the ballistic coefficient of the entry vehicle, and so the value for Mars descent/landing was taken as the upper limit of 0.8 km/s^{-1}. The Δv values for each upcoming transfer window are available in Appendix B. The ascent Δv can change slightly based on the ascent profile and target altitude for low Mars orbit (LMO). Here, an altitude of 400 km was used and the Δv taken as 4.1 km/s^{-1}; the same as the proposed Hercules reusable Mars lander [166]. The various Δv values for the transits between Earth and Mars are sown in Figure 3.

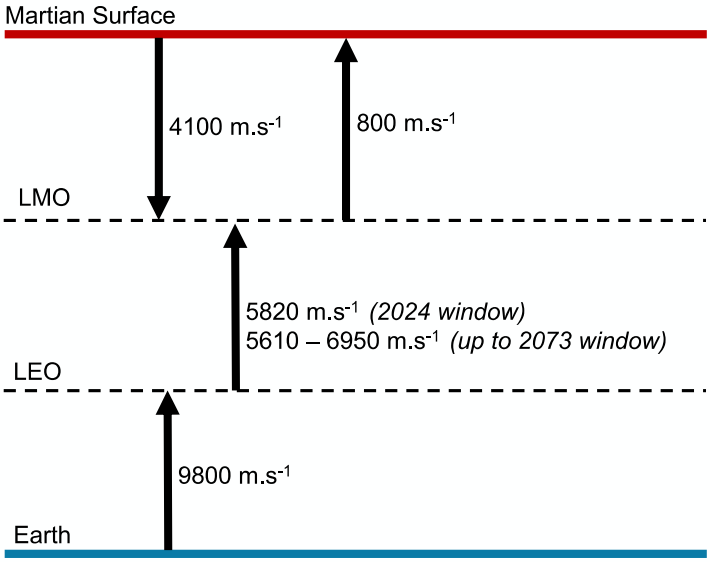

Figure 3: Δv map of Earth-Mars transfers

7.2 CO2 Sources

To calculate estimates of the CO2 emissions of each type of mission architecture we must limit ourselves to an incomplete, but sufficiently accurate, set of CO2 emissions sources. Within the scope of comparing different mission architectures we limit ourselves to three main sources for the carbon footprint. We make a key assumption that these three are the main contributors to the carbon footprint of a space mission, and that additional factors ranging from the construction down to the daily commutes of workers involved can be omitted, either because they occur regardless of the mission architecture, or because their overall contribution is expected to be several orders of magnitude lower that the principle contributors.

7.2.1 Materials of Construction (MoC)

The additional assumption was made that the entire mass of the vehicle was composed of the same material. The MoC for each vehicle and the calculation used to obtain a value of kgCO2/kg are outlined in the respective sections. Two different materials were considered as the MoC for launch vehicles (and subsequently also for spacecraft, tugs, and any additional mission infrastructure required); an Aluminium-Lithium alloy and Stainless steel.

Details regarding the carbon emissions of AlLi2195 production are scarce, and so a breakdown was performed such that a weighted sum of the individual carbon emissions of its components could be calculated to then obtain an estimate of the alloy's overall emissions value. This is outlined in Table 1. As previously stated, the conversion of the alloy from feed stock to final vehicle is not considered in the carbon emissions calculation.

The CO2 emissions of stainless steel can be split into 3 scopes. Scope 1 encompasses industry-direct emissions, such as from business-owned sources. Scope 2 encompasses indirect emissions, such as from the generation on purchased power. Scope 3 encompasses emissions associated with the supply chain for materials used in the production of stainless steel. The carbon footprint of stainless steel production also varies depending on the amount of scrap utilised, with scope 3 emissions ranging from 2.08 kgCO2/kg for 85% scrap to 6.82 kgCO2/kg for 30% scrap. The most common range for recycled

Table 1: AlLi2195 material breakdown

Material	Composition				
AlLi2195	Element	Al	Li	Cu	Mg
	Mass Fraction [167]	0.945	0.010	0.040	0.005
	kgCO2/kg	6.8 [168]	15 [169]	4.1 [170]	21.8 [171]
	Overall kgCO2/kg	6.853			

content in stainless steel production is between 50-85% scrap, allowing us to make an estimate of around 2.50 kgCO2/kg for the scope 3 carbon emissions of stainless steel production [172]. Scope 1 and scope 2 kgCO2/kg emissions are 0.38 and 0.45 respectively, giving a summed carbon emissions value for stainless steel production of 3.33 kgCO2/kg.

7.2.2 Propellant Production

Depending on the type of propellant mix used, the kgCO2/kg will vary. This is not only a factor of propellant mix ratio but also of the industrial plant used to produce the propellant. Within this study we consider two propellant mixes; Methalox (liquid oxygen and methane) and Cryogenic (liquid oxygen and liquid hydrogen). In order to calculate the carbon emissions of propellant production, first the propellant types were identified, then the emissions of each component calculated. To this end, different industrial plants were identified, and the kgCO2/kg product calculated using the formula

$$Carbon\ Emissions = Specific\ Energy \cdot\ Grid\ Carbon\ Intensity \tag{3}$$

$$\left[\frac{kgCO2}{kg}\right] = \left[\frac{kWh}{kg}\right] \cdot \left[\frac{kgCO2}{kWh}\right]$$

We can then look at publicly available data sheets for industrial plants to obtain the neccesary values. The calculated carbon emission values for the components of rocket propellant are listed in Table 2. We can then combine this data with the known propellant mix ratios, to obtain a total emissions value per propellant type (Table 3).

Table 2: Propellant component specific carbon emissions

Product	Plant	Specific energy [kWh/kg]	Grid Carbon Intensity [kgCO2/kWh]	Specific Carbon Emissions [kgCO2/kg]
LOX	Yango™– Standard Air Separation Unit [173]	0.4-0.6 [173]	0.25 [174]	0.125
LH2	Air Liquide Hydrogen Liquefier [173]	7.0 [173]	0.25 [174]	1.750
CH4	Smartfin™ (Single Mixed Refrigerant Cycle) [173]	0.35 [173]	0.25 [174]	0.0875

Table 3: Final propellant specific carbon emissions

Propellant type	Mix Ratio	Specific Carbon Emissions [kgCO2/kg]		
		fuel	*oxidiser*	*overall*
Cryogenic	6	1.75	0.125	0.357
Methalox	3.6	0.0875	0.125	0.117

7.2.3 Propellant Combustion

For existing launchers there exist already comprehensive calculations regarding the emissions from rocket launches [175]. However, this data was not available for all the launch vehicles used within

the concept of operations selected for comparison, so instead the nozzle exit mass fraction data was used to calculate the quantity of CO2 emitted per launch. Clearly different types of rocket engines operate at different design points, so it is expected that each have their own set of nozzle exit species mass fractions. Of the three launch vehicles under consideration for the various mission architectures (New Glenn, Superheavy, and SLS) only SLS has performed a successful launch to orbit. Nonetheless we can perform an initial estimate of the carbon emissions per launch for those not yet operational.

Given the lack of public information regarding the New Glenn launch vehicle being developed by Blue Origin, an estimate of the expected propellant mass was obtained via supplementary calculations. Knowing that the mass flow of a rocket engine can be expressed as

$$\dot{m} = \frac{F}{Isp \cdot g_0} \tag{4}$$

we can obtain an initial estimate of the total mass flow of the launch vehicle. Current specifications state a first stage thrust of 1.71×10^4 kN supplied over 7 engines. Each BE-4 engine produces approximately 2.442×10^3 kN of thrust and has an estimated[16] Isp of 315 s [176]. Given the proposed ascent profile [177], the lower density of methane *w.r.t.* RP-1, and comparison with similar engines, the Isp was lowered to 300 s for a more conservative estimate. This gives a mass flow per engine of 829.7 kg.s^{-1}. For seven engines, and a main engine cut off (MECO) of 198 seconds [177], we obtain a total propellant mass for New Glenn's first stage (NGS1) of just shy of 1150 tonnes. Calculations for New Glenn's second stage (NGS2) and for the Blue Moon lander are outlined in subsection 9.1. Their propellant combustion will not have an impact on emissions given the altitude at which they operate.

Table 4: Launch vehicle carbon emissions

Vehicle	Propellant Mass [tonnes]	CO2 nozzle exit mass fraction	CO2/launch [tonnes]
Superheavy	4,600 [178]	0.4118 [179]	1,894
New Glenn	1,150	0.3820 [176]	439.3
SLS	-	-	538 [180]

7.3 Solving Algorithms

The dependency of the propellant mass on the payload mass, which itself is dependant on the maximum wet mass limit minus the varying propellant mass results in a recursive equation. An iterative calculation method was developed that permits the solver to converge on a solution that results in the maximum deliverable payload per manoeuvre. Here we will outline two solving algorithms, both of which employ a creeping methodology to converge by iteratively modifying parameters. Depending on the mission architecture, a combination of both algorithms is used.

7.3.1 Single Manoeuvre

The single-manoeuvre scenario is used when maximising payload mass for a given vehicle with a given desired Δv and fixed maximum wet mass and dry structural mass. This process (Figure 4) is said to have converged when the available mass value is sufficiently small (< 0.001).

7.3.2 Multiple Manoeuvres

The multiple-manoeuvre scenario is identical to the first, but with the addition of required payload masses per iteration that represent the propellant mass required for subsequent manoeuvres. These

[16] Based on simulations by Rocket Propulsion Analysis and estimated engine parameters

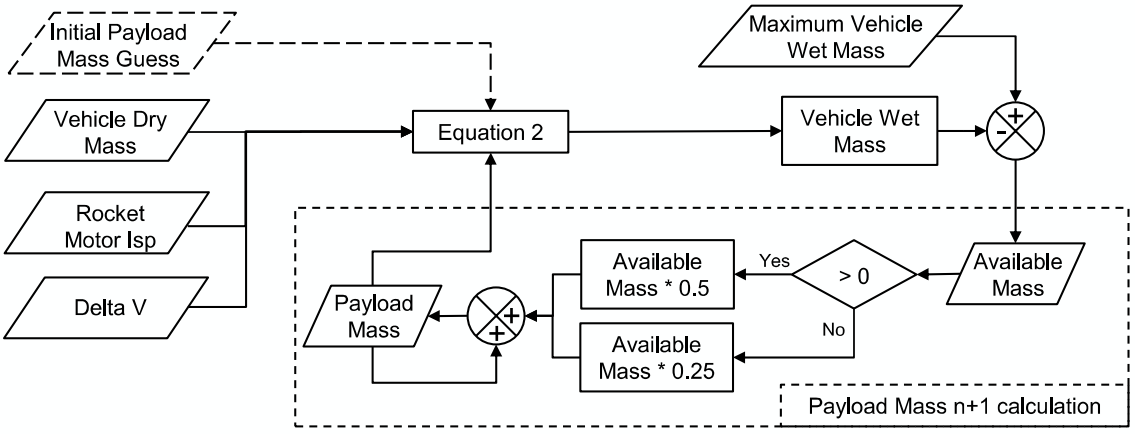

Figure 4: Single Manoeuvre solving algorithm

can be stacked where neccesary, and required propellant payload mass per manoeuvre can be modified to account for ISRU capabilities in different locations of the operational chain. The algorithm process for a three-manoeuvre event timeline is depicted in Figure 5. As for the single manoeuvre algorithm, the process is said to have converged when the available mass value is sufficiently small (< 0.001).

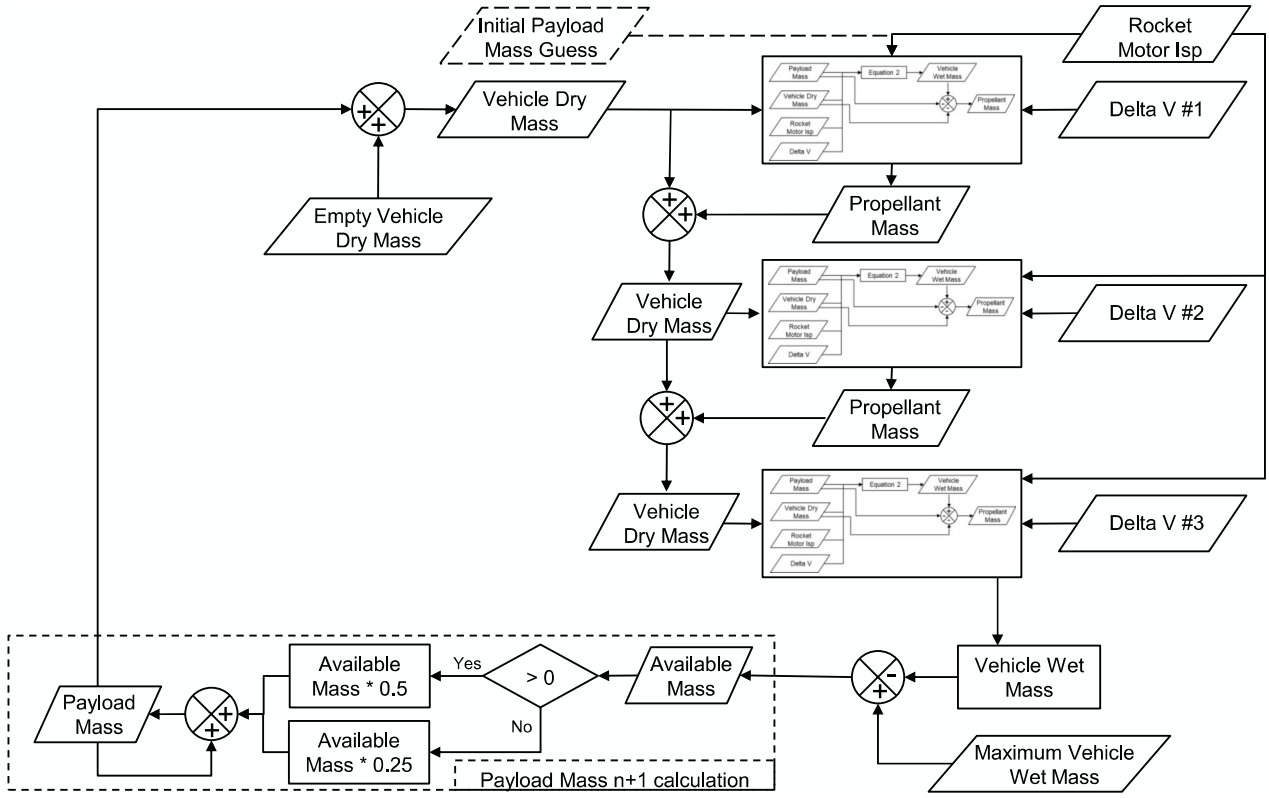

Figure 5: Multiple Manoeuvre solving algorithm

Within this process, the dry mass of a vehicle in all but the initial calculation is considered to be both the structural and payload mass. Furthermore, the three manoeuvres in Figure 5 are in inverse chronological order, such that "Delta V #3" refers to the first of the three manoeuvres, and such that the comparison to the maximum vehicle wet mass is done in the state where the vehicle is at its

maximum load.

7.4 ISRU Plant Sizing

Appendix D outlines various ISRU plant sizing results from reference Mars mission designs [181, 182, 183]. These results are tailored to Mars ISRU, and as such should not be used as accurate estimates of plant mass:output ratio for Lunar ISRU. Consequently, results from an internal ESA analysis were used to obtain an initial estimate for the output rates of three plant efficiencies.

Table 5: Estimated production rates of Lunar ISRU plants

Plant Efficiency	**Daily output: Mass**
Pessimistic	0.001
Baseline	0.005
Optimistic	0.01

8 Space X Model

The Space X model used in this study is based on the current launch vehicle/spacecraft combination being developed by Space Exploration Technologies Corp. The launch system uses a first stage booster, called Superheavy, and a second stage, called Starship. Both are designed to be fully reusable. In this reusable configuration, 150 tonnes can be delivered to LEO, with this increasing to 250 tonnes if the Starship second stage does not return to the surface. To achieve this, the first stage uses 3,600 tonnes and the second stage uses 1,200 tonnes. Both are powered by methalox-burning Raptor engines developed in-house.

8.1 Concept of Operations

The following three concepts of operations use ISRU-capabilities at different levels. The first is a one-way cargo delivery trip to the lunar surface facilitated by a LEO refuelling of the Starship before departure into cislunar space. The second is also a one-way cargo delivery to the lunar surface, but with the possibility to refuel LOX in low lunar orbit (LLO) before final descent. The third is where an outbound Starship can refuel LOX both in LEO and in LLO. In this scenario, the LOX available in LEO is the return payload of the previous Starship.

8.1.1 Con Ops 1

Con Ops 1 is the cargo-delivery variant of the currently envisioned architecture. Unlike the HLS mission plan which returns the Starship to lunar orbit [184], Con Ops 1 remains on the surface. This allows the deliverable payload to be maximised, as the ascent propellant does not need to be carried along. If the lunar-bound Starship is launched fully loaded in its expendable configuration, it arrives in LEO with 250 tonnes of payload. This vehicle (red in Figure 6) is now in orbit with 350 tonnes of dry mass, and requires 950 tonnes of propellant to return to its fully loaded configuration.

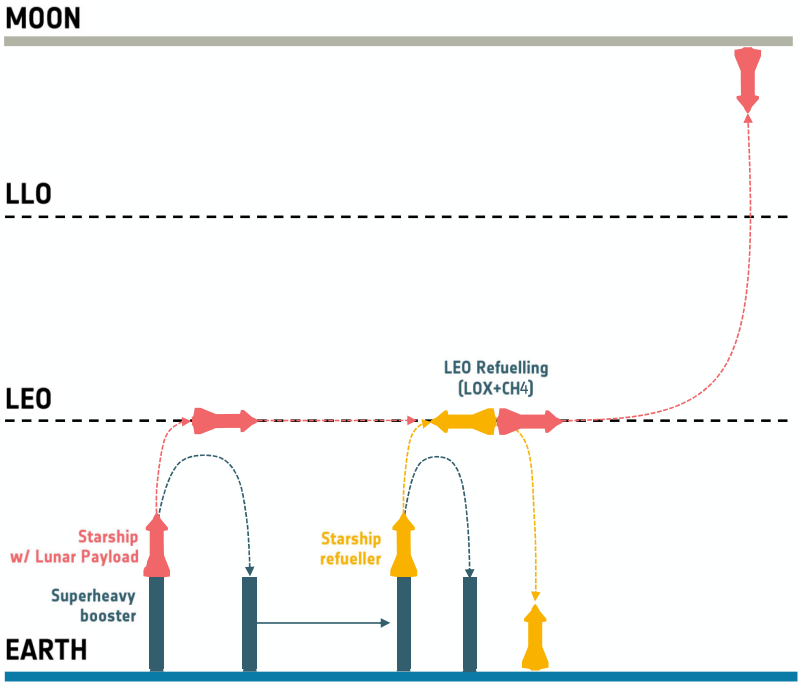

Figure 6: Space X Model Concept of Operations 1

These 950 tonnes of propellant require 7 additional launches of a Starship tanker (yellow in Figure 6), each delivering 150 tonnes per launch. Once fully loaded in LEO, the lunar-bound Starship must perform a 5986 m.s^{-1} manoeuvre to arrive at the lunar surface (Figure 2). Using its vacuum-optimised variant of the Raptor engines (Isp increases from 350s to 380s with a larger expansion nozzle [185]), Starship requires 1,039 tonnes of propellant to make this trip. Thus, in its one-way non-ISRU-enabled architecture, the Space X model concept of operations can deliver 161 tonnes of payload to the lunar surface per trip.

8.1.2 Con Ops 2

Con Ops 2 introduced ISRU capabilities into cislunar space. Within this architecture, a surface ISRU plant is operational and making LOX, which is then delivered to a LLO depot. Outbound Starships thus do not have to carry the LOX required to perform the final LLO to lunar surface descent, and can instead dedicate that capacity to extra deliverable payload.

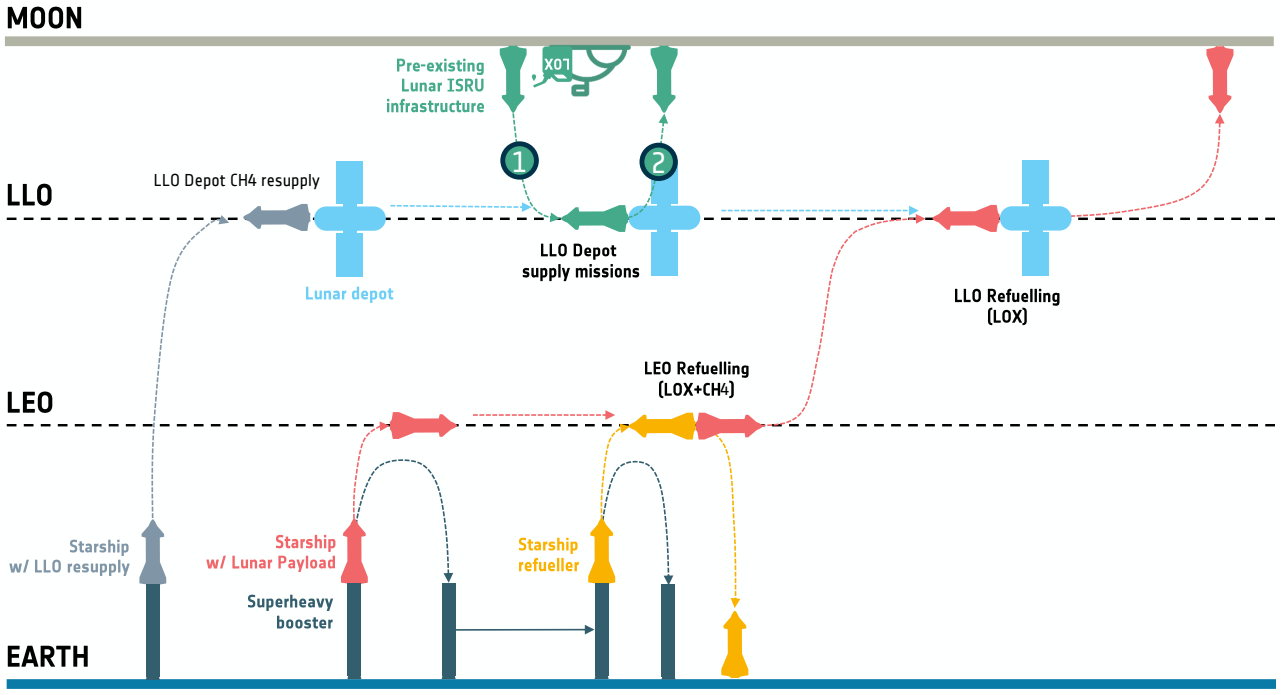

Figure 7: Space X Model Concept of Operations 2

Using the procedure outlined in Figure 5, and a maximum wet mass of 1,300 tonnes, we calculate a maximum lunar-bound payload of 291.9 tonnes. With this payload and a methalox mix ratio of 1:3.6, 63.6 tonnes of CH4 are needed for the descent from LLO to the lunar surface. This makes the effective payload for the LEO-LLO transit equal to 355.5 tonnes, the propellant required for the transit equal to 844.5 tonnes, and the wet mass equal to 1,300 tonnes. Since the payload is above the 250 tonne limit per Starship trip to LEO, an extra launch is required to fully load the lunar-bound Starship. If this extra payload can be launched aboard a tanker Starship, only 7 additional launches are required before LEO departure, and if not, 8 are required.

This architecture also requires the periodic resupply of CH4 at the cislunar depot to facilitate the lunar shuttle trips to and from the ISRU plant. Again using the procedure outlined in Figure 5, we calculate a [Earth-CH4 delivery to LLO]:[Lunar-LOX delivered to LLO] ratio of 0.23 (refer to Figure 8 for the mass distributions of lunar shuttle trips). Per cargo Starship landing on the lunar surface,

229 tonnes of LOX are required at a LLO depot. These 229 tonnes of LOX require the delivery of 53 tonnes of CH4 from Earth. Given that the periodic resupply of CH4 delivers 355 tonnes per trip to LLO, each cargo Starship requires 0.15 CH4 resupplies to LLO.

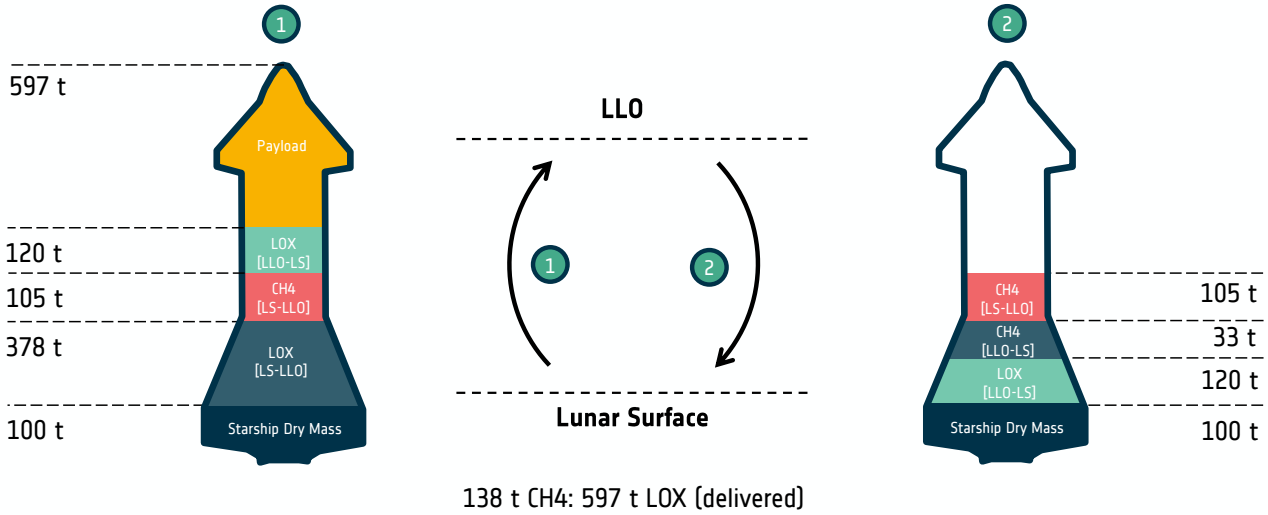

Figure 8: SX Con Ops 2: Lunar shuttle composition

8.1.3 Con Ops 3

Con Ops 3 introduces the additional capability of returning lunar-produced LOX to LEO, where it can be used to refuel a vehicle on the its outbound flight to reduce reliance on LOX sourced from within the Earth's gravity well (Figure 9). Unlike Con Ops 1 and 2, the third concept of operations introduces an additional consideration regarding the mission goals. Whereas before the optimum solution was defined as that with the most lunar-bound payload, now we must also consider the return of LOX from cislunar space. Let us quickly examine the two extremes of the problem. If we prioritise payload delivery to the surface and neglect LOX return to LEO we only bring back an empty Starship, which whilst useful for reusability means we reduced our effective cargo delivery with no accompanying benefit. On the other end of the spectrum we can consider prioritising LOX return to LEO by first sending a Starship to the lunar surface loaded with methane neccesary to bring back LOX. In this case we bring back LOX to LEO but delivered no payload to the lunar surface, nullifying our comparison.

There will clearly be a trade-off; more outbound payload from LEO mean less lunar-LOX returned to LEO - the choice of which payload trip should be more important is dependent on mission goals. We can, nonetheless, see the linear relationship between outbound and inbound payload for this concept of operations. Within Figure 10 only the extremes of the data set have been highlighted, but intermediate points were also calculated to validate the linear relationship. For comparison, a hydrolox propellant mix is also shown, and as expected the lower mass fraction of the fuel component results in a higher maximum payload both on the outbound and inbound phases of flight. For the mission architecture, we make the assumption that a previous mission has been conducted with the same inbound/outbound mass distribution, such that, for example, a mission carrying 50 tonnes of outbound payload has access to 191.8 tonnes of inbound lunar-produced LOX in LEO.

8.2 Carbon Dioxide Emissions

With the mission architecture outlined for each of the three concept of operations, we can proceed with calculating the associated carbon emissions.

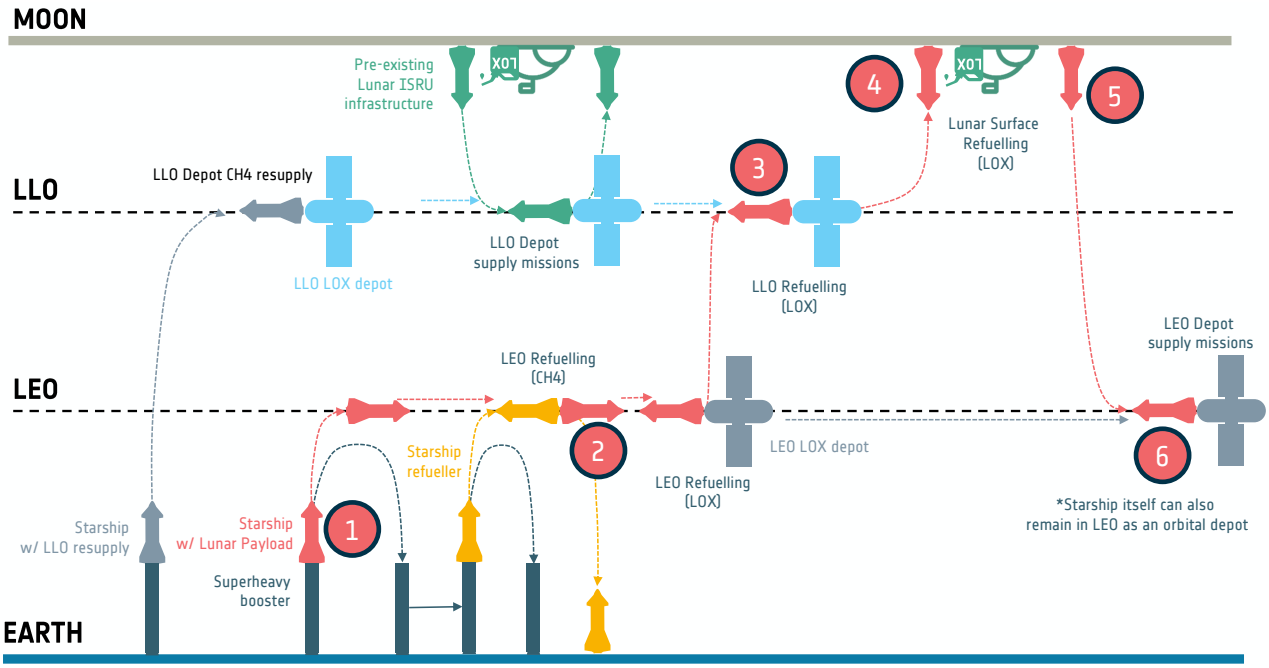

Figure 9: Space X Model Concept of Operations 3

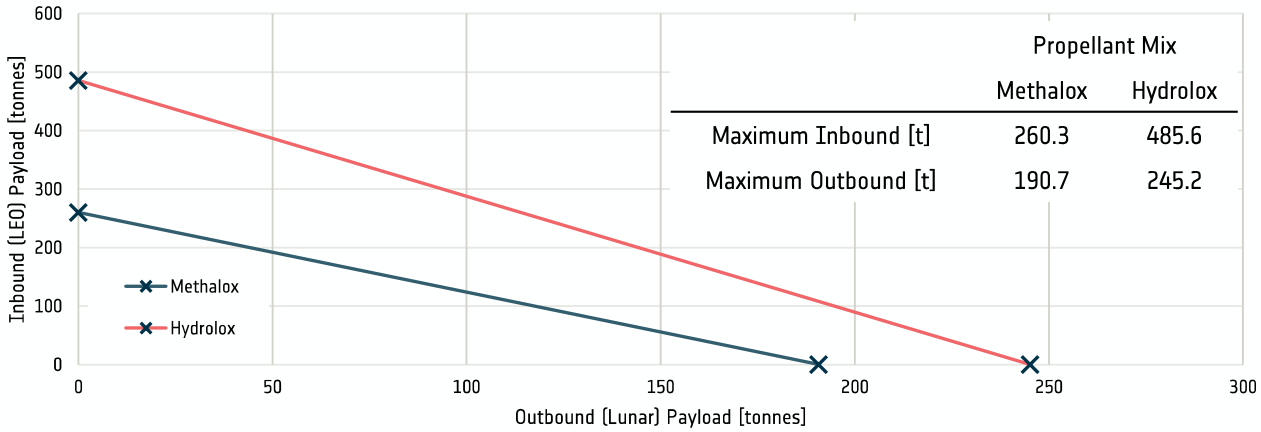

Figure 10: SX Con Ops 3: Inbound vs Outbound payload combinations

8.2.1 Con Ops 1

As previously mentioned, Con Ops 1 requires an initial launch to LEO of the lunar-bound Starship, and 7 subsequent launches to fully load before its departure to the lunar surface. Assuming full reusability of the Superheavy booster stage and the Starship tanker, we can outline the emissions per mission element (Table 6).

With 161 tonnes of payload delivered to the surface for every 22,314 tonnes of CO2 emitted, Space X Con Ops 1 has a payload emissions ratio of 1:139.

8.2.2 Con Ops 2

In terms of launch requirements, Con Ops 2 is similar to Con Ops 1 in that the lunar-bound Starship requires an initial launch plus 7 refuels in LEO. However, unlike Con Ops 1, it requires a resupply

Table 6: SX Con Ops 1: Carbon Emissions

Elements		**Con Ops 1**	
Name	CO2 Emissions [kg]	Quantity	CO2 Emissions [kg]
Superheavy MoC	1,370,600.00	1	1,370,600.00
Starship MoC	685,300.00	2	1,370,600.00
Launch Prop. Burn	1,894,000.00	8	15,152,000.00
Launch Prop. Prod	537,500.00	8	4,300,000.00
LOX:CH4/kg	0.117	1,039,000.00	121,404.89
LOX/kg	0.125	0	0
CH4/kg	0.0875	0	0
Total			**22,314,604.89**

of CH4 to a LLO depot so that it can then refuel the neccesary LOX before its descent to the lunar surface. Since this resupply of CH4 only needs to happen every 6.7 cargo mission, we can take the fractional emissions for this element of the mission architecture

Table 7: SX Con Ops 2: Carbon Emissions per mission element

Elements		**Cargo Mission**		**LLO Resupply of CH4**	
Name	CO2 Emissions [kg]	Quantity	CO2 Emissions [kg]	Quantity	CO2 Emissions [kg]
Superheavy MoC	1,370,600.00	1	1,370,600.00	0	0
Starship MoC	685,300.00	2	1,370,600.00	1	685,300.00
Launch Prop. Burn	1,894,000.00	8	15,152,000.00	8	15,152,000.00
Launch Prop. Prod	537,500.00	8	4,300,000.00	8	4,300,000.00
LOX:CH4/kg	0.117	908,100.00	106,109.51	845,000.00	98,736.41
LOX/kg	0.125	0	0	0	0
CH4/kg	0.0875	0	0	355,000.00	31,062.50
Element Total			**22,299,309.51**		**20,267,098.91**
		x1	**22,299,309.51**	**x0.15**	**3,040,064.84**
Overall Weighted Total					**25,339,374.35**

With 291.9 tonnes of payload delivered to the surface for every 25,339 tonnes of CO2 emitted, Space X Con Ops 2 has a payload emissions ratio of 1:87.

8.2.3 Con Ops 3

One of the most evident implications of our modified mission architecture within Con Ops 3 is that the payload emissions ratio will no longer be a constant, but instead dependent on the proportion of outbound-to-inbound payloads. We thus need to verify what the effect of our returning Starship is on the payload emissions ratio. Figure 11 shows the relationship between outbound payload and the payload emissions ratio. Perhaps not surprisingly, for all combinations of outbound and inbound payloads, the emissions ratio is higher than for the ISRU-enabled Con Ops 2. There is, also not too surprisingly, a range of outbound payloads in which Con Ops 3 has a lower payload emissions ratio than the non ISRU-enabled mission architecture of Con Ops 1. However, below $\approx$ 183 tonnes of outbound payload, Con Ops 1 has a lower payload emissions ratio, indicating that the penalty of having to return the 100 tonne Starship to LEO quickly outweighs the benefits of ISRU (at least within the scope of a direct comparison between Con Ops 1 and 3).

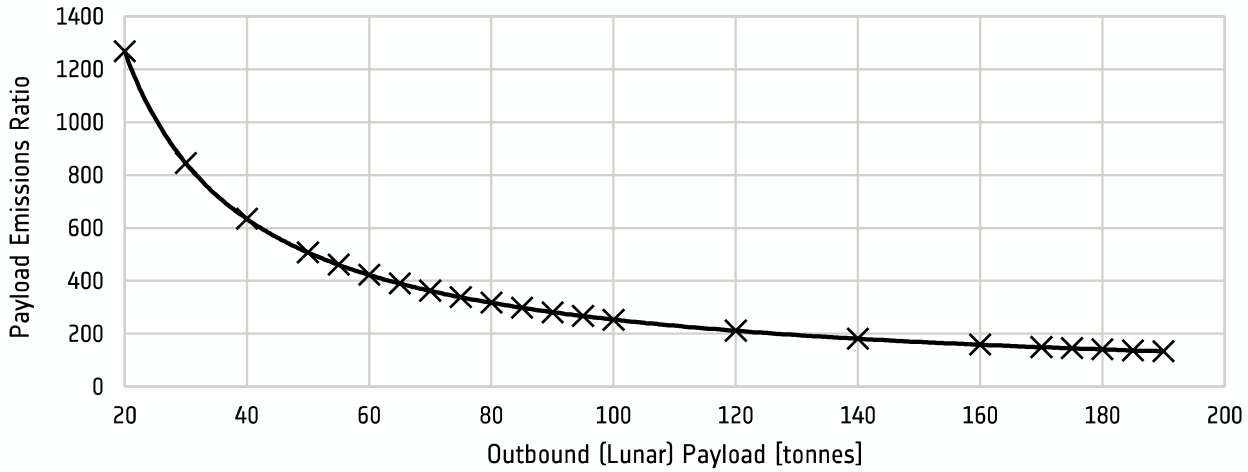

Figure 11: SX Con Ops 3: Outbound payload and corresponding payload emissions ratio

For reference, Table 8 shows the breakdown of CO2 emissions of a mission with 120 tonnes of outbound payload that returns 95.9 tonnes of lunar-produced LOX to LEO.

Table 8: SX Con Ops 3: Emissions breakdown for 120 tonnes outbound payload

Elements		**Cargo Mission**		**LLO Resupply of CH4**	
Name	CO2 Emissions [kg]	Quantity	CO2 Emissions [kg]	Quantity	CO2 Emissions [kg]
Superheavy MoC	1,370,600.00	1	1,370,600.00	0	0
Starship MoC	685,300.00	2	1,370,600.00	1	685,300.00
Launch Prop. Burn	1,894,000.00	8	15,152,000.00	8	15,152,000.00
Launch Prop. Prod	537,500.00	8	4,300,000.00	8	4,300,000.00
LOX:CH4/kg	0.117	0.00	0.00	845,000.00	98,736.41
LOX/kg	0.125	614,786.96	76,848	0	0
CH4/kg	0.0875	465,213.04	40,706	355,000.00	31,062.50
Element Total			**22,310,754.51**		**20,267,098.91**
		x1	**22,310,754.51**	**x0.15**	**3,040,064.84**
Overall weighted total					**25,350,819.35**

With 120 tonnes of payload delivered to the surface for every 25,350 tonnes of CO2 emitted, Space X Con Ops 3 with this outbound:inbound ratio has an emissions ratio of 1:211.

We can also check if there are benefits to combining different distributions of inbound vs. outbound payload to achieve a lower overall emissions ratio. Consider a first mission tasked with bringing lunar-produced LOX to LEO. With 0 tonnes outbound payload and 260.3 tonnes of LOX brought back to LEO, 27.8 million kilos of CO2 are emitted. For a subsequent mission that takes advantage of this LOX in LEO, 190.7 tonnes of payload can be delivered to the lunar surface, but with a reduced CO2 footprint of 25.3 million kilos. The second mission, as expected, has a reduction in carbon emissions ratio *w.r.t.* Con Ops 1 (with 1:139 emissions ratio Con Ops 1 outputs 26.5 million kg CO2 for 190.7 tonnes of payload). However, if the prior LOX-sourcing mission in included and the payload emission ratio over the two is averaged, it raises to 1:280, a clear and unwanted increase in emissions.

If we breakdown the LOX production requirements for a single (190.7 tonnes outbound) mission within

Con Ops 3 we get

- 216 tonnes of LOX are required in LLO per Starship cargo landing (where landing dry mass is 100 t structural, 190.7 t payload, and 78.9 t CH4 for LEO return).
- 180 tonnes of LOX required to place the previous 216 tonnes into LLO (with 498 t LOX required for a full load of 597 t payload).
- 284 tonnes of LOX for Starship's LEO return.

This totals 680 tonnes of LOX produced on the lunar surface per mission. A quick reference to the ISRU plant sizing in subsection 7.4 we expect a relatively large total system mass required to achieve this output. At its upper limit for outbound payload, Con Ops 3 has an emissions ratio of 1:133. Its marginal (-1:6) reduction of the payload emissions ratio, combined with this large expected ISRU system mass, remove it from further consideration within the break-even calculations[17]

8.2.4 Break-even Timeline

The relative carbon emissions savings between each of the Con Ops is outlined in Table 9.

Table 9: Relative reduction in payload emissions ratio between different Con Ops

	Con Ops		
	1	2	3
Savings *w.r.t.* ConOps 1	N.A.	-1:52	-1:6

Let us now consider the LOX production requirements for the ISRU plants outlined in Con Ops 2 and 3. Starting with Con Ops 2, each lunar-bound Starship mission requires 229 tonnes of LOX at a LLO depot. Each lunar shuttle trip from the ISRU plant to the depot requires 1,095 tonnes of LOX from the plant (378 t for the ascent, 120 t for the descent, and 597 t payload to orbit). Since each inbound mission only requires 0.38 lunar shuttle trips (229/597), the plant must output 420 tonnes of LOX per inbound mission. With a trip rate of 2/year, we require an ISRU plant that can produce 2.869 tonnes per day[18]. The resulting ISRU plant masses are outlined in Table 10 using plant sizing estimates from subsection 7.4.

Table 10: SX: Estimated ISRU plant mass

Plant Efficiency	**Plant Mass [tonnes]**	
	Con Ops 2	Con Ops 3
Pessimistic	2,869.00	N.A.
Baseline	573.80	N.A.
Optimistic	286.90	N.A.

[17]This is further confirmed by looking ahead to the results of Con Ops 2's break even calculations, where ≈ 60% of the LOX output is required, the emissions ratio reduction is 8.6 times higher, and the break even point at baseline efficiency is 5.5 years. We can quickly estimate Con Ops 3's break even point with a baseline ISRU plant output would be approximately 7 decades.

[18]One trip per 183 days, considering 20% plant downtime.

Table 11: SX model emissions break even points: ConOps 2

Plant efficiency	**Total System Mass [tonnes]**	**CO2 emissions [tonnes]**	**Break even point**		
			Cargo [tonnes]	Trips	Years
Pessimistic	5,738.00	797,582.00	15,338.12	53	26.5
Baseline	1,147.60	159,516.40	3,067.62	11	5.5
Optimistic	573.80	79,758.20	1,533.81	6	3

9 Blue Origin Model

The following section outlines the carbon emissions calculations associated with a lunar exploration model based on that currently being developed by Blue Origin. In some instances, changes were made *w.r.t.* their publicly stated architecture - it is clearly stated when this was done.

9.1 New Glenn Second Stage Calculations

In subsubsection 7.2.3 the calculations for the NGS1 were outlined. For NGS2 we need the propellant mass, but additionally also the vehicle dry mass. NGS2 uses 2 BE-3U engines for a total stage thrust of 1,060 kN. Engine data is not publicly available, but from images we can estimate an expansion ratio of ≈ 80, making it comparable to the HM7B engine developed by Ariane[19]. We know the HM7B has an Isp of 446 s, and other comparable rockets have values ranging from 440-450 s. If we take an estimated Isp of 450 for the BE-3U we can again use Equation 4 to obtain a mass flow per engine of 120 kg.s^{-1}. When delivering payload to LEO, NGS2 has a burn time of 600 s, giving it a total propellant mass of 144 tonnes (in its LEO delivery configuration) [177].

Given the orbital parameters of the parking/transfer orbits we can estimate a required Δv of ≈ 2.4 km.s^{-1}. With the stated 99 s burn used to transit from parking to transfer orbit [177], 23,760 kg of propellant are required. Using Equation 1 we can calculate the ratio of initial mass to propellant mass as 1.72. This allows us to estimate NGS2's dry mass as 32.9 tonnes. If we subtract the stated 13.6 tonne payload it delivers to GTO, and account for a 1 tonne fuel reserve, we obtain a NGS2 structural mass of 18.3 tonnes. Here we should note that in its payload-to-GTO configuration NGS2 requires 168 tonnes of propellant, not 144 tonnes.

9.2 Cislunar Transporter

Part of the Blue Origin architecture relies on a cislunar transporter (CT) currently being developed by Lockheed Martin [186, 187, 188]. Publicly available mission architecture for Blue Origin depicts only a single refuelling in LEO once New Glenn launches the CT into LEO [189]. Knowing New Glenn is capable of launching 45 tonnes into LEO, and assuming that the second launch is fully dedicated to refuelling the CT, we can assume that the total wet mass of the outbound CT from LEO is 90 tonnes. This value is also reliant on the assumption that the 45 tonne payload of the second launch is all propellant, an assumption that can be made by presuming a retrofit of NGS2 into a 'tanker variant', and presuming any additional structural mass is negligible *w.r.t.* its payload-to-LEO counterpart. From here it is neccesary to estimate the dry mass of the CT to estimate its payload capacity. We know it is a cryogenic propellant vehicle [186], and so can look at comparable vehicles (Appendix C). Here we calculate an average dry:wet mass fraction of 11.4% (Table 23), and thus estimate the dry mass of the CT as 10.4 tonnes, which we lower slightly to 10 tonnes assuming improvements in cryogenic stage design. Thus, the CT is capable of carrying 80 tonnes of propellant, usable for both its own propulsion and as deliverable payload.

9.3 BE-7 Engine

Both the Blue Moon lunar lander and the CT are planned to use the BE-7 engine currently under development by Blue Origin [190]. It is a cryogenic propellant engine designed with high specific impulse and reusability in mind. Its Isp is not publicly available, and so we estimate based on similar

[19] Both have similar expansion ratios and use the same cryogenic propellant mix, although the BE-3U uses an open expander cycle whereas the HM7B uses a gas generator cycle. An overview of other hydrolox engines is available in Appendix E.

high-Isp engines of comparable class. The RS-25 engine developed by Aerojet Rocketdyne has powered the Space Shuttle on all its 135 flights and is now used on the SLS [191]; it is also a cryogenic rocket engine designed with high-Isp in mind. It has an Isp of 452 s in a vacuum. This is extremely close to the theoretical maximum Isp for a LOX:LH2 propellant mix, where a maximum nozzle exit velocity of 4462 $m.s^{-1}$ gives an Isp of 455 s assuming a nozzle area ratio of 40:1 [192]. It is important to note that these values are calculated under the assumptions of:

1. adiabatic combustion,
2. isentropic expansion,
3. one-dimensional expansion, and
4. shifting equilibrium [193]

As such, we assume an Isp for the BE-7 engine of 450 s.

9.4 Concept of Operations

Unlike the Space X model explored in section 8, the Blue Origin model uses significantly fewer orbital refuellings in LEO. This is predominantly due to the reduced vehicle dry mass (from 100 tonnes for Starship to either 16 or 18.3 tonnes for the Blue Moon lander and NGS2 respectively) which require less propellant to deliver the same payload. There are several important point to be highlighted with the Blue Origin mission architecture (as it is currently envisioned by NASA/Blue Origin). Firstly, is that despite its life support capabilities (neccesary since it must ferry astronauts to the lunar surface and back to Gateway), the Blue Moon lander does not carry astronauts to cislunar space nor does it return them to Earth. All human transits from Earth to cislunar space are performed by the Orion/European Service Module (ESM) architecture as outlined in the Artemis mission plans [189]. In both version of the concept of operations used for the Blue Origin architecture, the Gateway station in NRHO is presumed to already be operational.

9.4.1 Con Ops 1

The first concept of operations considered for the Blue Origin model is that proposed by NASA for the Artemis missions [189], visible in Figure 12. This is the concept of operations for the Blue Origin mission architecture that does not implement ISRU-capabilities.
Here we encounter an incongruence between Blue Moon's stated capabilities and its calculated performance. A round-trip from Gateway's NRHO to the lunar surface and back requires 5609 $m.s^{-1}$ (Figure 2). Given the stated 16 tonne dry mass of the Blue Moon lunar lander (BMLL), this trip would require an initial starting mass of just over 57 tonnes. However, the stated maximum wet mass of BMLL is only 45 tonnes. Importantly, being a human-rated vehicle necessitates safety margins and manoeuvring capabilities, increasing the propellant mass further. Therefore, we can only conclude that either

1. The mission architecture is incomplete (in that an additional, currently undepicted, vehicle performs an initial braking burn to lower the Δv needed by the BMLL)
2. The BMLL dry mass is lower that currently stated or the wet mass is higher (given the wet:dry mass ratio of 3.56 neccesary for the manoeuvre, a maximum dry mass of 12.6 tonnes is permissible for the BMLL without exceeding the 45 tonne wet mass limit)
3. The propulsion architecture is significantly different to what is currently stated (with other factors remaining unchanged, an Isp of at least 553 s is required).

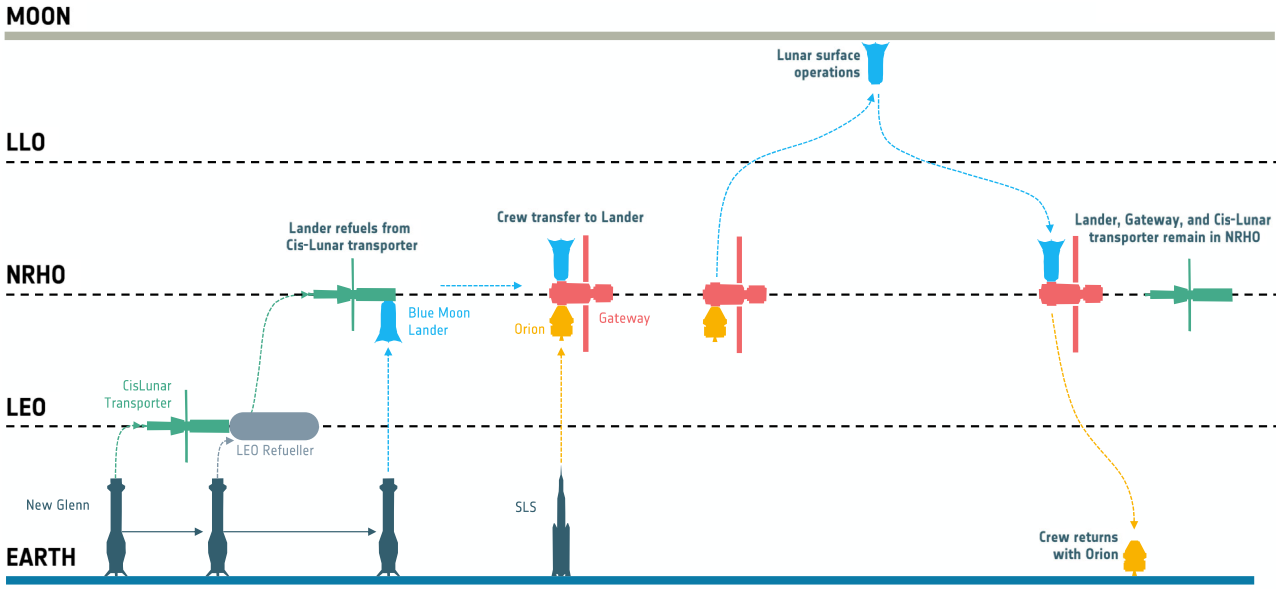

Figure 12: Blue Origin Model Concept of Operations 1

There are doubts related to each of these three solutions. The first seems unlikely, since not only is the mission architecture already published, but also any vehicle that performs the braking burn will crash into the lunar surface, making it a non-reusable part of the mission architecture which does not fall into the Artemis design goal

> *NASA will work with Artemis providers to ensure spacecraft are built ... with as many reusable components as possible for long-term sustainability at the Moon.*

as outlined by NASA's lunar exploration programme overview [194]. The third solution requires the adoption of a different propulsion architecture, something that is unlikely to happen for reasons including but not limited to (1) both the BMLL and CT are purposefully designed to use the same engine, (2) a hydrolox propellant was selected for its compatibility with lunar ice ISRU, (3) despite their significantly higher *Isp*, a move to nuclear engines would introduce additional operational risks, and (4) electric propulsion does not provide the neccesary thrust. The second is likely to be the probable solution as it entails the least operational hurdles - either an additional launch or two is required in LEO to fully refuel the BMLL before leaving for cislunar space, or the BMLL is made lighter. Therefore, for the purposes of a meaningful comparison, the dry mass of the BMLL was reduced to 10 tonnes, which allows us to also consider some payload delivery capabilities to the lunar surface from NRHO without exceeding the 45 tonne wet mass limit.

Here there are also some additional considerations to make. The first is that NGS2 is incapable of delivering the BMLL to a NRHO. However, a fully fuelled BMLL is capable of making the 3350 $m.s^{-1}$ transit from LEO-NRHO. This requires 23.9 tonnes of propellant, and in addition to its own 10 tonne dry mass can deliver 11.1 tonnes of payload to NRHO. Simultaneously, the CT makes the trip from LEO-NRHO fully loaded with 80 tonnes of propellant. Of those 80 tonnes, 47.88 tonnes are required as propellant, leaving 32.12 tonnes as deliverable payload to NRHO. Of this 32.12 tonne propellant payload delivered to NRHO, 23.9 tonnes can be resupplied to the BMLL, returning it to its fully-fuelled configuration. This also leaves 8.22 tonnes in NRHO as additional payload that can be used for a multitude of purposes such as the resupply of consumables, Gateway maintenance/expansion, and cislunar satellite delivery.

We can now calculate the payload deliverable to the lunar surface by a single round trip mission of the BMLL. As outlined in Figure 5, we first consider the final manoeuvre, where an empty BMLL returns to NRHO. With a 10 tonne vehicle, this requires 8.15 tonnes of propellant. If on the preceding descent the BMLL carried this neccesary propellant as payload, the *effective* dry mass of the vehicle would have been 18.15 tonnes, which means to achieve the required Δv the vehicle would have needed 17.49 tonnes of propellant. This would have given the departing vehicle a wet mass of 35.64 tonnes, almost 10 tonnes lighter than its maximum capacity. By employing the multiple-manoeuvre algorithm, the maximum lunar-bound payload from NRHO was calculated to be 4.76 tonnes per BMLL round-trip.

Finally, we consider the different elements required per mission type. Here we looked at a reusable CT that returns to LEO following the refuelling of the BMLL in NRHO. This return to LEO by the CT requires 11.37 tonnes of propellant, which means there are 3.15 tonnes of propellant that need to be sourced from somewhere (8.22 of the 11.37 can be taken from the propellant delivered on the outbound trip). Let us assume that these 3.15 tonnes of propellant have been already placed into NRHO by some previous mission[20]. Now that the CT is capable of returning to LEO, subsequent missions benefit from a reduction in MoC, but not in a reduction in launches, since two NG launches are still required to fully refuel the CT. Given that 90 tonnes will be put into LEO with those two launches, let us presume the CT is also capable of transporting these additional 10 tonnes of payload *w.r.t.* its initial LEO-NRHO trip. This increases its deliverable propellant payload to NRHO to 36.81 tonnes, which also increases the surplus (post BMLL refuel) propellant to 12.91. With this increase, future CT returns to LEO are now possible, closing the case.

We subsequently outline the elements required per mission type (Figure 13). The first is the initial mission. Two variations of the cargo missions are depicted, one fully autonomous and one that requires an accompanying human crew. The fourth is a human mission with no cargo-dedicated BMLL travelling from LEO-NRHO.

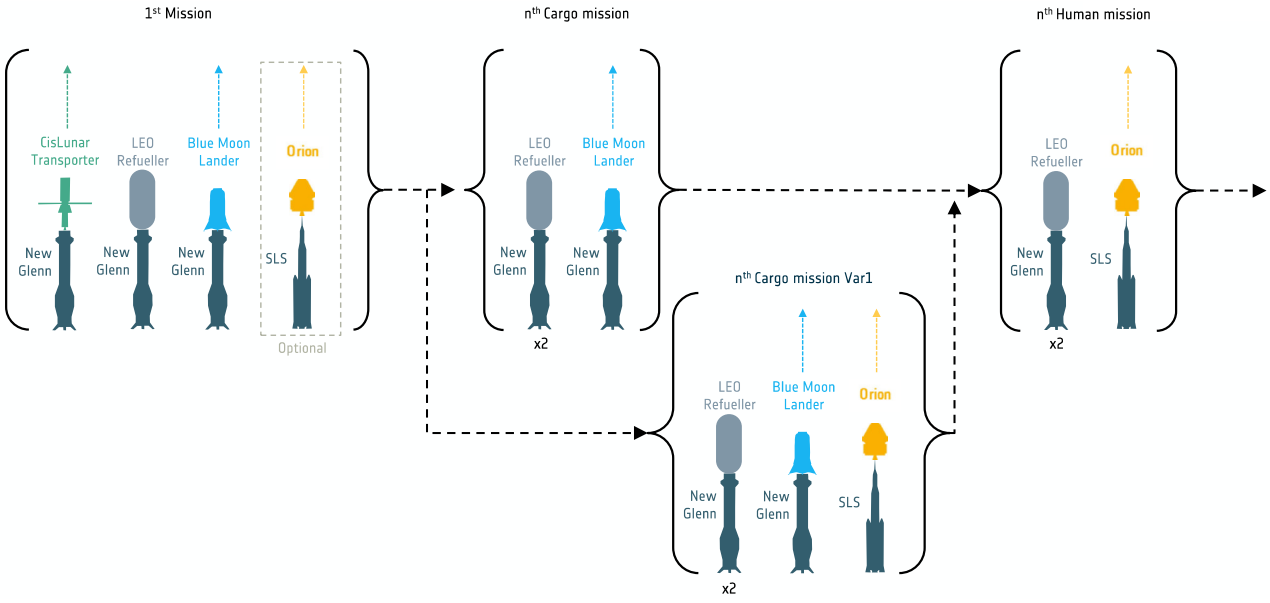

Figure 13: BO Con Ops 1 - elements required per mission type

[20]Somewhat sketchy but neccesary to continue without modifying the architecture - maybe a small disposable tank has been sent beforehand.

9.4.2 Con Ops 2

The second concept of operations considered for the Blue Origin model is a variation of Con Ops 1 where an ISRU capability has been introduced both on the Lunar surface and in cislunar space. Here it is assumed that an ISRU plant and the accompanying infrastructure (cislunar depot, resupply shuttle, power generation, feed stock collection etc.) are already operational. It is also assumed that the landing accuracy of the Blue Moon lander is sufficiently high to allow for precision landings on the lunar surface, that in turn allow for surface refuelling when near the ISRU plant. This architecture is shown in Figure 14.

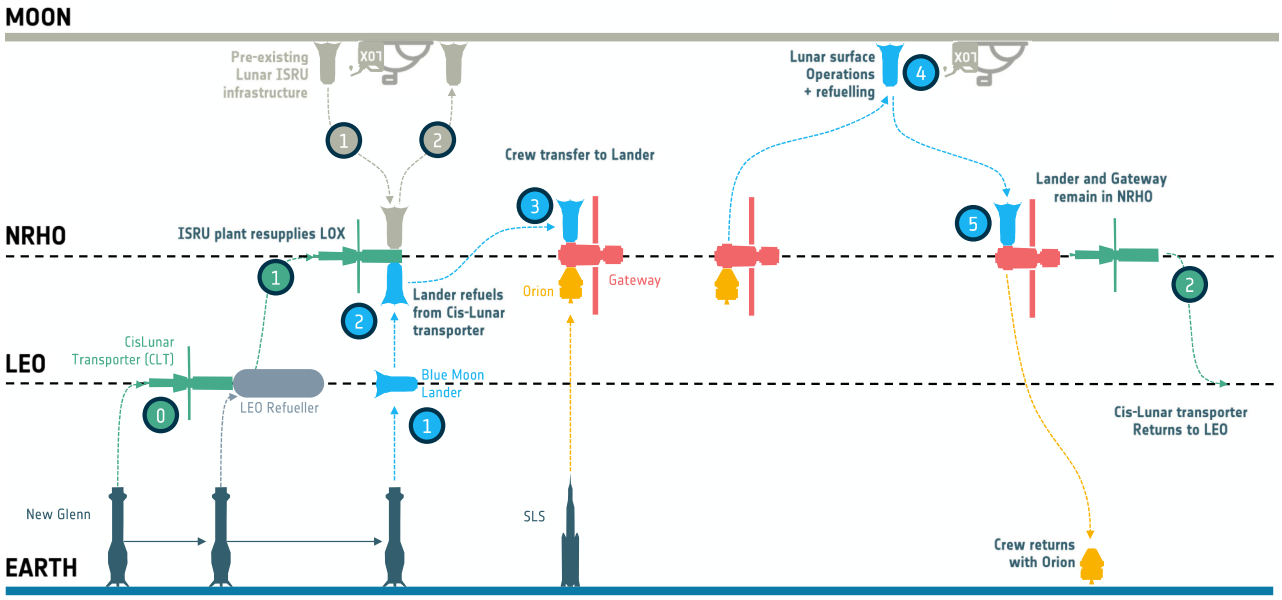

Figure 14: Blue Origin Model Concept of Operations 2

Here, different mission operations have been separated by colour and numbered to allow us to more clearly follow the composition of different vehicles. Let us consider the composition of the BMLL throughout the mission. Figure 15 shows the different composition as the mission progresses. Propellant resupply in NRHO and oxidiser resupply on the lunar surface are shown at points 2 and 4 respectively. The composition chain of the BMLL shown in Figure 15 depicts its role as both a cargo delivery vehicle to the lunar surface and also its capability to deliver lunar-produced LOX to a NRHO depot such as Gateway.

Within Con Ops 2 we also make the assumption that an ISRU plant has already been set up and is operational. An element of this operational ISRU plant on the lunar surface is a lunar shuttle (likely to be a surplus BMLL from when the plant was delivered). This lunar shuttle is tasked with resupplying a NRHO depot with lunar-ISRU produced oxygen. To facilitate these multiple operations, LH2 is taken from the orbital depot. Again, the iterative procedure outlined in subsubsection 7.3.2 was used to converge on a solution that maximised the payload delivery to NRHO whilst allowing the shuttle to perform a return trip. We calculated a maximum payload of 4,144 kg per lunar shuttle trip. The mass distributions for the two trips are shown alongside the landers in Figure 16. Note that the LH2 used for the ascent (1) is the same brought down as payload in (2), and that the LOX brought up as payload in (1) is the same as the LOX used for descent in (2).

To allow inbound BMLL to fully refuel in NRHO, and to allow the lunar shuttle to perform its resupply

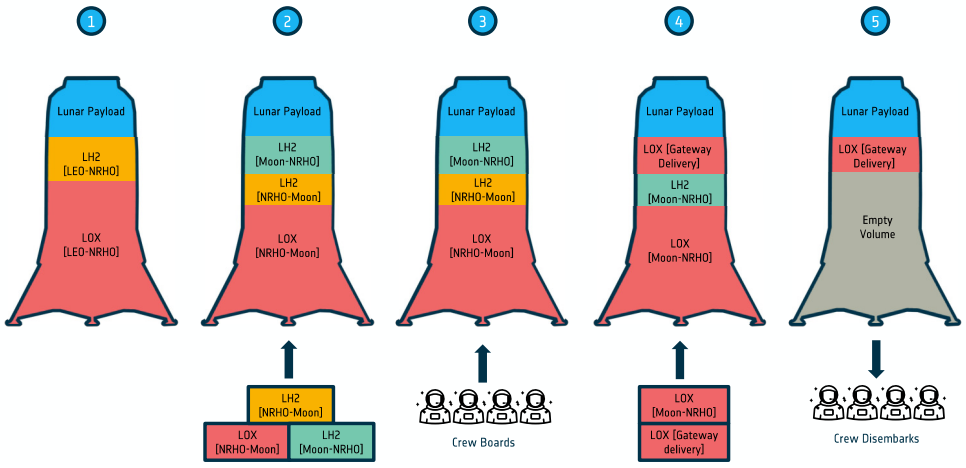

Figure 15: BO Con Ops 2 - BMLL composition over mission stages

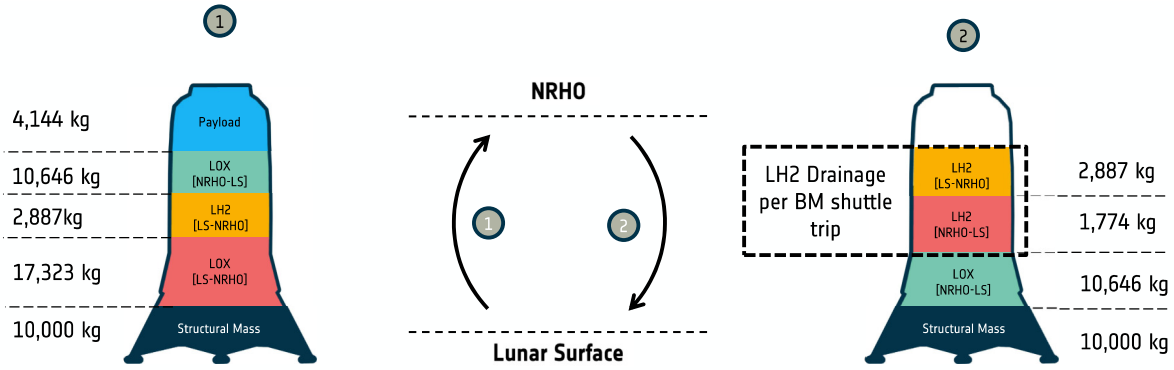

Figure 16: BO Con Ops 2 - LS composition over mission stages

trips from the surface ISRU plant, there must be a supply of LH2 in NRHO. Given the availability of lunar-produced LOX, the CT can be repurposed to deliver only LH2 from LEO to NRHO. In this configuration, the CT returns empty from NRHO to LEO, and sources the LOX it needs for the outbound trip from a terrestrial source. This choice in architecture was made to reduce the propellant required on the return trip, and maximise the LH2 delivery to NRHO. The mass distributions for the two trips are shown alongside the CT's in Figure 17.
From Figure 16 we can see that each lunar shuttle trip drains an LH2 orbital depot of 4,661 kg. From Figure 17 we can see that each CT trip resupplies a depot with 30,501 kg of LH2, meaning that one CT resupply is required per 6.54 NRHO depot resupply trips. In turn, those 6.54 trips can bring 27,117 kg of lunar-produced LOX to a NRHO depot.

Now we consider the BMLL that performs the cargo mission. In order to maximise the descent payload, we assume that it returns empty and thus only has to carry 1,164 kg of LH2 as descent payload to then perform the ascent back. Fully loaded, the BMLL requires 22,078 kg of propellant to land on the lunar surface, leaving 22,922 kg for dry/payload. If 11,164 is already fixed, each BMLL can deliver 11,758 kg of payload to the lunar surface. This confirms, as expected, that an ISRU capability augments payload delivery.

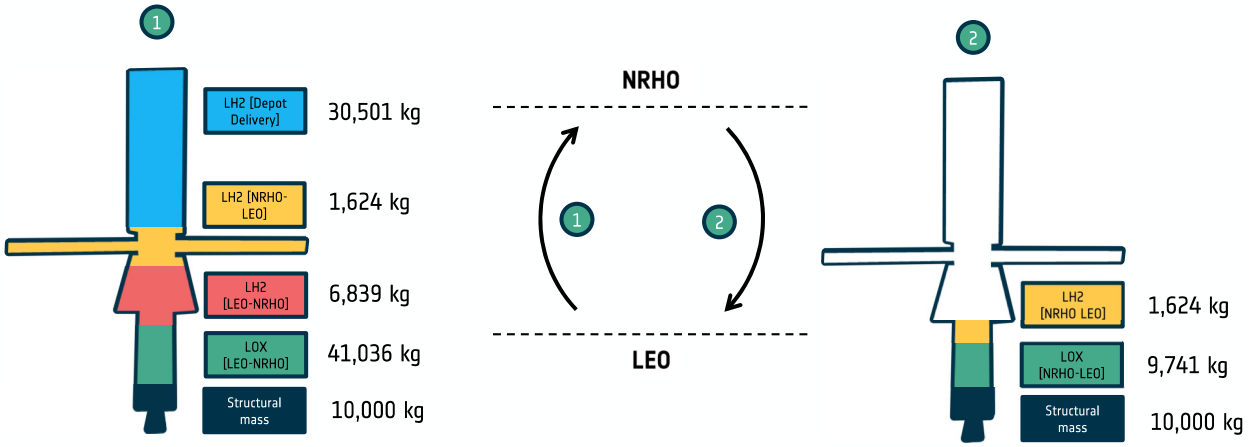

Figure 17: BO Con Ops 2 - CT composition over mission stages

9.5 Carbon Dioxide Emissions

With the concept of operations outlined for non-ISRU and with-ISRU cases, we can calculate the payload emissions ratio for each. From there, we can begin to see what the effect of ISRU capabilities are on the carbon emissions, and make preliminary estimates as to the break-even timeline.

9.5.1 Con Ops 1

Let us recall that within ConOps1, the maximum deliverable payload to the lunar surface per BMLL is 4.76 tonnes. To consider all three CO2 emissions sources as outlined in subsection 7.2 we also had to make some additional estimates. The first is that New Glenn's design is comparable to Starship's, and that as such we can use Starship's dry:propellant ratio as an indicator. This 1:12 ratio gives us a dry mass of 95.83 tonnes for NGS1 when considering 1150 tonnes of propellant. We increase this to 100 tonnes to account for the reduced mass of NGS1 *w.r.t.* Starship. There are also some estimates to be made regarding the SLS/Orion architecture. SLS has a core section and two boosters; the core carries 2,000,000 litres of liquid hydrogen and 742,000 litres of liquid oxygen, giving it a propellant mass of 988.3 tonnes [195]. With a core wet mass of 1088 tonnes, its dry mass is approximately 100 tonnes. Each SLS booster burns propellant at a rate of 5500 $kg.s^{-1}$ for two minutes. This gives each booster an approximate propellant mass of 660 tonnes, and knowing the boosters wet mass of 726 tonnes, allows us to deduce a dry mass of 66 tonnes each. The CM and ESM dry masses are 9,300 kg and 6,185 kg respectively, and the Orion module has 8,550 kg of propellant [196]. The two boosters in SLS use solid fuel called PBAN, the manufacturing of which (at large scale) is not well documented in public literature. As such, we roughly estimate an emissions of 500 tonnes to produce the 1,320 tonnes of PBAN required for both boosters. A summary of the carbon emissions per mission element is available in Table 12.

Now let us consider the payload:emissions ratio for such an architecture. Each one is capable of delivering 4.76 tonnes of payload to the lunar surface. If all mission elements were fully reusable, only the initial mission would require the launch of a CT, and all subsequent cargo missions could use the n^{th} cargo mission elements. This would mean that the additional 3.7 million kg of CO2 emitted from launching a CT and SLS/Orion combination on the first mission would then be shared over subsequent missions. However, there is likely to be a reusability limit for each element. As such, we compare the payload emissions ratio for different reusability levels.

Table 12: BO Con Ops 1: Carbon Dioxide emissions per mission variation

Elements		1st Mission		Cargo		Human		Cargo Var	
Name	CO2 emissions [kg]	Quantity	CO2 emissions [kg]	Quantity	CO2 emissions [kg]	Quantity	CO2 emissions [kg]	Quantity	CO2 emissions [kg]
NGS1 MoC	685,300.00	1	685,300.00	0	0.00	0	0.00	0	0.00
NGS2 MoC	125,409.00	3	376,227.00	3	378,000.00	2	252,000.00	3	378,000.00
NGS1 Burn	439,300.00	3	1,317,900.00	3	1,317,900.00	2	878,600.00	3	1,317,900.00
NGS1 PropProd	134,550.00	3	403,650.00	3	517,500.00	2	345,000.00	3	517,500.00
NGS2 PropProd	51,408.00	3	154,224.00	3	147,600.00	2	98,400.00	3	147,600.00
CT MoC	68,530.00	1	68,530.00	0	0.00	0	0.00	0	0.00
BMLL MoC	68,530.00	1	68,530.00	1	67,400.00	0	0.00	1	67,400.00
LOX:LH2/kg	0.357	80,000.00	28,560.00	90,000.00	32,130.00	90,000.00	32,130.00	90,000.00	32,130.00
		35,000.00	11,970.00	35,000.00	11,970.00			35,000.00	11,970.00
SLS Core MoC	685,300.00	1	685,300.00	0	0.00	1	685,300.00	1	685,300.00
SLS Booster MoC	904,596.00	1	904,596.00	0	0.00	1	904,596.00	1	904,596.00
SLS Core PropProd	352,823.00	1	352,823.00	0	0.00	1	352,823.00	1	352,823.00
SLS Booster PropProd	500,000.00	1	500,000.00	0	0.00	1	500,000.00	1	500,000.00
SLS Burn	538,000.00	1	538,000.00	0	0.00	1	538,000.00	1	538,000.00
Orion MoC	106,118.00	1	106,118.00	0	0.00	1	106,118.00	0	0.00
Orion PropProd	3,052.00	1	3,052.00	0	0.00	1	3,052.00	1	3,052.00
Total			**6,204,780.00**		**2,472,500.00**		**4,696,019.00**		**5,456,271.00**

Table 13: BO Con Ops 1: Payload Emissions Ratio

Reusability	**Payload:Emissions**	
# trips	*Cargo*	*Cargo Var*
5	1 : 676	1 : 1,178
10	1 : 598	1 : 1,162
30	1 : 546	1 : 1,152
50	1 : 535	1 : 1,149

As is evident from Table 13, the payload emissions ratios are higher for the Blue Origin model than for the Space X model.

9.5.2 Con Ops 2

Within the concept of operations there is not a clear block structure per mission - i.e. mission elements are not aligned as depicted in Figure 13. In order to calculate a payload emissions ratio, we consider the elements neccesary to facilitate the delivery of one fully-loaded BMLL to the lunar surface (11,758 kg payload). However, in it's transit from LEO-NRHO, a BMLL has a maximum payload of only 11,063 kg. Given this bottleneck in payload delivery to NRHO, the maximum deliverable payload per BMLL in ConOps 2 is reduced from 11,758 kg to 11,063 kg. From the NRHO depot, 18,925 kg of LOX are required in addition to 4,318 kg of LH2. We assume the LH2 is available in NRHO since it is required by the lunar shuttle resupplying the depot from the ISRU plant. To source the 18,925 kg of LOX needed for the descent, 4.6 lunar shuttle trips are required. These 4.6 lunar shuttle trips require 21,441 kg of earth-sourced LH2, which in addition to the 4,318 kg needed by the BMLL for descent totals 25,759 kg of LH2 required in NRHO per cargo mission. Each CT trip from LEO can supply 30,501 kg of LH2, meaning 0.84 CT trips are required per cargo delivery. By considering a fractional contribution of this resupply trip we can better represent the carbon emissions required per BMLL mission to the lunar surface. Table 14 shows this breakdown of carbon emissions per cargo BMLL mission to the surface, assuming a NGS1 is available and a CT is in orbit performing refuellings to cislunar space.

We can thus calculate the payload emissions ratio for ISRU-enabled mission architectures using the Blue Origin architecture.

Note here that a SLS/Orion launch represents a 25% increase of CO2 emissions *w.r.t.* a BMLL/double refuel mission. Clearly, any mission architecture using SLS/Orion will have a significantly higher pay-

Table 14: BO Con Ops 2: Carbon Emissions per mission element

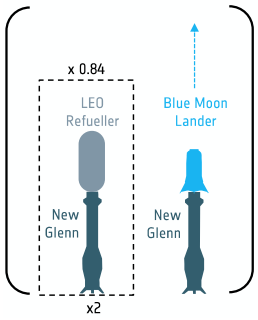

Elements		**BMLL Launch**		**x2 LEO Resupplies to CT**	
Name	CO2 emissions [kg]	Quantity	CO2 emissions [kg]	Quantity	CO2 emissions [kg]
NGS1 MoC	685,300.00	0	0.00	0	0.00
NGS2 MoC	125,409.00	1	125,409.00	2	250,818.00
NGS1 Burn	439,300.00	1	439,300.00	2	878,600.00
NGS1 PropProd	134,550.00	1	134,550.00	2	269,100.00
NGS2 PropProd	51,408.00	1	51,408.00	2	102,816.00
CT MoC	68,530.00	0	0.00	0	0.00
BMLL MoC	68,530.00	1	68,530.00	0	0.00
LH2/kg	1.75	0	0.00	80,000.00	140,000.00
LOX:LH2/kg	0.357	23,936.00	8,545.15	0	0.00
SLS Core MoC	685,300.00	0	0.00	0	0.00
SLS Booster MoC	904,596.00	0	0.00	0	0.00
SLS Core PropProd	352,823.00	0	0.00	0	0.00
SLS Booster PropProd	500,000.00	0	0.00	0	0.00
SLS Burn	538,000.00	0	0.00	0	0.00
Orion MoC	106,118.00	0	0.00	0	0.00
Orion PropProd	3,052.00	0	0.00	0	0.00
Element Total			**827,742.15**		**1,641,334.00**
		x1	**827,742.15**	**x0.84**	**1,378,720.56**
Overall Weighted Total					**2,206,462.71**

Table 15: BO Con Ops 2: SLS/Orion Launch Emissions

Elements		**SLS/Orion**	
Name	CO2 emissions [kg]	Quantity	CO2 emissions [kg]
SLS Core MoC	685,300.00	1	685,300.00
SLS Booster MoC	904,596.00	1	904,596.00
SLS Core PropProd	352,823.00	1	352,823.00
SLS Booster PropProd	500,000.00	1	500,000.00
SLS Burn	538,000.00	1	538,000.00
Orion MoC	106,118.00	1	106,118.00
Orion PropProd	3,052.00	1	3,052.00
Total			**3,089,889.00**

Table 16: BO Con Ops 1: Payload Emissions Ratio

Payload:Emissions	
Cargo	Cargo Var
1:199	1:411

load emissions ratio, as evident in Table 16[21].

9.5.3 Break-even Timeline

Recall the estimates for ISRU plant sizing presented in subsection 7.4. For our preliminary prediction of the break-even timeline, we look at the scenario depicted in Figure 14, where the plant must refuel the neccesary LOX to the lunar shuttle servicing the depot, and also refuel the neccesary LOX for the BMLL to return to NRHO. In this scenario the LOX requirements at the orbital depot are:

[21] Refer to Figure 13 for clarification on Cargo and Cargo Var mission composition.

- 18,925 kg for the BMLL descent from NRHO to the lunar surface

and thus the LOX requirements on the Lunar surface are:

- 6,984 kg for the BMLL ascent from the lunar surface to NRHO
- 127,730 kg to perform the 4.6 lunar shuttle trips needed to place the neccesary LOX into NRHO

If we assume a trip rate of 2/year, we require an ISRU plant that can produce 1,049 kg of LOX per day[22]. The resulting ISRU plant masses for both scenarios at three different efficiency levels are shown in Table 17.

Table 17: BO: Estimated ISRU plant mass

Plant efficiency	**Plant Mass [tonnes]**
Pessimistic	1,049.00
Baseline	209.8
Optimistic	104.90

We also make the assumption that the mass required for power generation and regolith feed stock collection is equal to the plant mass, and that the setup of the plant does not use ISRU capabilities (Concept of operations 1). Recalling that per BMLL in Con Ops 1, 4.76 tonnes can be delivered to the lunar surface, we can calculate the CO2 emissions of each plant setup, and knowing the relative emissions savings when moving from non-ISRU to ISRU-augmented missions, can calculate the point of emissions break even. Assuming mission elements can be used ten times before being replaced, Con Ops 1's payload emissions ratio is 1:598 and Con Ops 2's ratio is 1:214. This represents a -1:384 (64%) savings in carbon emissions.

Table 18: BO model emissions break even points

Plant efficiency	**Total System Mass [tonnes]**	**CO2 emissions [tonnes]**	**Break even point**		
			Cargo [tonnes]	Trips	Years
Pessimistic	2,098.00	1,254,604.00	3,267.20	295	148
Baseline	419.6	250,920.80	653.44	59	29.5
Optimistic	209.80	125,460.40	326.72	30	15

Table 18 outlines the calculated break even points in cargo mass, number of trips, and years[23] for the carbon emissions related to setting up ISRU capabilities on the lunar surface. It shows that, with a Blue Origin architecture, even optimistic ISRU plant throughputs require 15 years to achieve a carbon emissions breakeven.

[22] One trip per 183 days, considering 20% plant downtime.
[23] Assuming bi-annual BMLL trips.

10 Larger Cislunar Architecture

The system sizing for calculations within this section on larger cislunar architecture were based on the relationships between system mass and total mass as defined by an analysis of currently existing launch systems [197]. Unlike previous sections (section 8 and 9), both the dry mass of the tug and the mass of the payload tanks were not treated as constant but instead modified to be related to propellant and payload mass.

We can identify a minimum of two systems neccesary to form a cislunar transportation network: a tug to bring payload between LEO and NRHO, and a lunar shuttle that supplies a NRHO depot with LOX payload. As discussed in subsection 7.1, for use within missions with low time-criticality we explored the use of WSB orbits and in particular, ballistic lunar transfers (BLT's). BLT's are of particular interest for our investigation into larger cislunar architecture given the extremely low Δv required in cislunar space for both departing and entering NRHO [198, 165].

10.1 LEO-NRHO tugs

We chose NRHO as the parking orbit for the initial cislunar depot due to the very low Δv required to enter a disposal orbit with targeted Earth impact (as low as 10 $m.s^{-1}$)[198]. The flight time of these disposal orbits is not listed in the reference literature, but given their resemblance to BLT's and the assumption they have similar flight times in reverse, we can estimate a time of flight for a return to LEO from NRHO via WSB disposal orbits to be approximately 80-130 days [198, 165].

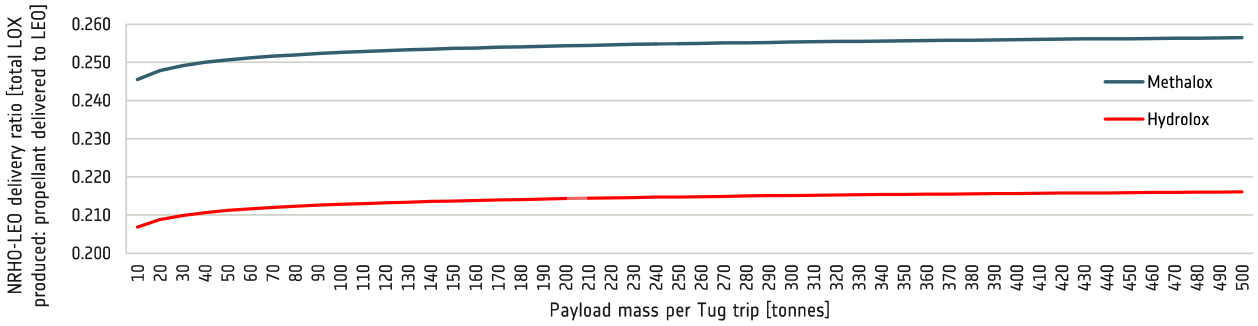

Figure 18: Delivery ratio with increasing payload mass

The values presented in Figure 18 were calculated using a lunar shuttle dry:wet mass ratio of 0.1. Although not constant, Figure 18 shows that the delivery ratio is not significantly impacted by the quantity of outbound payload per tug round-trip from NRHO to LEO. Henceforth we introduce a quasi-static assumption regarding the payload size per tug trip from NRHO to LEO, and take 250 tonnes as our payload mass per trip.

10.2 Lunar Shuttles

By keeping the outbound payload to LEO constant at 250 tonnes, we can investigate the effect of changing the dry:wet mass ratio of the lunar shuttle. Figure 19 shows how the quantity of LOX produced on the surface to the moon decreases for the same delivery to LEO when the dry:wet mass ratio of the lunar shuttle is reduced.

Here we can see that a lunar shuttle mass ratio of above 0.19 is not feasible, and results in a negative mass delivery ratio (i.e. mission does not work; rocket goes kerplunk). We can also see that even if

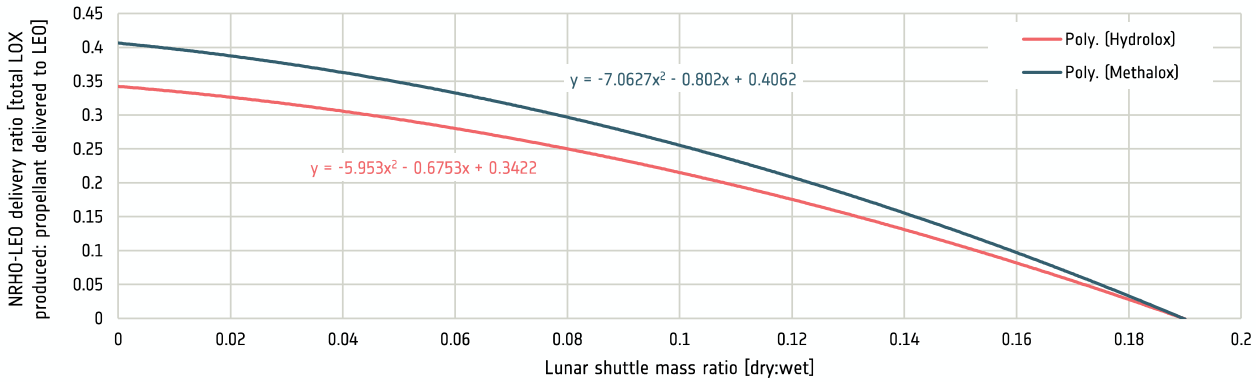

Figure 19: Delivery ratio with increasing dry:wet mass ratio of a lunar shuttle

the dry mass of the system is negligible (0 kg rocket, only propellant for propellant) the maximum achievable delivery ratio is still only 0.34 or 0.41 for hydrolox and methalox respectively. Clearly, any larger cislunar architecture utilising traditional chemical propulsion requires an ISRU plant who's majority output is not deliverable (and thus sellable) LOX, but is instead LOX used to facilitate cislunar transports. In any case, a mass ratio on the order of 0.19 is not yet technically feasible, with Appendix F giving an overview of lunar landers to date.

11 Mars

For our consideration of Mars ISRU-enabled cargo delivery, we consider an initial Con Ops identical to that presented in Figure 6, with the final destination as Mars instead of the Moon. The ISRU-enabled architecture under consideration for Mars is shown in Figure 20, and is very similar to that discussed in Space X's Con Ops 2 (subsubsection 8.1.2), except without the recurring resupply of fuel from Earth.

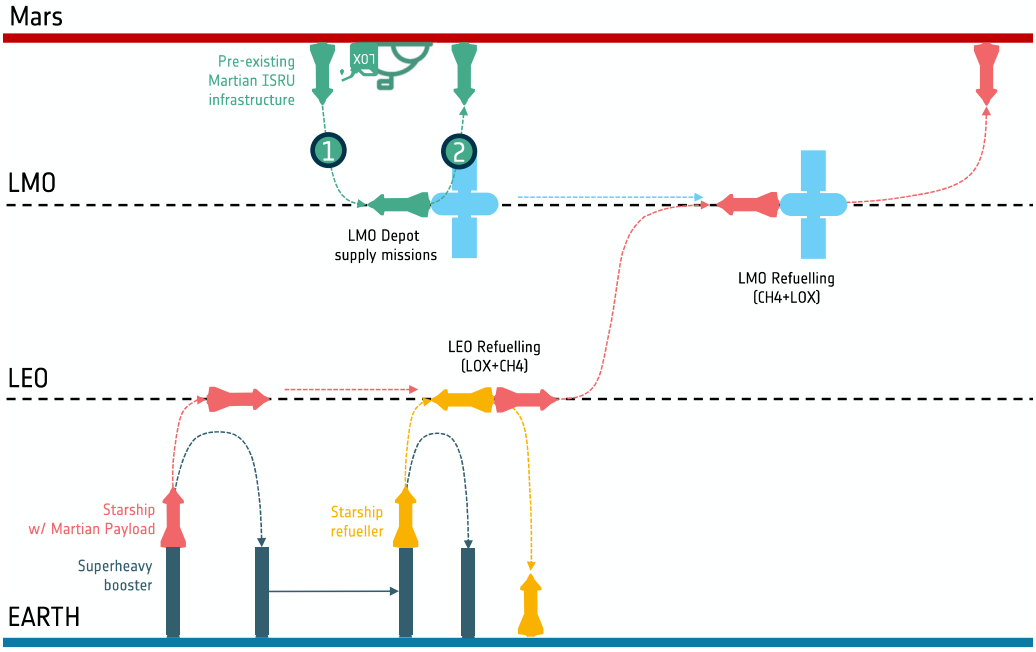

Figure 20: Mars mission Concept of Operations

11.1 Emissions

Consider a direct trip from LEO to the Mars in the 2024 launch window. Using Starship and modifying its dry mass to account for a 10 tonne thermal protection system designed for both aerocapture and atmospheric descent [199, 200], 110 tonnes of payload can be sent to the Martian surface. Like Space X Con Ops 1, this mission requires an initial launch of a Starship into LEO carrying 250 tonnes of payload and some propellant, and 7 additional launches of a tanker to fully refuel the outbound Starship. The carbon emissions associated with this are identical to those outlined in Table 6. Thus for 22,315 tonnes of carbon emissions 110 tonnes of payload can be delivered to the martian surface, giving a direct-to-Mars Starship mission a payload emissions ratio of 1:203.

Let us now consider an ISRU architecture similar to that shown in Figure 7, where an outbound Starship can refuel in low orbit before its final descent. Although the reduction in Δv for the mission leg departing from LEO is still present by not going directly for a landing, it is much less *w.r.t.* a lunar architecture given the atmospheric landing opportunity on Mars. Nonetheless, reducing the neccesary Δv from 6,620 to 5,820 m.s^{-1} allows for a payload increase to 162.6 tonnes. Since both components of Methalox can be produced in-situ on Mars, there is no need to account for emissions related to a resupply of fuel to a low Mars orbit (LMO) depot. As such, the carbon emissions related to the ISRU-enabled mission remain the same as Space X Con Ops 1 and the associated payload emissions ratio is reduced to 1:137.

11.2 Break-even Timeline

As in previous sections, we first need to establish the propellant requirements needed both on the Martian surface and in LMO. Arriving with 162.6 tonnes of payload, Starship requires 69.3 tonnes of propellant refuelled in LMO to perform its descent[24]. Similar to section 8 and 9, we can optimise the composition of a surface shuttle to maximise delivery of propellant to orbit.

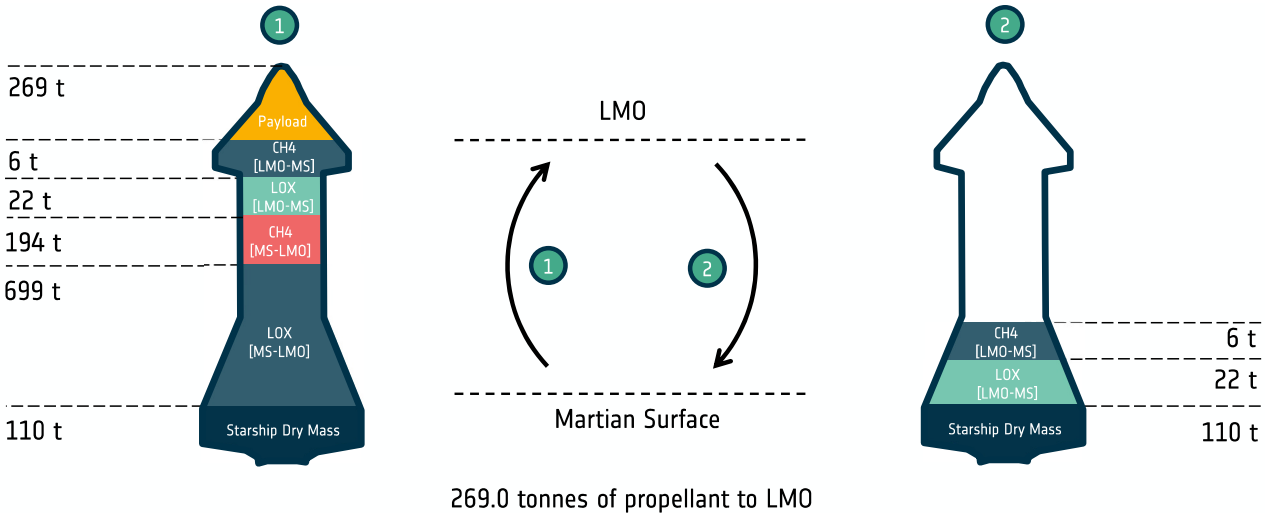

Figure 21: Mars surface shuttle composition

Figure 21 shows the optimised payload of a Martian surface shuttle. Unlike previously discussed shuttles, this one does not require any orbital refuel for its own descent, and instead carries all neccesary propellant from its initial surface launch. We calculate a propellant payload per shuttle trip of 269 tonnes. Per shuttle trip, a surface based Martian-ISRU plant must produce 1,190 tonnes of methalox propellant. Since each inbound Starship requires 0.26 shuttle trips, the propellant production requirement per trip is 309 tonnes.

Mars transfer windows open approximately once every 26 months and thus Mars arrivals are staggered by such. Assuming one inbound cargo mission per transfer window, surface methalox production rates need to be 495 kg.day^{-1}[25]. Utilising subsection 7.4 we obtain the following plant masses.

Table 19: Mars: Estimated ISRU plant mass

Plant efficiency	**Plant Mass [tonnes]**
Pessimistic	495.00
Baseline	99.00
Optimistic	49.50

Here we again assume that the total system mass is composed of plant + power generation + feedstock collection systems, and that it is equal to double the plant mass. With a payload emissions reduction of -1:66, we calculate the following break even timeline estimates for different plant efficiencies.

[24] Assume a Raptor engine Isp reduction from 380 s to 360 s to account for atmospheric conditions.
[25] Again assuming a 20% plant downtime.

Table 20: Mars emissions break even points

Plant efficiency	**Total System Mass [tonnes]**	**CO2 emissions [tonnes]**	**Break even point**		
			Cargo [tonnes]	Trips	Years
Pessimistic	990.00	200,970.00	3,045.00	19	41.2
Baseline	198.00	40,194.00	609.00	4	8.7
Optimistic	99.00	20,097.00	304.50	2	4.3

11.3 Additional Considerations

Like its lunar counterpart, the use of Starship combined with an optimistic plant efficiency would allow relatively few initial cargo launches to be required for ISRU plant setup. In particular, given the lower propellant production rate required *w.r.t.* the lunar case, this Mars mission architecture requires only two initial cargo launches, from which one Starship can be used as a surface shuttle and the other as an orbital depot location. This reduction of initial cost *w.r.t.* the lunar case is on account of the aerobraking capabilities for inbound missions to Mars, and the absence of a Starship refuel-for-ascent requirement. If we begin to consider human missions, the ISRU plant production rate requirements will rise, bringing the break even time with it.

12 Results

Within the Space X model several important results can be observed, The first is that at current plant output:mass ratios not only is an extremely large initial mass required, but it also takes close to three decades to break even. Furthermore, the 36 initial launches neccesary to deliver the required plant mass to the lunar surface would undoubtedly dissuade even the most keen of investors. By increasing the plant efficiency, however, we can see that not only does the break even time fall to half a decade (or even only three years in the optimistic case) but that also the number of initial launches required to set-up the plant drops to 8 (or 4 if optimistic). This undoubtedly drops the initial cost and raises the likelihood of investment.

The Blue Origin model, with its very low payload to the lunar surface for non-ISRU enabled missions, is unlikely to be adopted for the set-up of a surface plant. At current output:mass ratios the two-tonne ISRU plant would require 524 initial launches; clearly unfeasible. Additionally, even at optimistic plant output:mass ratios, the 210 tonnes of mass required by the ISRU plant would still require 53 trips; also unfeasible. The culprit is the low payload delivery per mission in the Blue Origin model. Even with ISRU capabilities, its payload per mission is approximately 3.7% of a Starship mission (11 tonnes vs. 292 tonnes) utilising similar ISRU-enabled architecture. Interestingly, the entire system mass required for a Blue Origin ISRU architecture can be delivered by one disposable and one returning Starship (1x SX Con Ops 1 + 1x SX Con Ops 3), meaning that a combination of launch systems could be used to quickly establish ISRU capabilities on the lunar surface. Although this will not facilitate Starship-level ISRU architecture, it would allow for a stand-alone lunar shuttle in the form of a BMLL, allowing for frequent human transport to-and-from the lunar surface to Gateway.

With the limited thrust-to-weight available from electric propulsion it is clear that, at least for the ascent to LLO/NRHO, chemical propulsion is required. We see that the amount of LOX required to facilitate a larger cislunar refuelling network is highly dependent on the dry:wet mass ratio of the lunar ascender, and that the upper limit is fixed at 0.19 regardless of propellant type. Furthermore, even with a mass-less ascender, more LOX is required as propellant than can be delivered to LEO (delivered:consumed is 35:65 for hydrolox and 40:60 for methalox). This is an unavoidable cost resulting from the unending tyranny of the rocket equation, but it can be mitigated by reducing the dry mass of our shuttle and increasing its payload capacity.

When considering the Mars architecture we can see the reduced plant output requirements that come from having aerobraking capabilities on the descent. Furthermore, the reduced ISRU plant requirements for Mars mission architectures also bring the break even time within very reasonable values. Considering a baseline plant output:mass ratio, only two initial cargo trips to the surface are required, after which break even is achieved within nine years. With an optimistic estimate of plant efficiency, this is reduced to one initial launch and break even within five years. These results, like within the assessment of lunar architecture, stress the importance of continued research into ISRU technology, particularly in increasing their efficiency.

References

[1] Peng Zhang, Wei Dai, Ran Niu, Guang Zhang, Guanghui Liu, Xin Liu, Zheng Bo, Zhi Wang, Haibo Zheng, Chengbao Liu, et al. Overview of the lunar in situ resource utilization techniques for future lunar missions. *Space: Science & Technology*, 3:0037, 2023.

[2] Gerald B Sanders and William E Larson. Integration of in-situ resource utilization into lunar/mars exploration through field analogs. *Advances in Space Research*, 47(1):20–29, 2011.

[3] RR King, KM Edmondson, CM Fetzer, GS Kinsey, H Yoon, RA Sherif, and NH Karam. 40% efficient metamorphic gainp/ gainas/ ge multijunction solar cells. *Applied physics letters*, 90(18), 2007.

[4] Masafumi Yamaguchi, Frank Dimroth, John F Geisz, and Nicholas J Ekins-Daukes. Multijunction solar cells paving the way for super high-efficiency. *Journal of Applied Physics*, 129(24), 2021.

[5] Allen Barnett, Douglas Kirkpatrick, Christiana Honsberg, Duncan Moore, Mark Wanlass, Keith Emery, Richard Schwartz, Dave Carlson, Stuart Bowden, Dan Aiken, Allen Gray, Sarah Kurtz, Larry Kazmerski, Myles Steiner, Jeffery Gray, Tom Davenport, Roger Buelow, Laszlo Takacs, Narkis Shatz, John Bortz, Omkar Jani, Keith Goossen, Fouad Kiamilev, Alan Doolittle, Ian Ferguson, Blair Unger, Greg Schmidt, Erie Christensen, and David Salzman. Very high efficiency solar cell modules. *Progress in Photovoltaics: Research and Applications*, 17(1):75–83, 2009.

[6] Allen Barnett, Xiaoting Wang, Nick Waite, Paola Murcia, Christiana Honsberg, Doug Kirkpatrick, Dan Laubacher, Fouad Kiamilev, Keith Goossen, Mark Wanlass, et al. Initial test bed for very high efficiency solar cell. In *2008 33rd IEEE Photovoltaic Specialists Conference*, pages 1–7. IEEE, 2008.

[7] R.K. Jones, P. Hebert, P. Pien, R.R. King, D. Bhusari, R. Brandt, O. Al-Taher, C. Fetzer, and J. Ermer. Progress in high-efficiency terrestrial concentrator solar cells. In *2009 34th IEEE Photovoltaic Specialists Conference (PVSC)*, pages 002111–002116, 2009.

[8] Anthony J Colozza. Analysis of lunar regolith thermal energy storage. Technical report, 1991.

[9] Brian Tillotson. Regolith thermal energy storage for lunar nighttime power. In *Conference on Advanced SEI Technologies*, page 3420, 1991.

[10] Miranda Fateri, Reinhard Sottong, Matthias Kolbe, Julie Gamer, Matthias Sperl, and Aidan Cowley. Thermal properties of processed lunar regolith simulant. *International Journal of Applied Ceramic Technology*, 16(6):2419–2428, 2019.

[11] Scott W Richter. Experimental determination of in situ utilization of lunar regolith for thermal energy storage. Technical report, 1993.

[12] Sam Schreiner, Laurent Sibille, Jesus Dominguez, Aislinn Sirk, Jeffrey Hoffman, and Gerald Sanders. Development of a molten regolith electrolysis reactor model for lunar in-situ resource utilization". In *8th Symposium on Space Resource Utilization*, page 1180, 2015.

[13] Carlos Montes, Kaylin Broussard, Matthew Gongre, Neven Simicevic, Johanna Mejia, Jessica Tham, Erez Allouche, and Gabrielle Davis. Evaluation of lunar regolith geopolymer binder as a radioactive shielding material for space exploration applications. *Advances in Space Research*, 56(6):1212–1221, 2015.

[14] Rongrong Zhang, Siqi Zhou, and Feng Li. Preparation of geopolymer based on lunar regolith simulant at in-situ lunar temperature and its durability under lunar high and cryogenic temperature. *Construction and Building Materials*, 318:126033, 2022.

[15] Shayan Gholami, Xiang Zhang, Young-Jae Kim, Yong-Rak Kim, Bai Cui, Hyu-Soung Shin, and Jangguen Lee. Hybrid microwave sintering of a lunar soil simulant: Effects of processing parameters on microstructure characteristics and mechanical properties. *Materials & Design*, 220:110878, 2022.

[16] Robert M Tute and Athanasios Goulas. Mechanical behaviour of sulphur-based martian regolith concrete processed under co2-rich conditions. *Icarus*, 417:116134, 2024.

[17] Yifan Sun, Siqi Ma, Qingze Chen, Guoliang Chen, Peigang He, Yaming Wang, Jun Qiu, and Dechang Jia. Lunar regolith simulant-derived 3d-printed geopolymers with optimized mechanical and thermal management properties. *Composites Part A: Applied Science and Manufacturing*, page 108989, 2025.

[18] Yuxin Li, Pengzhi Pan, Shuting Miao, and Yujie Feng. Basalt fiber reinforcement mechanism for geopolymer exposed to lunar temperature environment. *Construction and Building Materials*, 451:138845, 2024.

[19] Mahesh Anand. Lunar water: a brief review. *Earth, Moon, and Planets*, 107:65–73, 2010.

[20] Julie E Kleinhenz and Aaron Paz. Case studies for lunar isru systems utilizing polar water. In *ASCEND 2020*, page 4042. 2020.

[21] NASA Handbook. Nasa human integration design handbook (hidh)-nasa (vol. 3407). *SP-2010*, 2010.

[22] Robert D Green and Julie E Kleinhenz. In-situ resource utilization (isru) living off the land on the moon and mars. In *American Chemical Society National Meeting & Exposition*, number GRC-E-DAA-TN67217, 2019.

[23] Edgardo Santiago-Maldonado and Diane L Linne. Isru system model tool: From excavation to oxygen production. Technical report, 2007.

[24] Martin Elvis. How many ore-bearing asteroids? *Planetary and Space Science*, 91:20–26, 2014.

[25] George F Sowers. The business case for lunar ice mining. *New Space*, 9(2):77–94, 2021.

[26] Dana M Hurley, Matthew A Siegler, Joshua TS Cahill, Anthony Colaprete, Emily Costello, Ariel N Deutsch, Richard C Elphic, Wenzhe Fa, Cesare Grava, Paul O Hayne, et al. Surface volatiles on the moon. *Reviews in Mineralogy and Geochemistry*, 89(1):787–827, 2023.

[27] J Captain, R Elphic, A Colaprete, Kris Zacny, and A Paz. Resource prospector instrumentation for lunar volatiles prospecting, sample acquisition, and processing. In *15th Biennial ASCE Conference on Engineering, Science, Construction, and Operations in Challenging Environments*, pages 278–289. American Society of Civil Engineers Reston, VA, 2016.

[28] Myriam Lemelin, Shuai Li, Erwan Mazarico, Matthew A Siegler, David A Kring, and David A Paige. Framework for coordinated efforts in the exploration of volatiles in the south polar region of the moon. *The Planetary Science Journal*, 2(3):103, 2021.

[29] BG Marsden and AGW Cameron. The earth-moon system; proceedings of an international conference held january 20-21, 1964. *The Earth-Moon System*, 1966.

[30] Reginald A Daly. Origin of the moon and its topography. *Proceedings of the American Philosophical Society*, 90(2):104–119, 1946.

[31] Edward Anders. Origin, age, and composition of meteorites. *Space Science Reviews*, 3:583–714, 1964.

[32] Alastair Graham Walter Cameron. The formation of the sun and planets. *Icarus*, 1(1-6):13–69, 1962.

[33] James Richard Arnold, Masatake Honda, and Devendra Lal. Record of cosmic-ray intensity in the meteorites. *Journal of Geophysical Research*, 66(10):3519–3531, 1961.

[34] James R Arnold. The origin of meteorites as small bodies. ii. the model. *Astrophysical Journal, vol. 141, p. 1536-1547 (1965).*, 141:1536–1547, 1965.

[35] James R Arnold. The origin of meteorites as small bodies. iii. general considerations. *Astrophysical Journal, vol. 141, p. 1548*, 141:1548, 1965.

[36] Thomas B McCord. Spectral study of suggested apollo sites. Technical report, 1973.

[37] Carlé M Pieters, Rachel L Klima, and Robert O Green. Compositional analysis of the moon in the visible and near-infrared regions. *Remote compositional analysis: Techniques for understanding spectroscopy, mineralogy, and geochemistry of planetary surfaces*, pages 368–392, 2019.

[38] Thomas B McCord, Carle Pieters, and MA Feirberg. Multispectral mapping of the lunar surface using groundbased telescopes. Technical report, 1976.

[39] Brian Harvey. *Soviet and Russian lunar exploration*. Springer, 2007.

[40] Colin Trevor Pillinger and AP Gowar. The separation and subdivision of two 0.5 g samples of lunar soil collected by the luna 16 and 20 missions. *Philosophical Transactions of the Royal Society of London. Series A, Mathematical and Physical Sciences*, 284(1319):137–143, 1977.

[41] AL Albee, AA Chodos, AJ Gancarz, EL Haines, DA Papanastassiou, L Ray, F Tera, GJ Wasserburg, and T Wen. Mineralogy, petrology, and chemistry of a luna 16 basaltic fragment, sample b-1. *Earth and Planetary Science Letters*, 13(2):353–367, 1972.

[42] A Cimbalnikova, M Palivcova, J Frana, and A Mastalka. Chemical composition of crystalline rock fragments from luna 16 and luna 20 fines. In *NASA, Washington The Soviet-Am. Conf. on Cosmochem. of the Moon and Planets, pt. 1*, 1977.

[43] L Bakos, M Chayka, L Cher, A Cheke, NN Dogadkin, A Elek, K Kulchar, A Nagy, DL Nagy, and E Szabo. Investigation of the composition of the luna 16 lunar sample. In *NASA, Washington The Soviet-Am. Conf. on Cosmochem. of the Moon and Planets, pt. 1*, 1977.

[44] TRENDS IN APOLLO SAMPLES. Lunar samples: Apollo collection tools, curation handling, surveyor iii and.

[45] BA Lomax, M Conti, N Khan, and MD Symes. The metalysis-ffc-cambridge process for the efficient production of oxygen and metals on the lunar surface. *Lunar ISRU 2019-Developing a New Space Economy Through Lunar Resources and Their Utilization*, 2152:5023, 2019.

[46] WC Feldman, DJ Lawrence, RC Elphic, BL Barraclough, S Maurice, I Genetay, and AB Binder. Polar hydrogen deposits on the moon. *Journal of Geophysical Research: Planets*, 105(E2):4175–4195, 2000.

[47] David J Lawrence. Volatiles on the lunar surface and subsurface. In *Encyclopedia of Lunar Science*, pages 1244–1249. Springer, 2023.

[48] DL Mitchell, JS Halekas, RP Lin, S Frey, LL Hood, MH Acuña, and A Binder. Global mapping of lunar crustal magnetic fields by lunar prospector. *Icarus*, 194(2):401–409, 2008.

[49] DJ Lawrence, WC Feldman, BL Barraclough, AB Binder, RC Elphic, S Maurice, and DR Thomsen. Global elemental maps of the moon: The lunar prospector gamma-ray spectrometer. *Science*, 281(5382):1484–1489, 1998.

[50] Patrick Pinet, Priscilla Cerroni, J-L Josset, Stéphane Beauvivre, Serge Chevrel, Karri Muinonen, Yves Langevin, Maria Antonella Barucci, Maria Cristina De Sanctis, Yu Shkuratov, et al. The advanced moon micro-imager experiment (amie) on smart-1: Scientific goals and expected results. *Planetary and Space Science*, 53(13):1309–1318, 2005.

[51] Yu G Shkuratov, MA Kreslavsky, DG Stankevich, VG Kaydash, P Pinet, VV Shevchenko, BH Foing, and J-L Josset. The smart-1 mission: photometric studies of the moon with the amie camera. *Solar System Research*, 37:251–259, 2003.

[52] Priscilla Cerroni, Maria Cristina de Sanctis, Jean-Luc Josset, Stéphane Beauvivre, Detlef Koschny, Patrick Pinet, Serge Chevrel, Yves Langevin, Maria Antonella Barucci, P Plancke, et al. Preliminary analysis of colour information from amie on smart-1. In *37th Annual Lunar and Planetary Science Conference*, volume 37, page 1831, 2006.

[53] BH Foing. Smart-1 results and lessons for future exploration. In *EGU General Assembly Conference Abstracts*, page 13267, 2009.

[54] B. Foing. Combined analysis results from smart-1 archive data and recent lunar missions. 2:1076–1077, 01 2012.

[55] Carle M Pieters, JN Goswami, RN Clark, M Annadurai, J Boardman, B Buratti, J-P Combe, MD Dyar, R Green, JW Head, et al. Character and spatial distribution of oh/h2o on the surface of the moon seen by m3 on chandrayaan-1. *science*, 326(5952):568–572, 2009.

[56] R Sridharan, SM Ahmed, Tirtha Pratim Das, P Sreelatha, P Pradeepkumar, Neha Naik, and Gogulapati Supriya. 'direct'evidence for water (h2o) in the sunlit lunar ambience from chace on mip of chandrayaan i. *Planetary and Space Science*, 58(6):947–950, 2010.

[57] Akira Fujiwara, J Kawaguchi, DK Yeomans, M Abe, T Mukai, T Okada, J Saito, H Yano, M Yoshikawa, DJ Scheeres, et al. The rubble-pile asteroid itokawa as observed by hayabusa. *Science*, 312(5778):1330–1334, 2006.

[58] Hisayoshi Yurimoto, Ken-ichi Abe, Masanao Abe, Mitsuru Ebihara, Akio Fujimura, Minako Hashiguchi, Ko Hashizume, Trevor R Ireland, Shoichi Itoh, Juri Katayama, et al. Oxygen isotopic compositions of asteroidal materials returned from itokawa by the hayabusa mission. *Science*, 333(6046):1116–1119, 2011.

[59] Tetsuya Yokoyama, Nicolas Dauphas, Ryota Fukai, Tomohiro Usui, Shogo Tachibana, Maria Schönbächler, Henner Busemann, Masanao Abe, and Toru Yada. The chemical composition of ryugu: Prospects as a reference material for solar system composition. *arXiv preprint arXiv:2405.04500*, 2024.

[60] Steven Squyres and Claude Canizares. Science results from the mars exploration rover mission. *Bulletin of the American Academy of Arts and Sciences*, 61(4):23–28, 2008.

[61] Steven W Squyres, Raymond E Arvidson, Diane Bollen, James F Bell III, Johannes Brueckner, Nathalie A Cabrol, Wendy M Calvin, Michael H Carr, Philip R Christensen, Benton C Clark, et al. Overview of the opportunity mars exploration rover mission to meridiani planum: Eagle crater to purgatory ripple. *Journal of Geophysical Research: Planets*, 111(E12), 2006.

[62] DS Lauretta, SS Balram-Knutson, Eea Beshore, WV Boynton, C Drouet d'Aubigny, DN DellaGiustina, HL Enos, DR Golish, CW Hergenrother, ES Howell, et al. Osiris-rex: sample return from asteroid (101955) bennu. *Space Science Reviews*, 212:925–984, 2017.

[63] Dolan E Highsmith and Roger C Thompson. Osiris-rex conjunction screenings: Earth gravity assist and earth return analysis and results. In *AAS/AIAA Astrodynamics Specialist Conference*, 2024.

[64] Dante S. Lauretta, Harold C. Connolly Jr, Jeffrey N. Grossman, Anjani T. Polit, and the OSIRIS-REx Sample Analysis Team. Osiris-rex sample analysis plan – revision 3.0, 2023.

[65] Daniel R Wibben, Andrew Levine, Samantha Rieger, Jason M Leonard, Coralie Adam, Leilah McCarthy, Eric Sahr, Derek Nelson, Peter G Antreasian, Michael C Moreau, et al. Osiris-rex post-tag observation trajectory design and navigation performance. In *Proceedings of the 44th Annual American Astronautical Society Guidance, Navigation, and Control Conference, 2022*, pages 1551–1571. Springer, 2022.

[66] DS Lauretta, CD Adam, AJ Allen, R-L Ballouz, OS Barnouin, KJ Becker, T Becker, CA Bennett, EB Bierhaus, BJ Bos, et al. Spacecraft sample collection and subsurface excavation of asteroid (101955) bennu. *Science*, 377(6603):285–291, 2022.

[67] David W. Brown. How nasa brought an asteroid to earth. *The New Yorker*, 2023. Accessed 23 May 2025.

[68] Chunlai Li, Yan Su, Elena Pettinelli, Shuguo Xing, Chunyu Ding, Jianjun Liu, Xin Ren, Sebastian E. Lauro, Francesco Soldovieri, Xingguo Zeng, Xingye Gao, Wangli Chen, Shun Dai, Dawei Liu, Guangliang Zhang, Wei Zuo, Weibin Wen, Zhoubin Zhang, Xiaoxia Zhang, and Hongbo Zhang. The moon's farside shallow subsurface structure unveiled by chang'e-4 lunar penetrating radar. *Science Advances*, 6(9):eaay6898, February 2020. Published 26 February 2020.

[69] Chunlai Li, Hao Hu, Meng-Fei Yang, Zhao-Yu Pei, Qin Zhou, Xin Ren, Bin Liu, Dawei Liu, Xingguo Zeng, Guangliang Zhang, Hongbo Zhang, Jianjun Liu, Qiong Wang, Xiangjin Deng, Caijin Xiao, Yonggang Yao, Dingshuai Xue, Wei Zuo, Yan Su, Weibin Wen, and Ziyuan Ouyang. Characteristics of the lunar samples returned by the chang'e-5 mission. *National Science Review*, 9:nwab188, 2022. Advance access publication 14 October 2021.

[70] Chengxiang Yin, Jian Chen, Xiaohui Fu, Haijun Cao, Xuejin Lu, Yiheng Liu, Jin Li, Siyue Chi, Xiaojia Zeng, and Zongcheng Ling. Petrogenesis of chang'e-6 basalts and implication for the young volcanism on the lunar farside. *The Astrophysical Journal Letters*, 981:L2, March 2025.

[71] Weiren Wu, Qiong Wang, Yuhua Tang, Guobin Yu, Jizhong Liu, Wei Zhang, Yuanming Ning, and Liangliang Lu. Design of chang'e-4 lunar farside soft-landing mission. *Journal of Deep Space Exploration*, 4(2):111–117, 2017.

[72] Michael WM Jones, David T Flannery, Joel A Hurowitz, Michael M Tice, Christoph E Schrank, Abigail C Allwood, Nicholas J Tosca, David C Catling, Scott J VanBommel, Abigail L Knight, et al. In situ crystallographic mapping constrains sulfate precipitation and timing in jezero crater, mars. *Science Advances*, 11(16):eadt3048, 2025.

[73] KA Farley, KM Stack, DL Shuster, BHN Horgan, JA Hurowitz, JD Tarnas, JI Simon, VZ Sun, EL Scheller, KR Moore, et al. Aqueously altered igneous rocks sampled on the floor of jezero crater, mars. *Science*, 377(6614):eabo2196, 2022.

[74] Marc D Fries, Carina Lee, Rohit Bhartia, Joseph Razzell Hollis, Luther W Beegle, Kyle Uckert, Trevor G Graff, William Abbey, Zachary Bailey, Eve L Berger, et al. The sherloc calibration target on the mars 2020 perseverance rover: Design, operations, outreach, and future human exploration functions. *Space Science Reviews*, 218(6):46, 2022.

[75] Abigail C Allwood, Joel A Hurowitz, Benton C Clark, Luca Cinquini, Scott Davidoff, Robert W Denise, W Timothy Elam, Marc C Foote, David T Flannery, James H Gerhard, et al. The pixl instrument on the mars 2020 perseverance rover. *arXiv preprint arXiv:2103.07001*, 2021.

[76] S Hamran, D Paiges, HEF Amundsen, T Berger, S Brovoll, L Carter, TM Casademont, L Damsgård, H Dypvik, S Eide, et al. Exploring the martian subsurface with the rimfax ground penetrating radar on the mars 2020 perseverance rover. In *84th EAGE Annual Conference & Exhibition*, volume 2023, pages 1–5. European Association of Geoscientists & Engineers, 2023.

[77] Jeffrey A Hoffman, Michael H Hecht, Donald Rapp, Joseph J Hartvigsen, Jason G SooHoo, Asad M Aboobaker, John B McClean, Andrew M Liu, Eric D Hinterman, Maya Nasr, et al. Mars oxygen isru experiment (moxie)—preparing for human mars exploration. *Science Advances*, 8(35):eabp8636, 2022.

[78] John B McClean, Jeffrey A Hoffman, Michael H Hecht, Asad M Aboobaker, Koorosh R Araghi, S Elangovan, Christopher R Graves, Joseph J Hartvigsen, Eric D Hinterman, Andrew M Liu, et al. Pre-landing plans for mars oxygen in-situ resource utilization experiment (moxie) science operations. *Acta astronautica*, 192:301–313, 2022.

[79] Michael Hecht, J Hoffman, D Rapp, J McClean, J SooHoo, R Schaefer, A Aboobaker, J Mellstrom, J Hartvigsen, F Meyen, et al. Mars oxygen isru experiment (moxie). *Space Science Reviews*, 217:1–76, 2021.

[80] Jeffrey A Hoffman, Eric R Hinterman, Michael H Hecht, Donald Rapp, and Joseph J Hartvigsen. 18 months of moxie (mars oxygen isru experiment) operations on the surface of mars-preparing for human mars exploration. *Acta Astronautica*, 210:547–553, 2023.

[81] Donald Rapp and Eric Hinterman. Adapting a mars isru system to the changing mars environment. *Space: Science & Technology*, 3:0041, 2023.

[82] European Space Agency. Exomars discovers new gas and traces water loss on mars, 2021. Accessed 23 May 2025.

[83] European Space Agency. First results from the exomars trace gas orbiter, 2019. Accessed 23 May 2025.

[84] European Space Agency. Exomars mission (2022) – mission overview, 2020. Last updated 12 Mar 2020.

[85] European Space Agency. Exomars rover, 2020. Accessed 23 May 2025.

[86] E. Sefton-Nash, J. L. Vago, L. Joudrier, F. Haessig, A. Williams, P. Mitschdoerfer, D. Koschny, T. Lim, A. Toni, R. Fonteyne, C. Orgel, and R. Bahia. Exomars 2022 rover science operations preparations. In *European Planetary Science Congress*, pages EPSC2021–773, September 2021. Provided by the SAO/NASA Astrophysics Data System.

[87] Engineering National Academies of Sciences, Medicine, et al. Report series: Committee on biological and physical sciences in space: Using commercial lunar payload services (clps) to achieve lunar biological and physical science objectives: Proceedings of a workshop. 2021.

[88] Sally Cahill and David Mauro. Commercial lunar payloads services (clps). In *NASA Ames Research*, 2022.

[89] NASA Office of Inspector General. Nasa's commercial lunar payload services initiative. Audit Report IG-24-013, National Aeronautics and Space Administration, Washington, D.C., June 2024. Published 6 June 2024.

[90] Paul B Niles. Summary of the contracted deliveries of nasa payloads to the moon via commercial lunar payload services (clps). In *56th Lunar and Planetary Science Conference (LPSC)*, 2025.

[91] Daniel Andrews. Viper: Systems integration status. In *74th International Astronautical Congress (IAC)*, 2023.

[92] Daniel Andrews. Viper rover: Flight build and environmental test status. In *75th International Astronautical Congress (IAC)*, 2024.

[93] Francesco Latini, Simone Pirrotta, Raffaele Mugnuolo, Michéle Lavagna, Alice Dottori, Ivan Troisi, et al. Oracle: an isru technological demonstrator for oxygen production on the moon. In *11th European Lunar Symposium*, 2023.

[94] Francesco Latini, Simone Pirrotta, Raffaele Mugnuolo, M Lavagna, I Troisi, A Dottori, et al. Development status of oracle, the isru demonstrator for oxygen extraction on the moon. In *IAF Space Exploration Symposium (75th International Astronautical Congress)*, pages 265–271. International Astronautical Federation (IAF), 2024.

[95] I G Mitrofanov, A B Sanin, WV Boynton, G Chin, JB Garvin, D Golovin, LG Evans, K Harshman, AS Kozyrev, ML Litvak, et al. Hydrogen mapping of the lunar south pole using the lro neutron detector experiment lend. *science*, 330(6003):483–486, 2010.

[96] LO Magaña, KD Retherford, BD Byron, AR Hendrix, C Grava, KE Mandt, U Raut, E Czajka, PO Hayne, DM Hurley, et al. Lro-lamp lunar south pole cold traps: Assessment of h2o and potential co2 and nh3 reserves. *Journal of Geophysical Research: Planets*, 128(8):e2023JE007863, 2023.

[97] ES Costello and PG Lucey. The age and evolution of lunar micro cold traps at the scale of surface exploration. *Geophysical Research Letters*, 51(1):e2023GL105369, 2024.

[98] LO Magaña, KD Retherford, BD Byron, AR Hendrix, C Grava, KE Mandt, U Raut, E Czajka, PO Hayne, DM Hurley, et al. Lro-lamp survey of lunar south pole cold traps: Implication for the presence of condensed h2o. *Journal of Geophysical Research: Planets*, 127(11):e2022JE007301, 2022.

[99] Carolyn H van der Bogert, Harald Hiesinger, Isacco Pretto, Floriano Venditti, Alexander Lewang, Lutz Richter, David Binns, and Philipp Gläser. Science-rich sites for in situ resource utilization characterization and end-to-end demonstration missions. *The Planetary Science Journal*, 2(2):84, 2021.

[100] Molly S Anderson, Sean M Fuller, and Jon Olansen. Gateway at the crossroads of sustainable lunar exploration. In *74th International Astronautical Congress (IAC 2023)*, number IAC-23-D3. 2A. 1, 2023.

[101] Roger Dendy, Daniel J Zeleznikar, and Michael J Zemba. Nasa lunar exploration–gateway's power and propulsion element communications links. In *38th International Communications Satellite Systems Conference (ICSSC 2021)*, volume 2021, pages 1–8. IET, 2021.

[102] MS Uludag, Najla Alahmadi, Emma Lehnhardt, Jackelynne Silva-Martinez, Eric Dahlstrom, Aaron Thornton, ELISABETTA MARRUCCI, NA Duursma, A Battegazzore, et al. Defining mars-forward capabilities of the lunar gateway space station. 2024.

[103] National Aeronautics and Space Administration. Moon to mars architecture white papers: 2024 architecture concept review. White-paper compilation, Exploration Systems Development Mission Directorate, NASA, Washington, D.C., 2024. Accessed 23 May 2025.

[104] National Aeronautics and Space Administration. The artemis plan: Nasa's lunar exploration program overview. Program Plan NP-2020-05-2853-HQ, NASA, September 2020. Released September 2020.

[105] Gerald B. Sanders, Julie E. Kleinhenz, and Diane L. Linne. Nasa plans for *In Situ* resource utilization (isru): Development, demonstration, and implementation. Presentation at the 44th COSPAR Scientific Assembly, July 2022. Slides available from NASA JSC.

[106] Julie Kleinhenz and Gerald B. Sanders. Isru potential water-mine sites: Preliminary evaluation for the nasa artemis campaign. In *Space Resources Roundtable XXIV*, Golden, CO, June 2022. 7–10 June 2022.

[107] Julie E. Kleinhenz and Gerald B. Sanders. Evaluation of the nasa artemis regions of interest for isru water-mine potential. In *Proceedings of AIAA ASCEND 2022*, Las Vegas, NV, 2022. Paper presented 24 Oct 2022.

[108] Gerald B. Sanders and Julie E. Kleinhenz. Update on nasa's isru development and mission plans for the artemis program. In *75th International Astronautical Congress (IAC 2024)*, pages IAC–24–A5–x82120, Milan, Italy, October 2024.

[109] Diane L Linne, Gerald B Sanders, Stanley O Starr, David J Eisenman, Nantel H Suzuki, Molly S Anderson, Terrence F O'Malley, and Koorosh R Araghi. Overview of nasa technology development for in-situ resource utilization (isru). In *International Astronautical Congress*, number GRC-E-DAA-TN46532, 2017.

[110] Matthew G Shaw, Geoffrey A Brooks, M Akbar Rhamdhani, Alan R Duffy, and Mark I Pownceby. Thermodynamic modelling of ultra-high vacuum thermal decomposition for lunar resource processing. *Planetary and Space Science*, 204:105272, 2021.

[111] JOHN Matchett. Production of lunar oxygen through vacuum pyrolysis. *School of Engineering and Applied Science. George Washington University Washington, DC, USA*, 2006.

[112] HM Sargeant, FAJ Abernethy, SJ Barber, IP Wright, M Anand, S Sheridan, and A Morse. Hydrogen reduction of ilmenite: Towards an in situ resource utilization demonstration on the surface of the moon. *Planetary and Space Science*, 180:104751, 2020.

[113] HM Sargeant, FAJ Abernethy, M Anand, SJ Barber, P Landsberg, S Sheridan, I Wright, and A Morse. Feasibility studies for hydrogen reduction of ilmenite in a static system for use as an isru demonstration on the lunar surface. *Planetary and Space Science*, 180:104759, 2020.

[114] Matthew Shaw. The carbothermal reduction of lunar regolith under high-vacuum conditions. *Vacuum*, 233:114039, 2025.

[115] Jack Robinot, Sylvain Rodat, Stéphane Abanades, Alexis Paillet, and Aidan Cowley. Review of in-situ oxygen extraction from lunar regolith with focus on solar thermal and laser vacuum pyrolysis. *Acta Astronautica*, 2025.

[116] Ivan Troisi, Paolo Lunghi, and Michéle Lavagna. Oxygen extraction from lunar dry regolith: Thermodynamic numerical characterization of the carbothermal reduction. *Acta astronautica*, 199:113–124, 2022.

[117] Shuai Li, Paul G Lucey, Ralph E Milliken, Paul O Hayne, Elizabeth Fisher, Jean-Pierre Williams, Dana M Hurley, and Richard C Elphic. Direct evidence of surface exposed water ice in the lunar polar regions. *Proceedings of the National Academy of Sciences*, 115(36):8907–8912, 2018.

[118] Qinggong Wang, Juping Gu, Yong Pang, Yang Zuo, Guidong Mo, and Xingwang Zhang. Water extraction and collection from icy lunar regolith by microwave heating. *Acta Astronautica*, 2025.

[119] James D Cole, Sungwoo Lim, Hannah M Sargeant, Simon Sheridan, Mahesh Anand, and Andrew Morse. Water extraction from icy lunar simulants using low power microwave heating. *Acta astronautica*, 209:95–103, 2023.

[120] NASA. Polar resources ice mining experiment-1 (prime-1). `https://www.nasa.gov/mission/polar-resources-ice-mining-experiment-1-prime-1/`, 2022. Accessed: 2025-05-18.

[121] JJ Cilliers, JN Rasera, and K Hadler. Estimating the scale of space resource utilisation (sru) operations to satisfy lunar oxygen demand. *Planetary and Space Science*, 180:104749, 2020.

[122] Xiao Chen, Shiyu Yang, Guoxin Chen, Wei Xu, Lijian Song, Ao Li, Hangboce Yin, Weixing Xia, Meng Gao, Ming Li, et al. Massive water production from lunar ilmenite through reaction with endogenous hydrogen. *The Innovation*, 5(5), 2024.

[123] Geoffrey A Landis. Materials refining on the moon. *Acta astronautica*, 60(10-11):906–915, 2007.

[124] Geoffrey A Landis. Materials refining for solar array production on the moon. In *29th Photovoltaic Specialists Conference*, number NASA/TM-2005-214014, 2005.

[125] Carsten Schwandt, Greg R Doughty, and Derek J Fray. The ffc-cambridge process for titanium metal winning. *Key Engineering Materials*, 436:13–25, 2010.

[126] Timon Schild, Bethany A Lomax, Melchiorre Conti, Gwenaelle Aridon, Dennis Harries, and Kathryn Hadler. Characterization of metal products from the molten salt electrolysis of lunar highland regolith simulants. *Acta Astronautica*, 232:1–13, 2025.

[127] Bethany A Lomax, Áron Selmeci, Alexander Rützler, Timon Schild, Mark D Symes, Emily Bonsall, Christian Schröder, Melchiorre Conti, Robert Lindner, and James D Carpenter. Identifying an efficient endpoint for oxygen extraction from lunar regolith simulant pellets using molten salt electrolysis. *Acta Astronautica*, 2025.

[128] NASA. Polar ice mining system for lunar resource acquisition. `https://techport.nasa.gov/projects/116413`, 2023. Accessed: 2025-05-18.

[129] Francisco J Guerrero-Gonzalez and Paul Zabel. System analysis of an isru production plant: Extraction of metals and oxygen from lunar regolith. *Acta Astronautica*, 203:187–201, 2023.

[130] Gerald B Sanders, Aaron Paz, Lara Oryshchyn, Koorosh Araghi, Anthony Muscatello, Diane L Linne, Julie E Kleinhenz, and Todd Peters. Mars isru for production of mission critical consumables-options, recent studies, and current state of the art. In *AIAA SPACE 2015 Conference and Exposition*, page 4458, 2015.

[131] Angel Abbud-Madrid, David Beaty, Dale Boucher, Ben Bussey, Richard Davis, Leslie Gertsch, Lindsay Hays, Julie Kleinhenz, Michael Meyer, Michael Moats, et al. Mars water in-situ resource utilization (isru) planning (m-wip) study. *Report of the Mars Water In-Situ Resource Utilization (ISRU) Planning (M-WIP) Study*, 90, 2016.

[132] Jeffrey A Hoffman, Donald Rapp, and Michael Hecht. The mars oxygen isru experiment (moxie) on the mars 2020 rover. In *AIAA Space 2015 Conference and Exposition*, page 4561, 2015.

[133] Yu Chang Kim. Exploring water production dynamics in a sabatier reactor: A comprehensive experimental investigation. *Fuel*, 396:135298, 2025.

[134] Tony Muscatello. Atmospheric capture on mars (and processing). In *The Technology and Future of In-Situ Resource Utilization (ISRU) Seminar*, number KSC-E-DAA-TN39558, 2017.

[135] Anthony C. Muscatello and Edgardo Santiago-Maldonado. Mars in situ resource utilization technology evaluation. Technical Report NASA/TM–2012–217775, NASA Kennedy Space Center, 2012. Accessed: 2025-05-19.

[136] Carolina Franco, Robert W. Devor, Sarah J. Snyder, Elspeth Petersen, and Paul E. Hintze. Study of sabatier catalyst performance for a mars isru propellant production plant. In *49th International Conference on Environmental Systems (ICES)*, number ICES-2019-077, Boston, Massachusetts, 2019. Accessed: 2025-05-19.

[137] NASA. *Human Exploration of the Moon: A Comprehensive Framework for Future Missions*. Number SP-2009-566 in NASA Special Publication. NASA Headquarters, 2009. Accessed: 2025-05-19.

[138] Sylvain Piqueux, Jennifer Buz, Christopher S Edwards, Joshua L Bandfield, Armin Kleinböhl, David M Kass, Paul O Hayne, MCS, and Themis Teams. Widespread shallow water ice on mars at high latitudesand midlatitudes. *Geophysical Research Letters*, 46(24):14290–14298, 2019.

[139] Colin M Dundas, Michael T Mellon, Susan J Conway, Ingrid J Daubar, Kaj E Williams, Lujendra Ojha, James J Wray, Ali M Bramson, Shane Byrne, Alfred S McEwen, et al. Widespread exposures of extensive clean shallow ice in the midlatitudes of mars. *Journal of Geophysical Research: Planets*, 126(3):e2020JE006617, 2021.

[140] Hongqing Song, Jie Zhang, Yang Liu, Yueqiang Sun, and Dongdong Ni. Investigation of in situ thermal mining of shallow excess ice at martian northern midlatitudes. *Advances in Space Research*, 72(11):4997–5012, 2023.

[141] Kris Zacny, Gale Paulsen, Christopher P McKay, et al. Reaching 1 m deep on mars: The icebreaker drill. *Astrobiology*, 13(12):1166–1198, 2013.

[142] K. Zacny and G. Cooper. Considerations, constraints and strategies for drilling on mars. *Planetary and Space Science*, 54(4):345–356, 2006.

[143] Dominik Höber, Andreas Taschner, and Eric Fimbinger. Excavation and conveying technologies for space applications. *Berg- und Hüttenmännische Monatshefte*, 166(2):95–103, 2021.

[144] Anthony C. Muscatello and Edgardo Santiago-Maldonado. Mars in situ resource utilization technology evaluation. Technical Report NASA/TM–2012–217775, NASA Kennedy Space Center, 2012.

[145] G. Sanders and J. Smith. Vacuum–scale demonstration of molten salt electrolysis for lunar oxygen. In *Proceedings of the AIAA Propellant and Energy Forum*, Orlando, FL, 2024. NASA–KSC internal report KSC-ISRU-24-17.

[146] J. A. Hoffman and M. H. Hecht. Scaling solid-oxide electrolysis from the MOXIE flight unit to a human-class oxygen plant. *Journal of Aerospace Engineering*, 35(4):04022055, 2022.

[147] B. G. (Ed.) Drake. Mars Design Reference Architecture 5.0. Technical Report NASA/SP–2009-566, NASA, Washington, DC, 2009.

[148] P. O. Hayne, O. Aharonson, and D. A. Paige. The distribution and stability of surface water ice on the moon. *Nature Astronomy*, 5:169–177, 2021.

[149] NASA. Apollo 11 mission report: Preflight, flight, and postflight of apollo 11. Technical Memorandum NASA-TM-X-62633, MSC-00171, NASA, November 1969. Work of the US Gov. Public Use Permitted.

[150] NASA. Nasa's artemis iv: Building first lunar space station, May 2024. Accessed: 2025-05-18.

[151] Christopher McLean, Shuvo Mustafi, Laurie Walls, Brian Pitchford, Mark Wollen, and Jeff Schmidt. Simple, robust cryogenic propellant depot for near term applications. In *2011 Aerospace Conference*, pages 1–24. IEEE, 2011.

[152] Joe T Howell, John C Mankins, and John C Fikes. In-space cryogenic propellant depot stepping stone. *Acta Astronautica*, 59(1-5):230–235, 2006.

[153] Christopher A Jones, Alejandro R Pensado, Matteo Clark, Marie Ivanco, Emily Judd, Jordan Klovstad, and David M Reeves. Cost breakeven analysis of lunar in-situ propellant production for human missions to the moon and mars. In *ASCEND 2020*, page 4041. 2020.

[154] Michael Galluzzi, Edgar Zapata, Oliver De Weck, and Martin Steele. Foundations of supply chain management for space application. In *Space 2006*, page 7234. 2006.

[155] Bartosz Sawik. Space mission risk, sustainability and supply chain: review, multi-objective optimization model and practical approach. *Sustainability*, 15(14):11002, 2023.

[156] Charles W Pierce, Patrick S McRight, Jonathan Stephens, Wesley Johnson, Brian Nufer, and Benjamin Reed. A review of in-space propellant transfer capabilities and challenges for missions involving propellant resupply. 2020.

[157] Alessia Simonini, Michael Dreyer, Annafederica Urbano, Francesco Sanfedino, Takehiro Himeno, Philipp Behruzi, Marc Avila, Jorge Pinho, Laura Peveroni, and Jean-Baptiste Gouriet. Cryogenic propellant management in space: open challenges and perspectives. *npj Microgravity*, 10(1):34, 2024.

[158] Gerald Sanders, Julie Kleinhenz, and Diane Linne. Nasa plans for in situ resource utilization (isru) development, demonstration, and implementation. In *Committee on Space Research (COSPAR) 2022*, 2022.

[159] Robert L Bayt. Crewed deep space systems human rating certification requirements and standards for nasa missions. Technical report, National Aeronautics and Space Administration, 2024.

[160] National Aeronautics and Space Administration. Nasa technical requirements for human-rating. NASA Technical Standard NASA-STD-8719.29, NASA, 2023. Baseline version approved on 2023-12-11.

[161] IN-SPACE PROPELLANT. In-space propellant logistics. 1972.

[162] David Kornuta, Angel Abbud-Madrid, Jared Atkinson, Jonathan Barr, Gary Barnhard, Dallas Bienhoff, Brad Blair, Vanessa Clark, Justin Cyrus, Blair DeWitt, et al. Commercial lunar propellant architecture: A collaborative study of lunar propellant production. *Reach*, 13:100026, 2019.

[163] F Renk, M Landgraf, L Bucci, et al. Refined mission analysis for heracles-a robotic lunar surface sample return mission utilizing human infrastructure. In *2018 AAS/AIAA astrodynamics specialist conference*, pages 1–12, 2018.

[164] Max Braun, Nick Gollins, Veronica Trivino, Shahrzad Hosseini, Rogier Schonenborg, and Markus Landgraf. Human lunar return: An analysis of human lunar exploration scenarios within the upcoming decade. *Acta Astronautica*, 177:737–748, 2020.

[165] Nathan L Parrish, Ethan Kayser, Shreya Udupa, Jeffrey S Parker, Bradley W Cheetham, and Diane C Davis. Survey of ballistic lunar transfers to near rectilinear halo orbit. In *AAS/AIAA Astrodynamics Specialists Conference*, pages 1–20, 2019.

[166] Dale C Arney, Christopher A Jones, Jordan Klovstad, DR Komar, Kevin Earle, Robert Moses, Dennis Bushnell, and Hilary Shyface. Sustaining human presence on mars using isru and a reusable lander. In *AIAA Space 2015 Conference and Exposition*, page 4479, 2015.

[167] Stanford Advanced Materials. Aluminum lithium (al-li) alloy 2195, 2023. `https://www.samaterials.com/aluminium/1774-2195-aluminum-lithium-alloy.html` [Accessed: 07/11/2023].

[168] European Aluminium. Global arrangement on sustainable aluminium, 2023. `https://european-aluminium.eu/wp-content/uploads/2022/10/22-08-31-european-aluminium_gasa-position-paper.pdf` [Accessed: 07/11/2023].

[169] R. PELL and J. J. LINDSAY. Comparative life cycle assessment study of solid state and lithium-ion batteries for electric vehicle application in europe, 2022. `https://www.transportenvironment.org/wp-content/uploads/2022/07/2022_07_LCA_research_by_Minviro.pdf` [Accessed: 07/11/2023].

[170] International Copper Association. Copper environmental profile, 2022. `https://copperalliance.org/wp-content/uploads/2021/07/ICA-EnvironmentalProfileHESD-201803-FINAL-LOWRES-1.pdf` [Accessed: 07/11/2023].

[171] Simone Ehrenberger. Carbon footprint of magnesium production and its use in transport applications. 2020.

[172] World Stainless. World stainless co2 emissions report, 2022. `https://www.worldstainless.org/files/issf/non-image-files/PDF/worldstainless_CO2_Emissions_Report.pdf#page=7` [Accessed: 07/11/2023].

[173] Air Liquide. Air liquide technology handbook, 2022. `https://engineering.airliquide.com/sites/engineering/files/2022-09/technohandbook11oct.pdf` [Accessed: 07/11/2023].

[174] European Environment Agency. Greenhouse gas emission intensity of electricity generation, 2022. https://www.eea.europa.eu/data-and-maps/daviz/co2-emission-intensity-14#tab-chart_7 [Accessed: 07/11/2023].

[175] Tyler FM Brown, Laura Revell, Michele T Bannister, Timofei Sukhodolov, and Eugene Rozanov. An inventory of global rocket launch emissions and projected near-future impacts on stratospheric ozone. *Authorea Preprints*, 2022.

[176] Alexander Ponomarenko. Rp/software engineering ug/rpa/download. http://www.rocket-propulsion.com/RPA/download.htm [Accessed: 07/11/2023].

[177] Blue Origin. New glenn payload user's guide. 2018. https://yellowdragonblogdotcom.files.wordpress.com/2019/01/new_glenn_payload_users_guide_rev_c.pdf[Accessed: 07/11/2023].

[178] SpaceX. Starship/superheavy, 2023. https://www.spacex.com/vehicles/starship/ [Accessed: 07/11/2023].

[179] Sierra Engineering & Software Inc. Exhaust plume calculations for spacex raptor booster engine. 2022.

[180] John D DeSain, Brian B Brady, and Air Force Space Command. Potential atmospheric impact generated by space launches worldwide—update for emission estimates from 1985 to 2013. *Aerospace Report Prepared for Space and Missile Systems Center, US Air Force Space Command, Aerospace Rept. TOR-2014-02140, El Segundo, CA*, pages 5–15, 2014.

[181] G Sanders and M Duke. In-situ resource utilization (isru) capability roadmap. *NASA/JSC*, 19, 2005.

[182] Stephen J Hoffman. *Human exploration of Mars: the reference mission of the NASA Mars exploration study team*, volume 6107. National Aeronautics and Space Administration, Lyndon B. Johnson Space Center, 1997.

[183] Bret G Drake, Stephen J Hoffman, and David W Beaty. Human exploration of mars, design reference architecture 5.0. In *2010 IEEE Aerospace Conference*, pages 1–24. IEEE, 2010.

[184] Lisa Watson-Morgan, Greg Chavers, John Connolly, Kathryn Crowe, Don Krupp, Laura Means, Thomas Percy, Tara Polsgrove, and Jason Turpin. Nasa's initial and sustained artemis human landing systems. In *2021 IEEE Aerospace Conference (50100)*, pages 1–11. IEEE, 2021.

[185] Elon Musk, September 2019. TweetID: 1171118891671490560, "Sea level Raptor's vacuum Isp is 350 sec, but 380 sec with larger vacuum-optimized nozzle".

[186] Lockheed Martin. Space exploration, 2023. https://www.lockheedmartin.com/en-us/capabilities/space/human-exploration.html [Accessed: 09/11/2023].

[187] Lockheed Martin. Lockheed martin on blue origin's national team selected to develop human lunar lander, 2023. https://news.lockheedmartin.com/2023-05-19-Lockheed-Martin-on-Blue-Origins-National-Team-Selected-to-Develop-Human-Lunar [Accessed: 09/11/2023].

[188] NASA. Nasa selects blue origin as second artemis lunar lander provider, 2023. https://www.nasa.gov/news-release/nasa-selects-blue-origin-as-second-artemis-lunar-lander-provider/ [Accessed: 09/11/2023].

[189] NASA Lisa Watson-Morgan, Marshall Space Flight Centre. Human landing system, 2023. https://ntrs.nasa.gov/api/citations/20230010065/downloads/10%207%20HLS%20101.pdf [Accessed: 08/11/2023].

[190] Air Force Research Laboratory. Afrl and blue origin partner on test site for be-7 lunar lander engine development, 2020. https://afresearchlab.com/news/afrl-and-blue-origin-partner-on-test-site-for-be-7-lunar-lander-engine-development/ [Accessed: 09/11/2023].

[191] Aerojet Rocketdyne. Rs-25 engine, 2023. https://www.l3harris.com/all-capabilities/rs-25-engine [Accessed: 09/11/2023].

[192] Dieter K Huzel. *Modern engineering for design of liquid-propellant rocket engines*, volume 147. AiAA, 1992.

[193] Robert A. Braeunig. Rocket propellants, 2008. http://www.braeunig.us/space/propel.htm [Accessed: 09/11/2023].

[194] NASA. Nasa's lunar exploration program overview, 2020. http://www.braeunig.us/space/propel.htm [Accessed: 09/11/2023].

[195] NASA. Nasa's space launch system reference guide, 2022. https://www.nasa.gov/wp-content/uploads/2022/03/sls_reference_guide_2022_v2_print_0.pdf [Accessed: 10/11/2023].

[196] NASA. Nasa's orion reference guide, 2023. https://www.nasa.gov/wp-content/uploads/2023/02/orion-reference-guide-111022.pdf [Accessed: 10/11/2023].

[197] Steven S. Pietrobon. Analysis of propellant tank masses. 2009. https://api.semanticscholar.org/CorpusID:195179426 [Accessed: 01/11/2023].

[198] Kenza K Boudad, Diane C Davis, and Kathleen C Howell. Disposal trajectories from near rectilinear halo orbits. In *AAS/AIAA Astrodynamics Specialists Conference*, number JSC-E-DAA-TN60056, 2018.

[199] Steven Sepka and Jamshid A Samareh. Thermal protection system mass estimating relationships for blunt-body, earth entry spacecraft. In *45th AIAA Thermophysics Conference*, page 2507, 2015.

[200] NASA. Nasa's aerothermodynamics course: Tps mass fraction requirements. https://tfaws.nasa.gov/TFAWS12/Proceedings/Aerothermodynamics%20Course.pdf [Accessed: 23/11/2023].

[201] Ryan C Woolley and Charles W Whetsel. On the nature of earth-mars porkchop plots. In *AAS/AIAA Spaceflight Mechanics Meeting*, number AAS 13-226, 2013.

[202] Aerojet Rocketdyne. Rl10 upper-stage engine: Product overview, 2024. Manufacturer data sheet with performance characteristics.

[203] Arianespace. *Ariane 5 User's Manual, Issue 5 Rev. 1.* Arianespace, 2016. Includes HM7B engine performance for the ESC-A stage.

[204] ArianeGroup / Arianespace. *Ariane 6 User's Manual, Issue 1*, 2023. VINCI upper-stage engine characteristics and duty cycle.

[205] KBKhA — Chemical Automatics Design Bureau. Kvd-1 (11d56) cryogenic engine, 2021. Manufacturer page with thrust, mixture ratio and Isp.

[206] Indian Space Research Organisation. Cryogenic upper stage (cus) ce-7.5, 2024. Official ISRO overview with performance parameters.

[207] Indian Space Research Organisation. Ce-20 cryogenic engine, 2024. Official ISRO engine page with thrust and Isp figures.

[208] China Great Wall Industry Corporation (CGWIC). *Long March 3A/3B/3C Series Launch Services User's Manual, Rev. 2015*, 2015. Lists YF-73 and YF-75 engine performance on LM-3 series.

[209] China Great Wall Industry Corporation (CGWIC). *Long March 5 Launch Services User's Manual*, 2020. Includes YF-75D expander-cycle upper-stage engine data.

[210] KBKhA — Chemical Automatics Design Bureau. Rd-0146 expander-cycle cryogenic engine family, 2022. Manufacturer page with variants and performance.

[211] Japan Aerospace Exploration Agency. *LE-5/LE-5A/LE-5B Engine Overview*, 2023. Official summaries with thrust, Isp, mixture ratio.

[212] Blue Origin. Be-3 liquid hydrogen/liquid oxygen engine, 2024. Manufacturer page with BE-3 and BE-3U performance.

[213] Lunar and Planetary Institute. Luna mission. `https://www.lpi.usra.edu/lunar/missions/luna/`. Accessed 2025-10-13.

[214] Lunar and Planetary Institute. Surveyor mission. `https://www.lpi.usra.edu/lunar/missions/surveyor/`. Accessed 2025-10-13.

[215] National Aeronautics and Space Administration. Apollo program overview, 2025. Official NASA overview summarising lunar landings.

[216] China National Space Administration. China lunar exploration project (chang'e) – overview, 2025. Official programme background and missions.

[217] Indian Space Research Organisation. Chandrayaan programme overview, 2025. ISRO's official page on the Chandrayaan missions.

[218] SpaceIL. Beresheet mission, 2025. Programme/mission overview and landing outcome.

[219] ispace, inc. Hakuto-r programme, 2025. Company's official programme page with mission status.

[220] Roscosmos State Corporation. Luna-25 (luna-glob) mission overview, 2025. Official programme/mission information and press communications.

[221] Japan Aerospace Exploration Agency. Slim: Smart lander for investigating moon, 2025. Official JAXA mission page confirming lunar landing.

[222] Astrobotic Technology Inc. Peregrine mission one, 2025. Official mission page with post-flight status.

A Lunar Regolith Composition

Below is a collection of data regarding the chemical composition of lunar soil/regolith. The average values, and upper/lower bounds are summarised in the table below.

Table 21: Chemical composition of lunar soil samples

Element	**Compound**	**Average wt%**	**Lower bound**	**Upper bound**
-	SiO_2	44	39	49
Si	-	21	18	23
-	Al_2O_3	19	6	34
Al	-	10	3	18
-	FeO	11	1	22
Fe	-	9	0	17

B Upcoming Mars Transfer Windows

The following values for upcoming Mars transfer windows are sourced from a NASA JPL analysis[201].

Table 22: Mars transfer windows from 2011-2073

Year	ΔV_{Tot} km/s	ΔV_1 km/s	ΔV_2 km/s	ν_{Earth} deg.	ν_{Mars} deg.	Transfer days	T_{angle} deg.	Type	e	LD	AD
2011	5.70	2.99	2.70	303.1	278.5	307	208.6	2	0.210	11/9/2011	9/11/2012
2013	6.24	3.07	3.17	330.8	312.4	295	214.7	2	0.190	12/6/2013	9/27/2014
2016	7.12	3.36	3.76	13.1	354.0	277	214.1	2	0.176	1/17/2016	10/20/2016
2018	5.76	2.80	2.96	128.0	47.6	204	152.8	1	0.175	5/12/2018	12/2/2018
2020	6.32	3.71	2.61	199.2	112.6	205	146.5	1	0.231	7/25/2020	2/15/2021
2022	6.49	3.84	2.65	236.2	215.4	351	212.3	2	0.251	9/2/2022	8/19/2023
2024	5.82	3.36	2.45	265.9	242.0	334	209.3	2	0.237	10/2/2024	9/1/2025
2026	5.61	3.04	2.57	294.2	266.8	311	205.7	2	0.218	10/31/2026	9/7/2027
2028	5.99	3.02	2.97	318.8	298.8	301	213.2	2	0.198	11/24/2028	9/21/2029
2030	6.75	3.22	3.53	353.8	336.3	285	215.7	2	0.180	12/29/2030	10/10/2031
2033	6.33	3.00	3.33	102.8	17.4	198	147.8	1	0.167	4/16/2033	10/31/2033
2035	5.85	3.21	2.64	170.7	86.4	201	148.8	1	0.208	6/26/2035	1/13/2036
2037	6.85	4.03	2.82	223.8	203.3	354	212.7	2	0.254	8/20/2037	8/9/2038
2039	6.03	3.54	2.49	254.3	232.0	342	210.9	2	0.243	9/21/2039	8/28/2040
2041	5.62	3.13	2.48	283.3	256.5	319	206.3	2	0.226	10/20/2041	9/4/2042
2043	5.79	3.00	2.79	308.8	285.7	305	210.1	2	0.206	11/15/2043	9/15/2044
2045	6.41	3.11	3.30	338.7	320.9	292	215.4	2	0.186	12/14/2045	10/2/2046
2048	6.95	3.26	3.69	76.3	350.2	199	147.1	1	0.171	3/20/2048	10/5/2048
2050	5.63	2.83	2.80	141.2	62.4	206	154.4	1	0.185	5/26/2050	12/18/2050
2052	6.59	3.98	2.61	213.3	126.6	210	146.5	1	0.241	8/9/2052	3/7/2053
2054	6.31	3.73	2.58	242.7	221.3	348	211.9	2	0.248	9/9/2054	8/23/2055
2056	5.72	3.27	2.45	272.5	247.0	328	207.6	2	0.233	10/9/2056	9/2/2057
2058	5.65	3.01	2.64	298.9	272.6	308	207.0	2	0.214	11/5/2058	9/9/2059
2060	6.13	3.04	3.08	325.6	306.5	298	214.1	2	0.194	12/1/2060	9/25/2061
2063	6.95	3.29	3.66	3.7	345.8	281	215.4	2	0.178	1/8/2063	10/16/2063
2065	5.98	2.86	3.12	117.1	34.3	201	150.4	1	0.169	5/1/2065	11/18/2065
2067	6.10	3.49	2.61	187.6	101.1	202	146.7	1	0.222	7/14/2067	2/1/2068
2069	6.64	3.91	2.72	231.2	210.5	353	212.5	2	0.252	8/28/2069	8/16/2070
2071	5.90	3.44	2.46	260.8	237.3	337	209.7	2	0.239	9/28/2071	8/30/2072
2073	5.60	3.08	2.52	290.0	261.6	313	204.8	2	0.222	10/27/2073	9/5/2074

C Previously Constructed Cryogenic Stage Masses

The following is a mass breakdown of previously constructed cryogenic (LOX/LH2) stages [197].

Table 23: Cryogenic Propellant Stage Masses

Stage	**Total Mass** [kg]	**Propellant Mass** [kg]	**Dry Mass** [kg]	**Engine Mass** [kg]	**Structural Mass** [kg]	**Dry:Wet Ratio**
S–IV	50580	45360	5220	6x131	4430	0.103203
S–IVB	117870	106125	11745	1x1,438	10307	0.099644
S–II	490780	451730	39050	5x1,438	31860	0.079567
Centaur C	15558	13604	1954	2x131	1692	0.125595
Centaur D/E	16258	13627	2631	2x131	2369	0.161828
Centaur I	15558	13880	1678	2x141	1396	0.107854
Centaur II	18833	16778	2055	2x141	1773	0.109117
Centaur IIA	19073	16778	2295	2x168	1959	0.120327
Centaur G	23877	21105	2772	2x141	2490	0.116095
Centaur 3A	18710	16805	1905	1x167	1738	0.101817
Centaur 3B	22956	20829	2127	2x167	1793	0.092656
Centaur V1	22825	20799	2026	1x167	1859	0.088762
Centaur V2	23050	20800	2250	2x167	1916	0.097614
Ariane H–8	9678	8221	1457	1x149	1308	0.150548
Ariane H–10	12000	10400	1600	1x155	1445	0.133333
Ariane H–10+	12310	10740	1570	1x155	1415	0.127539
Ariane H–155	170800	158100	12700	1x625	12075	0.074356
Ariane H–173	186000	173300	12700	1x811	11889	0.06828
Ariane ESC–A	16500	14400	2100	1x155	1945	0.127273
Ariane ESC–B	27500	24100	3400	1x280	3120	0.123636
CZ H–8	10500	8500	2000	4x236	1056	0.190476
CZ H–18	21000	18200	2800	2x550	1700	0.133333
Japan H–1–3	10600	8800	1800	1x245	1555	0.169811
Japan H–2–1	98100	86200	11900	1x1,714	10186	0.121305
Japan H–2–2	16700	14000	2700	1x242	2458	0.161677
Japan H–2A–1	113600	100000	13600	1x1,800	11800	0.119718
Japan H–2A–2	19600	16600	3000	1x269	2731	0.153061
GSLV–3	14600	12400	2200	1x282	1918	0.150685
Delta 3–2	19300	16824	2476	1x301	2175	0.12829
Delta IV–1	226400	199640	26760	1x6,597	20163	0.118198
Delta IV–2	24170	21320	2850	1x301	2549	0.117915
Delta IVH–2	30708	27220	3488	1x301	3187	0.113586
Energia	905000	820000	85000	4x3,450	71200	0.093923
Shuttle ET	747974	721212	26762	0	26762	0.035779
Ares–I US	151400	138000	13400	1x2,472	10928	0.088507
Ares–V Core	1761253	1603630	157623	6x6,747	117141	0.089495
Ares–V EDS	278460	254193	24267	1x2,472	21795	0.087147
Direct 2.0 Core	808687	735360	73327	3x6,747	53086	0.090674
Direct 2.0 EDS	381500	359065	22435	2x2,472	17491	0.058807
					Average Ratio	**0.113626**

D Previous ISRU plant sizing

Table 24: Mass and power estimated for an Mars ISRU plant [181]

Mission Name	Propellant Produced (mt)	ISRU Plant Mass (mt)	Mass Seed Hydrogen (mt)	Mass To Surface Saved (mt)	Mass In LEO Saved (4:1) (mt)
Bimodal NTR [26]	39.5	2.4	4.1	33.0	132.1
DRM 3 [27]	39.0	3.9	5.4	29.7	118.8
DRM 3 [28] (cache + rover fuel) 6 types	101.4	3.9-10.8	4.4-10.4	42.8-60.1	171.0-240.5
Mars Direct [29]	108	*~6*	6	96	384

Table 25: Mass and power estimated for a Mars ISRU plant [182]

Plant Component	Production Rate (per day)	Component Mass (kg)	Component Power (kWe)
Compressor	269.7 kg	716	4.09
CO_2 Electrolysis	53.2 kg	2128	63.31
Sabatier	22.9 kg	504	1.15
H_2O Electrolysis	27.8 kg	778	0.00
Buffer Gas Extraction	8.7 kg	23	0.13
Cryogenic Coolers	84.8 kg	653	3.59

Table 26: Mass and power estimated for a Mars ISRU plant [183]

	Quantity	Unit Mass (kg)	Total Mass (kg)	Volume (m3)	Power (kWe)
Atmospheric Acquisition Subsystem	2	-	492.12	0.66	17.86
Filter/Frit	4	0.10	0.40	-	-
Microchannel CO2 Adsorption Pump	4	57.50	230.00	0.01	17.86
check Valve	8	0.10	0.80	-	-
Buffer gas pump	4	1.23	4.92	0.00	0.00
Isolation Valve	8	0.50	4.00	-	-
Buffer gas tank	1	250.00	250.00	0.60	-
Flow Controller	4	0.50	2.00	-	-
Oxygen Generation System	2	-	38.80	0.10	2.59
Solid Oxide Electrolysis Stack	2	17.00	34.00	0.05	2.59
Isolation Valve	8	0.50	4.00	-	-
Filter/Frit	4	0.10	0.40	-	-
check Valve	4	0.10	0.40	-	-
Liquefaction Subsystem	1	-	34.60	0.10	3.26
Hydrogen Cooler	2	10.60	21.20	0.01	0.34
Methane Cooler	2	1.20	2.40	0.01	0.02
Oxygen Crycooler	2	5.50	11.00	0.03	2.90
ISRU System (each)	**-**	**-**	**565.52**	**0.86**	**23.71**

E Current Hydrolox Engines

Table 27: Overview of currently developed hydrolox rocket engines

	RL-10 [202]	**HM7B** [203]	**Vinci** [204]	**KVD-1** [205]
Country of origin	United States	France	France	Soviet Union
Thrust (vac.)	66.7 kN (15,000 lbf)	62.7 kN	180 kN	69.6 kN
Mixture ratio	5.5:1 or 5.88:1	5.0	5.8	-
Nozzle ratio	40	83.1	-	-
Isp (vac.)	433	444.2	465	462
Chamber pressure (MPa)	2.35	3.5	6.1	5.6
LH2 TP (rpm)	-	-	90,000	-
LOX TP (rpm)	-	-	18,000	-
Length (m)	1.73	1.8	2.2∼4.2	2.14
Dry mass (kg)	135	165	550	282

	CE-7.5 [206]	**CE-20** [207]	**YF-73** [208]	**YF-75** [208]
Country of origin	India	India	China	China
Thrust (vac.)	73 kN	186.36 kN	44.15 kN	83.585 kN
Mixture ratio	-	5.05	5.0	5.2
Nozzle ratio	-	100	40	80
Isp (vac.)	454	442	420	438
Chamber pressure (MPa)	5.8	6.0	2.59	3.68
LH2 TP (rpm)	-	-	-	42,000
LOX TP (rpm)	-	-	-	-
Length (m)	2.14	-	1.44	2.8
Dry mass (kg)	435	558	236	245

	YF-75D [209]	**RD-0146** [210]	**ES-702**	**ES-1001**
Country of origin	China	Russia	Japan	Japan
Thrust (vac.)	88.36 kN	98.1 kN (22,054 lbf)	68.6 kN (7.0 tf)	98 kN (10.0 tf)
Mixture ratio	6.0	-	5.2	6.0
Nozzle ratio	80	-	40	40
Isp (vac.)	442.6	463	425	425
Chamber pressure (MPa)	4.1	5.9	2.45	3.51
LH2 TP (rpm)	65,000	125,000	41,000	46,310
LOX TP (rpm)	-	-	16,680	21,080
Length (m)	-	2.2	-	-
Dry mass (kg)	265	242	255.8	259.4

	LE-5 [211]	**LE-5A** [211]	**LE-5B** [211]	**BE-3** [212]
Country of origin	Japan	Japan	Japan	United States
Thrust (vac.)	102.9 kN (10.5 tf)	121.5 kN (12.4 tf)	137.2 kN (14 tf)	710 kN
Mixture ratio	5.5	5	5	-
Nozzle ratio	140	130	110	-
Isp (vac.)	450	452	447	-
Chamber pressure (MPa)	3.65	3.98	3.58	-
LH2 TP (rpm)	50,000	51,000	52,000	-
LOX TP (rpm)	16,000	17,000	18,000	-
Length (m)	2.68	2.69	2.79	-
Dry mass (kg)	255	248	285	-

*Highlighted values are above the theoretical limit for hydrolox engines.

F Past and Current Lunar Landers

Table 28: Overview of Lunar Landers

Programme	Successful	Dry mass (kg)	Propellant mass (kg)	dry:wet ratio
Luna[213]	7/27	1,641	3,539	0.317
Surveyor[214]	5/7	306	734	0.294
Apollo[215]	6/7	4,280	10,920	0.282
Chang'e[216]	3/3	1,200	2,580	0.317
Chandrayaan[217]	1/2	626	845	0.426
Beresheet[218]	0/1	150	435	0.256
Hakuto-R[219]	0/1	340	660	0.340
Luna-Glob[220]	0/1	800	950	0.457
SLIM[221]	1/1	120	470	0.203
Peregrine[222]	0/1	833	450	0.649
			Average	**0.354**